

Identification and Characterization of GAS2L3 as a Novel Mitotic Regulator in Human Cells

Dissertation zur Erlangung des
naturwissenschaftlichen Doktorgrades
der Bayerischen Julius-Maximilians-Universität Würzburg



vorgelegt von

Kathrin Schmitt

aus

Freiburg im Breisgau

Würzburg, 2010

Eingereicht am:

.....

Mitglieder der Promotionskommission:

Vorsitzender:

1. Gutachter: Prof. Dr. Stefan Gaubatz

2. Gutachter: Prof. Dr. Georg Krohne

Tag des Promotionskolloquiums:

.....

Doktorurkunde ausgehändigt am:

.....

ABSTRACT

Precise control of mitotic progression is vital for the maintenance of genomic integrity. Since the loss of genomic integrity is known to promote tumorigenesis, the identification of new G2/M regulatory genes attracts great attention.

LINC, a human multiprotein complex, is a transcriptional activator of a set of G2/M specific genes. By depleting LIN9 in MEFs, a core subunit of LINC, *Gas2l3* was identified as a novel LINC target gene. The so far uncharacterized *Gas2l3* gene encodes for a member of the family of growth arrest specific 2 (GAS2) proteins, which share a highly conserved putative actin binding CH and a putative microtubule binding GAS2 domain.

In the present study *GAS2L3* was identified as a LINC target gene also in human cells. Gene expression analysis revealed that *GAS2L3* transcription, in contrast to all other GAS2 family members, is highly regulated during the cell cycle with highest expression in G2/M. The *GAS2L3* protein showed a specific localization pattern during the M phase: In metaphase, *GAS2L3* localized to the mitotic spindle, relocated to the spindle midzone microtubules in late anaphase and concentrated at the midbody in telophase where it persisted until the end of cytokinesis. Overexpression of a set of different *GAS2L3* deletion mutants demonstrated that the localization to the mitotic microtubule network is dependent on the C-terminus, whereas the midbody localization is dependent on full length *GAS2L3* protein. Additionally, exclusive overexpression of the CH domain induced the formation of actin stress fibers, suggesting that the CH domain is an actin binding domain. In contrast, the GAS2 domain was neither needed nor sufficient for microtubule binding, indicating that there must be an additional so far unknown microtubule binding domain in the C-terminus. Interestingly, immunoblot analysis also identified the C-terminus as the domain responsible for *GAS2L3* protein instability, partially dependent on proteasomal degradation.

Consistent with its specific localization pattern, *GAS2L3* depletion by RNAi demonstrated its responsibility for proper mitosis and cytokinesis. *GAS2L3* depletion in HeLa cells resulted in the accumulation of multinucleated cells, an indicator for chromosome mis-segregation during mitosis. Also the amount of cells in cytokinesis was enriched, indicating failures in completing the last step of cytokinesis, the abscission. Strikingly, treatment with microtubule poisons that lead to the activation of the spindle assembly checkpoint (SAC) indicated that the SAC was weakened in *GAS2L3* depleted cells. Although the exact molecular mechanism is still unknown, first experiments support the hypothesis that *GAS2L3* might be a regulator of the SAC master kinase BUBR1.

In conclusion, this study provides first evidence for *GAS2L3* as a novel regulator of mitosis and cytokinesis and it might therefore be an important guardian against tumorigenesis.

Die Identifizierung und Charakterisierung von GAS2L3 als neuer Regulator der Mitose in humanen Zellen

KURZFASSUNG

Der korrekte Verlauf durch die Mitose des Zellzyklus trägt entscheidend zur Aufrechterhaltung der genomischen Integrität bei. Da ein Verlust der genomischen Integrität die Tumorentstehung begünstigt, ist die Identifizierung neuer G2/M regulatorischer Gene ein Forschungsbereich, der großes Interesse weckt.

Der humane Multiproteinkomplex LINC ist für die transkriptionelle Aktivierung einer Vielzahl G2/M spezifischer Gene verantwortlich. Durch die Depletion von LIN9 in MEFs, einer Kernkomponente von LINC, wurde *Gas2/3* als ein neues Zielgen von LINC identifiziert. Das bisher uncharakterisierte *Gas2/3* Gen codiert für ein der GAS2 (growth arrest specific 2) Familie zugehöriges Protein, deren Mitglieder sich durch eine hoch konservierte putative Aktin-bindende Domäne (CH) und eine putative Mikrotubuli-bindende Domäne (GAS2) auszeichnen.

In der vorliegenden Arbeit konnte gezeigt werden, dass *GAS2L3* auch in humanen Zellen ein Zielgen von LINC ist. Die Transkription von *GAS2L3* wies, im Gegensatz zu allen anderen GAS2 Familienmitgliedern, eine starke Regulation während des Zellzyklus auf, wobei die höchste Genexpression in der G2/M Phase vorlag. Das *GAS2L3* Protein zeigte eine spezifische Lokalisation während der M Phase: In der Metaphase findet sich *GAS2L3* an der mitotischen Spindel, wandert von dort an die Mikrotubuli der zentralen Spindel der Anaphase und konzentriert sich in der Telophase am Midbody, wo es bis zum Ende der Zytokinese verweilt. Der Einsatz unterschiedlicher Deletionsmutanten demonstrierte, dass die Lokalisation an die mitotischen Mikrotubuli vom C-Terminus abhängig ist, wohingegen die Lokalisation am Midbody von der gesamten Proteinsequenz abhängt. Die Ausbildung von Aktin-Streß-Filamenten nach alleiniger Überexpression der CH Domäne deutete darauf hin, dass die CH Domäne eine Aktin-bindende Domäne ist. Die GAS2 Domäne hingegen wurde weder für die Interaktion mit Mikrotubuli gebraucht, noch war sie alleine für diese ausreichend. Alle Daten weisen darauf hin, dass *GAS2L3* eine bisher unbekannte Mikrotubuli-bindende Domäne im C-Terminus trägt. Interessanterweise ist der C-Terminus auch für die hohe Instabilität des *GAS2L3* Proteins, die teilweise durch den Abbau im Proteasom verursacht wird, verantwortlich.

Entsprechend der spezifischen Lokalisation zeigte die Depletion von *GAS2L3* durch siRNA Transfektion dessen Wichtigkeit für den korrekten Verlauf der M Phase. *GAS2L3* depletierte HeLa Zellen zeigten eine Anreicherung von multinukleären Zellen, welche ein Indikator für die fehlerhafte Verteilung der Chromosomen in der Mitose sind. Ein Hinweis auf Probleme im Beenden der Zytokinese stellte die erhöhte Anzahl von Zellen dar, die sich in der Zytokinese befanden. Eines der auffallendsten Merkmale war ein geschwächter mitotischer Spindelkontrollpunkt, den *GAS2L3* depletierte Zellen nach der Behandlung mit den Kontrollpunkt aktivierenden Mikrotubuli-Giften aufwiesen. Auch wenn der exakte molekulare Mechanismus hierbei noch unbekannt ist, deuten erste Experimente darauf hin, dass *GAS2L3* die Aktivität von BUBR1, einer essentiellen Kinase des mitotischen Spindelkontrollpunkts, beeinflusst.

Alle Daten dieser Arbeit verdeutlichen die Wichtigkeit von *GAS2L3* als einen neuen Regulator der Mitose und Zytokinese. Somit ist anzunehmen, dass die korrekte Funktion von *GAS2L3* entscheidend zum Schutz vor Tumorentstehung beiträgt.

TABLE OF CONTENTS

1	INTRODUCTION	1
1.1	The human cell cycle	1
1.1.1	Cell cycle regulation by cyclin/CDK complexes	1
1.1.2	Cell division: the M phase	4
1.1.2.1	Mitosis.....	4
1.1.2.2	Cytokinesis.....	5
1.1.2.2.1	<i>Cleavage furrow formation</i>	6
1.1.2.2.2	<i>Midbody formation and abscission</i>	6
1.1.3	The Spindle assembly checkpoint	7
1.1.3.1	The spindle assembly checkpoint and cancer	9
1.2	The LIN complex	10
1.2.1	LINC characterization in vitro.....	10
1.2.2	LINC characterization in vivo	10
1.2.2.1	LINC target genes in mice	11
1.3	The family of growth arrest specific genes.....	12
1.3.1	The GAS2 family.....	13
1.3.1.1	The highly conserved CH and GAS2 domains	13
1.3.1.2	GAS2.....	14
1.3.1.3	GAS2L1 (GAR22).....	14
1.3.1.4	GAS2L2 (GAR17).....	14
1.3.1.5	GAS2L3	15
1.4	Aim of this study.....	15
2	MATERIAL & METHODS	16
2.1	Materials.....	16
2.1.1	Chemical Stocks & Reagents	16
2.1.2	Enzymes.....	17
2.1.3	Antibiotics	17
2.1.4	Buffers	18
2.1.4.1	General buffers.....	18
2.1.4.2	Buffers for whole protein lysates	19
2.1.4.3	Buffers for immunoprecipitation and immunoblot	19
2.1.4.4	Buffers for inclusion body purification.....	20
2.1.4.5	Buffers for flow cytometry (FACS).....	20
2.1.4.6	Buffers for immunofluorescence	20
2.1.5	Antibodies.....	21
2.1.5.1	Primary antibodies	21

2.1.5.2	Secondary antibodies	22
2.1.6	Plasmids.....	23
2.1.6.1	Plasmids for overexpression	23
2.1.6.2	Plasmids for recombinant proteins.....	23
2.1.6.3	Plasmids for retroviral knock down.....	23
2.1.7	Primers.....	24
2.1.7.1	Primers for cloning.....	24
2.1.7.2	Primer for shRNA design.....	25
2.1.7.3	Primers for quantitative RT-PCR.....	25
2.1.8	siRNA sequences	26
2.1.9	Cell lines / Cell culture media / Transfection reagents.....	26
2.1.10	Markers.....	27
2.1.11	Kits.....	27
2.1.12	Beads	27
2.2	Methods.....	28
2.2.1	Cell culture	28
2.2.1.1	Passageing of cells	28
2.2.1.2	Freezing of cells	28
2.2.1.3	Thawing of cells.....	28
2.2.1.4	Counting of cells	28
2.2.1.5	Transient transfection.....	28
2.2.1.5.1	<i>Calcium phosphate transfection</i>	28
2.2.1.5.2	<i>Lipofectamine / Metafectene transfection</i>	29
2.2.1.6	Infection of BJ-ET cells	29
2.2.1.7	Growth curve of BJ-ET cells	29
2.2.1.8	Synchronization of T98G cells by serum starvation	29
2.2.1.9	Synchronization of HeLa cells by thymidine.....	29
2.2.1.10	Cell treatment with different reagents.....	30
2.2.1.11	Determination of cell cycle phases by flow cytometry	30
2.2.1.12	Immunofluorescence	30
2.2.1.12.1	<i>PSP fixation</i>	30
2.2.1.12.2	<i>PSP / 0.3 % triton fixation</i>	31
2.2.1.12.3	<i>MesMetOh fixation</i>	31
2.2.1.12.4	<i>TCA fixation</i>	31
2.2.1.12.5	<i>Indirect immunofluorescence (standard procedure)</i>	31
2.2.1.12.6	<i>Direct immunofluorescence of actin filaments</i>	31
2.2.1.12.7	<i>Fixation method for specific immunofluorescence stainings</i>	32
2.2.2	Expression analysis.....	32
2.2.2.1	RNA isolation	32
2.2.2.2	Reverse transcription.....	32

2.2.2.3	Quantitative real-time PCR (qRT-PCR)	33
2.2.3	Biochemical methods	33
2.2.3.1	Whole cell lysates	33
2.2.3.2	Determination of protein concentration (Bradford)	34
2.2.3.3	Immunoprecipitation	34
2.2.3.4	SDS polyacrylamide gel electrophoresis (SDS-PAGE)	34
2.2.3.5	Immunoblotting	35
2.2.3.6	Purification of inclusion bodies from recombinant bacteria for antibody production	35
2.2.4	Molecular biology	36
2.2.4.1	Isolation of plasmid DNA from bacteria	36
2.2.4.1.1	<i>Mini preparation</i>	36
2.2.4.1.2	<i>Midi and Maxi preparation</i>	36
2.2.4.2	Isolation of plasmid DNA fragments from agarose gels	36
2.2.4.3	Isolation of PCR products after restriction	37
2.2.4.4	Standard cloning methods	37
2.2.4.4.1	<i>Primer design</i>	37
2.2.4.4.2	<i>PCR for cloning of DNA fragments</i>	37
2.2.4.4.3	<i>Agarose gelelectrophoresis</i>	38
2.2.4.4.4	<i>Restriction</i>	38
2.2.4.4.5	<i>Ligation</i>	39
2.2.4.4.6	<i>Transformation (heat shock)</i>	39
2.2.4.4.7	<i>Sequencing</i>	39
2.2.4.4.8	<i>Cloning of hGAS2L3 WT and Delmut 1-5</i>	39
3	RESULTS	40
3.1	The uncharacterized LINC target gene <i>GAS2L3</i>	40
3.2	<i>GAS2L3</i> is a LINC target gene in the human system	40
3.2.1	Transcriptional regulation during the cell cycle	41
3.2.2	G2/M specific expression pattern is LINC dependent	43
3.3	Localization pattern of overexpressed <i>GAS2L3</i>	44
3.3.1	Validation of the midbody localization	45
3.3.2	Mitotic distribution of <i>GAS2L3</i>	47
3.4	Localization of endogenous <i>GAS2L3</i>	50
3.5	Characterizing <i>GAS2L3</i> protein domains	51
3.5.1	Protein domains essential for specific localization pattern	52
3.5.2	Domains essential for <i>GAS2L3</i> protein stability	55
3.6	Immunoblot analysis of endogenous <i>GAS2L3</i> protein	57
3.7	Biological relevance	58
3.8	<i>GAS2L3</i> depletion under physiological conditions	58

3.8.1	GAS2L3 depletion in transformed cells	59
3.8.2	GAS2L3 depletion in untransformed cells	61
3.9	GAS2L3 depletion after induction of mitotic stress	62
3.9.1	Spindle assembly checkpoint activation by nocodazole.....	63
3.9.1.1	SAC activation over time.....	63
3.9.1.2	SAC recovery assay	65
3.9.2	Spindle assembly checkpoint activation by Taxol	66
3.9.2.1	SAC activation over time.....	66
3.9.3	Mechanism behind a compromised SAC	67
3.9.3.1	MAD2 protein characterization after GAS2L3 depletion.....	68
3.9.3.1.1	<i>MAD2 kinetochore localization after taxol treatment.....</i>	<i>68</i>
3.9.3.1.2	<i>MAD2/CDC20 interaction after taxol treatment.....</i>	<i>69</i>
3.9.3.2	BUBR1 protein characterization after GAS2L3 depletion	69
3.9.3.2.1	<i>BUBR1 kinetochore localization</i>	<i>70</i>
3.9.3.2.2	<i>BUBR1 protein levels after taxol treatment</i>	<i>71</i>
4	DISCUSSION.....	72
4.1	Characterization of GAS2L3.....	72
4.2	<i>GAS2L3</i> is a G2/M regulated LINC target gene.....	72
4.3	GAS2L3 localization during the cell cycle	72
4.3.1	GAS2L3 colocalizes with and stabilizes the interphase microtubule..... network	73
4.3.2	GAS2L3 colocalizes with the mitotic microtubule network	73
4.3.3	GAS2L3 localizes to the midbody during cytokinesis	73
4.4	Characterization of GAS2L3 protein domains.....	74
4.4.1	The GAS2 domain is neither needed nor sufficient for microtubule binding	74
4.4.2	The CH domain is an actin binding domain	75
4.4.3	Only full length GAS2L3 localizes to the midbody	75
4.4.4	GAS2L3 is highly regulated on protein level.....	75
4.5	Biological relevance: GAS2L3 is a regulator of mitosis and cytokinesis.....	77
4.5.1	GAS2L3 depletion results in mitosis and cytokinesis failure.....	77
4.5.2	GAS2L3 depletion weakens the spindle assembly checkpoint	79
4.5.3	Role of GAS2L3 in the SAC	80
4.5.3.1	MAD2 can still localize to kinetochores but MAD2/CDC20	81
4.5.3.2	BUBR1 phosphorylation is affected in GAS2L3 depleted cells.....	81
4.6	Hypothesis	83

5	APPENDIX.....	85
5.1	List of Figures & Tables	85
5.2	Abbreviations.....	86
5.3	References	87
5.4	Own publications.....	96
5.5	Curriculum Vitae	97
5.6	Eidesstattliche Erklärung	98
	Acknowledgements	

1 INTRODUCTION

1.1 The human cell cycle

The eukaryotic cell cycle is a fundamental evolutionarily conserved process that regulates cell division from simple unicellular organisms, such as yeast, through to higher multicellular organisms, such as humans. In multicellular organism, maintaining genomic integrity by precise control of the cell cycle is vital for development, survival and proliferation.

The human cell cycle can be divided into four main phases, termed G1, S, G2 and M phase. During G1 (gap1), the first gap phase, cells grow in size and synthesize RNA and proteins. These molecular events eventually commit the cell to progress into the next cell cycle phase, the S phase. In S (synthesis) phase, active replication of the parental chromosomes takes place resulting in the doubled DNA amount though the cell ploidy remains the same. During the following G2 (gap2) phase, correct duplication of the chromosomes is controlled before cells enter M phase, where cell division takes place. The M phase is composed of two tightly controlled important processes. First, in mitosis, the duplicated chromosomes get separated followed by cytokinesis, the process of dividing the cytoplasm in two identical daughter cells. The period of the cell cycle from the end of one M phase to the beginning of the next, including G1, S and G2 phase is also termed interphase. In humans, most differentiated cells stop dividing and leave the cell cycle in G1 to enter a quiescent cell cycle state called G0, where they survive for month to years (Coller, 2007; Pardee, 1974; Shackelford et al., 1999).

1.1.1 Cell cycle regulation by cyclin/CDK complexes

The transition from one cell cycle phase into the next is mainly regulated by the activities of various protein kinase complexes, the so called cyclin/CDK (cyclin dependent kinase) complexes. Different cyclin/CDK complexes are expressed in different phases of the cell cycle, with each cyclin, as regulatory subunit, having a specific time of appearance and a specific kinase to activate (Doree and Galas, 1994). In humans, mainly the four kinases CDK1, 2, 4 and 6 regulate the activity of several proteins involved in DNA replication and mitosis by phosphorylating them at specific regulatory sites, thereby promoting cell cycle progression (Morgan, 1997; Murray, 2004).

Cell cycle progression starts with external mitogenic signaling in G1. Mitogens induce, via conserved receptor tyrosine kinase pathways, the expression of CDK4 and CDK6, the G1 CDKs (Sherr, 1994a; Sherr et al., 1994). G1 cyclin/CDK complexes lead to the release of E2F transcription factors (E2F1-3) by phosphorylating their inhibitory subunit, the pRB protein (Nevins, 1992; Sherr, 1994b; Stevaux and Dyson, 2002). Once E2F1-3 are released, cells have

bypassed the so called restriction point, a point of no return (Planas-Silva and Weinberg, 1997). Further cell cycle progression is now independent from external mitogens. This highlights the important role of pRB as a negative regulator of proliferation, supported by the fact that pRB, product of the first identified tumorsuppressor gene *RB1*, is mutated in approximately one third of all human tumors (Lee et al., 1987a; Lee et al., 1987b; Sherr, 1996). After their release, E2F1-3 activate the expression of genes essential for S phase entry (Dyson, 1998; Humbert et al., 2000; Trimarchi and Lees, 2002). Amongst others, these are genes essential for DNA replication, nucleotide synthesis and the S phase cyclin/CDK genes, cyclin E and *CDK2*. Active S phase cyclin/CDK complexes are then the start signal for DNA replication. During S phase, the M phase cyclin, cyclin B, is synthesized and accumulates in the cytosol. As soon as cyclin B migrates into the nucleus it activates the kinase activity of CDK1 (Porter and Donoghue, 2003). Cyclin B/CDK1 complexes are also called the MPF (mitosis promoting factor), since directly after complex formation entry into mitosis takes place (Gavet and Pines, 2010). After successful chromosome segregation, mitotic exit is caused by the complete degradation of cyclin B in late mitosis. Responsible for cyclin B degradation is the so called destruction box, a specific APC (anaphase promoting complex)/CDH1 recognition site. The APC, an E3 ubiquitin ligase, polyubiquitinates cyclin B. This event is followed by proteasomal degradation (Kramer et al., 2000; Peters, 2006). After the complete loss of cyclin/CDK activity, constitutively active phosphatases dephosphorylate pRB, which in turn inhibits E2F transcription factors and the cell cycle restarts.

Under normal circumstances the cell cycle proceeds without interruptions. However, when damage occurs cells have the capacity to arrest proliferation in all phases of the cell cycle. Those control mechanisms that check cellular integrity before subsequent events in cell cycle progression are initiated, are referred to as cell cycle checkpoints. Checkpoints can generate a transient delay to allow the cell more time to repair damage before further progression. Alternatively, if the damage is too severe to be adequately repaired, cells undergo apoptosis or enter an irreversible senescence like state (Kastan and Bartek, 2004; Shackelford et al., 1999).

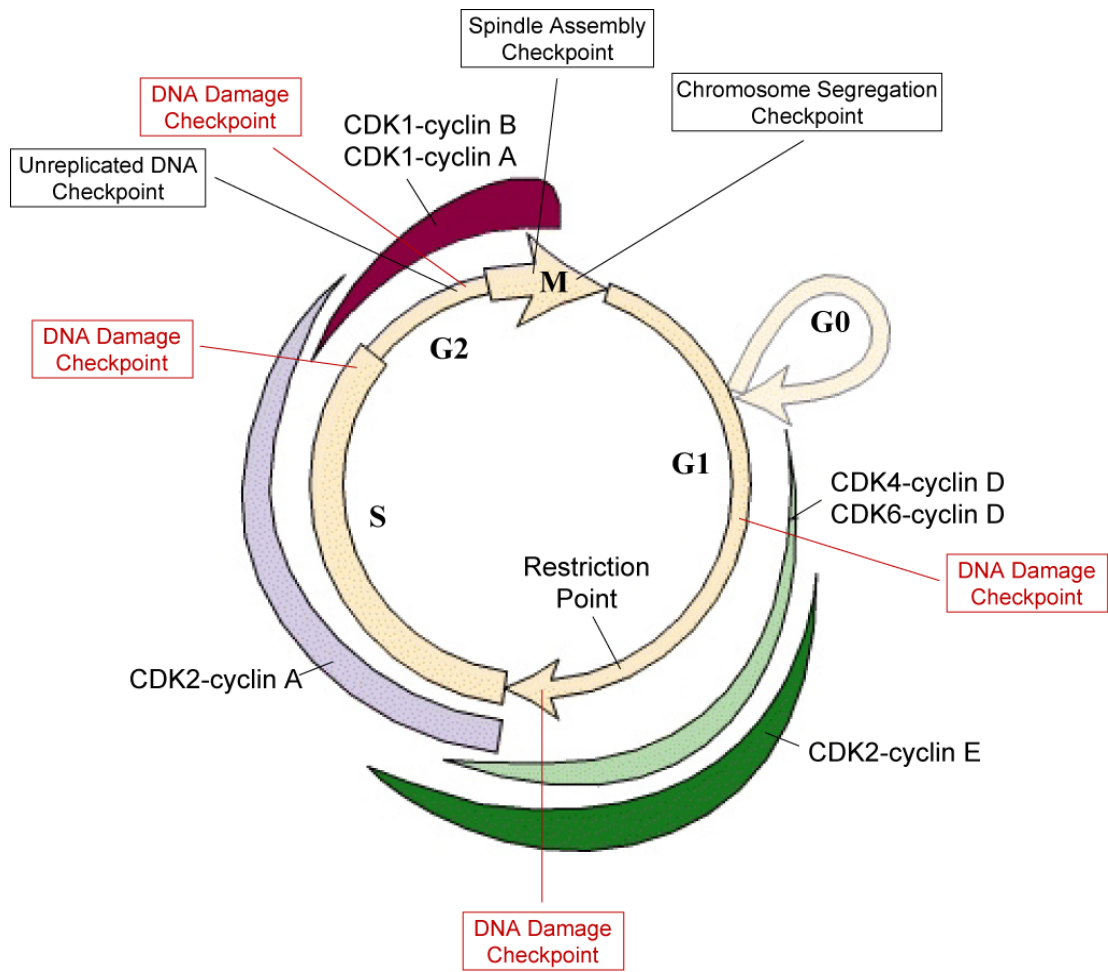


Fig. 1.1. Simplified illustration of the human cell cycle

Oscillating activity of different cyclin/CDK complexes guides the cell through the different phases of the cell cycle. Cell cycle checkpoints monitor for the correct progression through single cell cycle phases and for genomic integrity. Checkpoints depicted in black are constitutive active and have to be silenced for further progression. DNA damage checkpoints depicted in red get only activated when DNA damage has occurred. As soon as cells have bypassed the restriction point, cell cycle progression is no longer dependent on external mitogenic signaling. (Adapted and modified from Molecular Cell Biology 4th edition by Harvey Lodish)

1.1.2 Cell division: the M phase

Chromosome missegregation leads to genetic instability and alters the dosage of a large subset of genes, which can result in severe disease phenotypes. Therefore, chromosome segregation in M phase is one of the most important steps during the cell cycle and has to be tightly controlled.

The M phase, the last step during one cell cycle, is composed of mitosis and cytokinesis, including the separation of sister chromatids followed by the division of the mother cell cytoplasm in two new identical daughter cells. In contrast to the other cell cycle phases, M phase, with a duration of approximately 30 min, is extremely fast.

1.1.2.1 Mitosis

Mitosis can be divided into several stages, named prophase, prometaphase, metaphase, anaphase and telophase. Start signal for mitotic entry is the activation of CDK1/cyclin B complexes in late G2, also called mitotic promoting factor (MPF) (Gavet and Pines, 2010). In prophase, the MPF phosphorylates a variety of substrates, including nuclear lamins, microtubule binding proteins and condensins. Those early mitotic phosphorylation events lead to the initiation of chromatin condensation and the reorganization of microtubules in preparation of mitotic spindle formation. Chromosomes, containing two sister chromatids held together by cohesins at the centromeric region, start to get visible. Duplicated centrosomes divide and relocate to the opposite cell poles where they function as microtubule organizing centers (MTOCs), also called mitotic spindle poles (Cleveland et al., 2003; Nasmyth, 2002). Initiation of prometaphase starts with the nuclear envelope breakdown and chromosomes are captured by spindle microtubules at the kinetochores, an accumulation of proteins at the centromeric region (Hauf and Watanabe, 2004; Maiato et al., 2004a; Maiato et al., 2004b). Highly conserved proteins of the kinetochores are for example the specialized histone H3 variant CENP-A and the motor proteins dynein and kinesin. CENP-A helps the kinetochore to associate with DNA; the motor proteins generate forces that move chromosomes during later mitosis (Joglekar et al., 2010). As soon as chromosomes are aligned at the spindle equator, called metaphase plate, cells have entered metaphase. Chromosomes arrest in metaphase until every single kinetochore is correctly attached to spindle microtubules. This essential step is controlled by the spindle assembly checkpoint (SAC). Once the SAC is satisfied, anaphase onset is induced by APC/C^{CDC20} complex formation (Yu, 2002). The anaphase promoting complex/cyclosome (APC/C) is a specific mitotic E3 ubiquitin ligase (Peters, 2002). Binding of the co-activator CDC20 to APC/C targets the APC/C to securin and cyclin B (Kraft et al., 2006). This in turn leads to their ubiquitination and degradation by the proteasome. Securin degradation leads to the release of separase, a cysteine protease specifically cleaving the Scc1 subunit of cohesin, leading to sister chromatid separation (Nasmyth, 2002; Peters, 2002; Peters, 2006).

Additionally, spindle poles move further apart supporting sister chromatid separation. Finally, binding of the co-activator CDH1 to APC/C leads to complete cyclin B degradation and cells enter telophase, the last stage of mitosis (Peters, 2002; Peters, 2006). During telophase, the nuclear envelope reassembles, chromosomes decondense and first steps of cytokinesis are initiated.

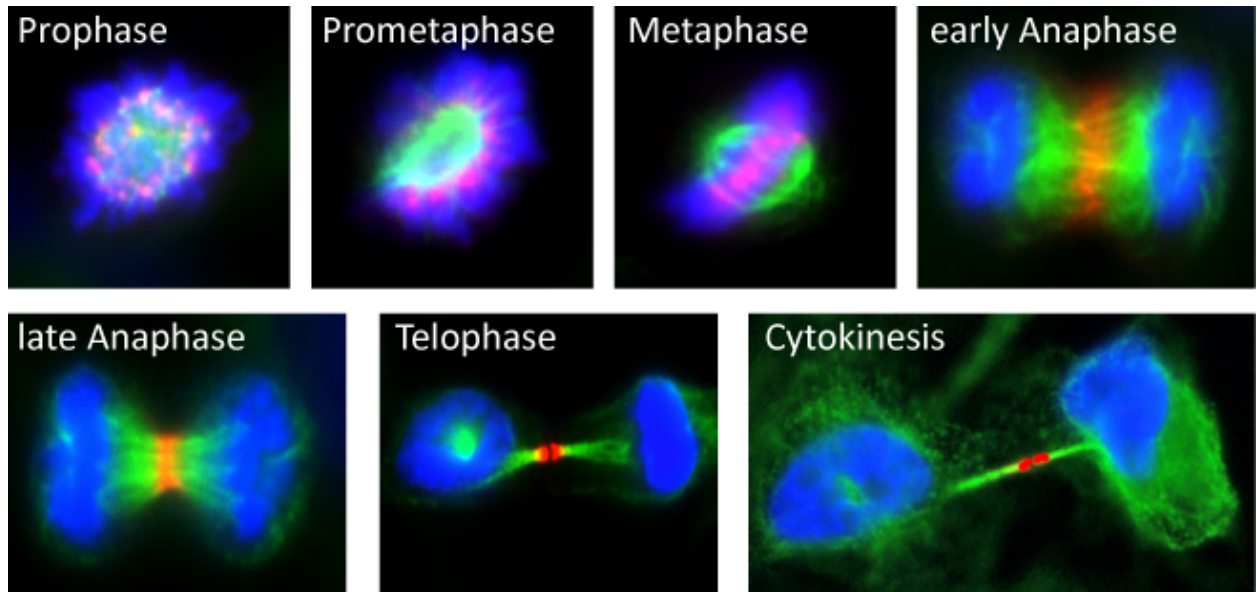


Fig. 1.2. Overview of different M phase stages

HeLa cells were stained with an antibody against Aurora B in red as a marker for the single mitotic stages. The microtubules were counterstained in green with an A-tubulin antibody. Aurora B, the enzymatic heart of the chromosomal passenger complex, colocalizes with centromeres from prophase until metaphase. During anaphase Aurora B localizes to the spindle midzone and finally accumulates at the midbody during telophase.

1.1.2.2 Cytokinesis

The final act of cell division is cytokinesis, the partition of cellular contents into two daughter cells. In the last years, research on cytokinesis has been attracting increasing attention, since it is proposed that failure of this process is associated with tumorigenesis (Sagona and Stenmark, 2010). Although many proteins could be identified as cytokinesis regulators, this process is still less well understood than earlier events during mitosis.

1.1.2.2.1 Cleavage furrow formation

Preparation of cytokinesis already starts during anaphase with the formation of the central spindle and the contractile ring (Glotzer, 2005; Glotzer, 2009a). The contractile ring is a network of actin and myosin filaments organized on a scaffold of cytoskeletal proteins, such as septins and the actin binding protein anillin (D'Avino, 2009). The contractile ring drives the constriction of the plasma membrane, generating two daughter cells connected by a cytoplasmic bridge. The right positioning of the contractile ring has to be tightly controlled since failure during cytokinesis causes abortive cytoplasmic abscission resulting in binucleated or multinucleated cells. The central spindle, also called spindle midzone, plays an important role in coordinating the site of contractile ring assembly (Glotzer, 2009b). Central spindle formation also starts during anaphase. Directly after chromatid separation, proteins essential for the assembly of the central spindle relocate from the cytoplasm and initiate a bundling of the plus ends of microtubules. One important protein concentrating at the central spindle is the guanine nucleotide exchange factor (GEF) ECT2. ECT2 leads to the central spindle localization and activation of RhoA, the key activator in contractile ring formation (Kamijo et al., 2006; Nishimura and Yonemura, 2006; Piekny et al., 2005). After contractile ring formation at the equatorial cortex, activation of myosin motor activity and sliding of actin filaments leads to the ingression of the cleavage furrow (Eggert et al., 2006). At the same time the central spindle becomes compacted and forms a dense structure called the midbody (Paweletz, 2001).

1.1.2.2.2 Midbody formation and abscission

By the end of cytokinesis, the dividing cells are still connected by a narrow intercellular bridge containing the midbody. The midbody (MB) is a dense structure formed in telophase and derived from the central spindle and a massive number of recruited proteins. By purification of MBs from mitotic HeLa cells following proteomic analysis, recent research identified more than 100 proteins to be involved in MB formation (Skop et al., 2004). However, due to its small size and its temporary appearance, molecular and functional aspects of the MB still remain poorly understood. Proteins of the MB are known to be responsible for many different processes in the cell. These are for example ribosomal proteins, heat shock proteins and proteins from various subcellular compartments such as mitochondria and the centrosomes. The concentration of proteins which are associated with vesicular transport finally leads to the last step of cytokinesis, the abscission (Schiel and Prekeris, 2010). During abscission three main processes have to be fulfilled. Firstly, membrane vesicles derived from the biosynthetic and endocytic recycling pathways are delivered to the plasma membrane of the constricting midbody in order to facilitate further narrowing. Secondly, central spindle microtubules of the midbody have to be severed. Thirdly, the final abscission of a membrane remnant that connects the two daughter cells is required. Not surprisingly, disruption of components of the MB can result in defective

cleavage furrow formation or completion (Skop et al., 2004). All those highly precise and spatiotemporal defined processes point up the intricacy of cytokinesis.

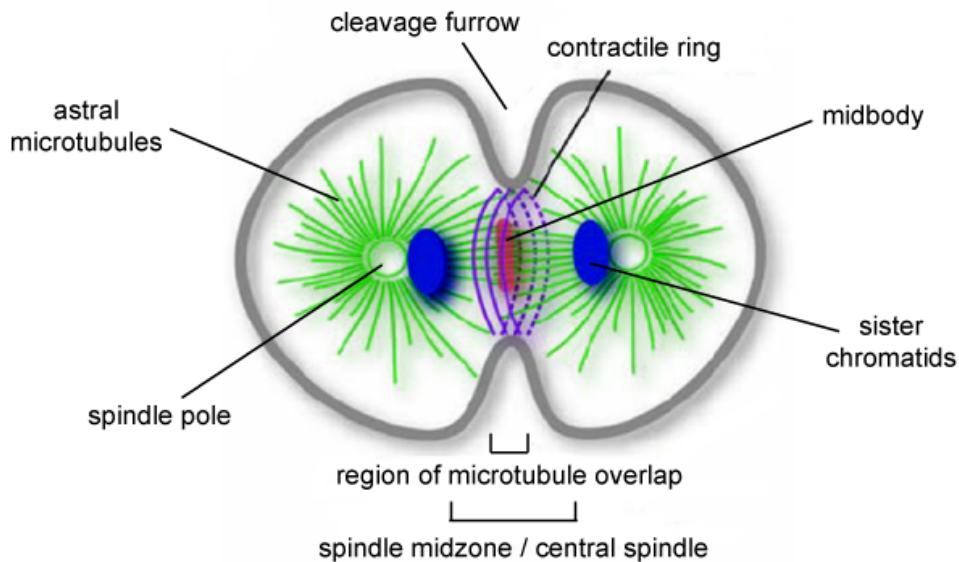


Fig. 1.3. Schematic illustration of a dividing cell in telophase

In telophase, after cleavage furrow ingression, the contractile ring compresses the spindle midzone to form the midbody. Proteins of the midbody are essential for the last step of cytokinesis, the abscission. (Adapted and modified from Glotzer 2005)

1.1.3 The Spindle assembly checkpoint

An indispensable checkpoint controlling chromosome segregation in early mitosis is the spindle assembly checkpoint (SAC). The SAC prevents premature sister chromatid separation prior to bi-orientation of all pairs of sister chromatids on the mitotic spindle (Li and Nicklas, 1995; Rieder et al., 1995).

Early research of the nineties could show that a single unattached kinetochore can generate sufficient amounts of an inhibitory signal to prevent a cell from mitotic exit (Rieder et al., 1995). Based on this result, the following model about SAC signaling was created, predicting that this pathway consists of three components. A sensor that detects the presence of unaligned chromosomes, a transducer that relays or amplifies the signal generated by the sensor, and an inhibitor capable to stop cell cycle progression until all chromosomes are properly aligned. Recent research confirmed the basic idea behind this model, but also revealed that it is oversimplified.

Today the SAC has been proposed to be bipartite, with one arm monitoring kinetochore occupancy with microtubules and the other arm monitoring spindle tension exerted on kinetochores (Shannon et al., 2002; Skoufias et al., 2001; Stern and Murray, 2001; Taylor et al., 2001; Waters et al., 1998). First evidence that a “lack of tension” alone is sufficient to activate the SAC came from experiments in yeast. By using a replication defective Cdc6-yeast strain, Stern and Murray demonstrated that unreplicated chromosomes, containing only one kinetochore, were still able to be captured by the mitotic spindle microtubules. Although all kinetochores were occupied by microtubules, still prolonged SAC activation was triggered, indicated by non decreasing levels of securin. This clearly demonstrated that monooriented chromatids, whose kinetochores are not under tension, can trigger the SAC (Stern and Murray, 2001).

The critical molecular target of the SAC is the APC/C (Bharadwaj and Yu, 2004; Yu, 2002). Important proteins concerning a functional SAC are the core components MAD2 (mitotic arrest deficiency 2), BUBR1 (mitotic arrest deficiency 3) and BUB3 (budding uninhibited by benzimidazole). The *BUB* and *MAD* genes were originally identified in yeast genetic screens, where their functional loss inhibited mitotic arrest upon exposure to microtubule destabilizing drugs (Hoyt et al., 1991; Li and Murray, 1991). Those proteins get recruited to unattached kinetochores where they bind CDC20, together representing the so called MCC (mitotic checkpoint complex) (Cleveland et al., 2003; Taylor et al., 2004) . Even though single MAD2 and BUBR1 have the potential to bind and inhibit CDC20, MCC formation leads to a 3.000 fold greater inhibition of APC/C^{CDC20} complex formation (Fang, 2002; Hardwick et al., 2000; Sudakin et al., 2001; Tang et al., 2001). Interestingly, signal for MCC formation is not generated from kinetochores, as MCC is also present and active in interphase cells. However, only APC/C isolated from mitotic cells is sensitive to inhibition by MCC (Sudakin et al., 2001). It is proposed that the interphase pool of MCC allows for rapid inhibition of APC/C when cells enter mitosis. Unattached kinetochores then target the APC/C for sustained inhibition by the MCC (Sudakin et al., 2001). In addition, MCC formation promotes CDC20 degradation, thus lowering CDC20 protein levels upon checkpoint activation. Upon correct attachment of all kinetochores to microtubules, the SAC is satisfied and stops producing APC/C inhibitors. However, the rate of spontaneous dissociation of these inhibitors is low, and it is widely accepted that an active process, called SAC silencing, must be triggered for APC/C^{CDC20} to be activated (Akiyoshi et al., 2009; Vanoosthuysse and Hardwick, 2009a; Vanoosthuysse and Hardwick, 2009b; Vanoosthuysse et al., 2009). To date, the mechanism of SAC silencing still raises many questions.

Like all checkpoints, the SAC does not arrest cells permanently. Even if the SAC cannot be satisfied, cyclin B is progressively destroyed by a proteasome dependent mechanism followed by mitotic exit. Interestingly, MAD2 and BUBR1 remain associated with kinetochores as cells bypass the SAC, indicating that the SAC is still active. Therefore, mitotic escape is not due to active adaption pathways. A feasible model predicts a leaky APC/C^{CDC20} inhibition over

time leading to a slow but continuous cyclin B degradation that ultimately drives the cell out of mitosis (Brito and Rieder, 2006; Rieder and Maiato, 2004).

1.1.3.1 The spindle assembly checkpoint and cancer

A hallmark of most human cancers is aneuploidy, a state of having abnormal numbers of chromosomes. Aneuploid cells can arise directly from diploid cells through errors in chromosome segregation. However, whether aneuploidy is cause or consequence of tumorigenesis is still a matter of debate (Weaver et al., 2007).

One possible candidate mechanism involved in chromosome segregation in relation to tumorigenesis is the SAC. In certain types of human cancers, including breast, colorectal and gastric cancers, mutations have been observed in SAC genes, although at very low frequency (Weaver and Cleveland, 2006). To learn more about the contribution of deregulated SAC genes and tumorigenesis, a multitude of mouse genetic models has been created in recent years. Extensive studies of those mouse genetic approaches could indeed demonstrate a strong link between deregulation of genes involved in controlling chromosome segregation and development of aneuploidy and cancer (Li et al., 2009).

For example, classical knockout mouse models of the important SAC genes *Bub1*, *BubR1* and *Mad2* results in early embryonic lethality (Baker et al., 2004; Dobles et al., 2000; Jeganathan et al., 2007). In contrast, haploinsufficiency or hypomorphism of these genes results in aneuploidy in both mouse embryonic fibroblasts (MEFs) and in tissues, albeit to varying degrees (Michel et al., 2001; Perera et al., 2007; Wang et al., 2004). Even though *Bub1* and *BubR1* heterozygous mice develop aneuploidy, they show no increase in spontaneous tumor formation (Baker et al., 2004; Jeganathan et al., 2007), while mice heterozygous for *Mad2* develop tumors after long latencies (Dobles et al., 2000; Michel et al., 2001). Additionally, those mouse models revealed that the potential of aneuploidy to drive tumorigenesis is highly dependent on the genetic context. As a specific example, *BubR1* hypomorphism has been analyzed in mice lacking either p16Ink4a or p19Arf (Baker et al., 2008). The incidence of lung tumorigenesis in *BubR1* hypomorphic mice increased nearly 20 fold in mice lacking the gene that encodes p16Ink4a. In contrast, when p19Arf instead of p16Ink4a was absent, tumorigenesis did not accelerate in any tissue.

This contrariness underlines the fact that there are still more open than answered questions about tumorigenesis in general.

1.2 The LIN complex

The coordinated expression of G2/M-specific genes is responsible for correct progression through mitosis, an important step for the maintenance of genomic integrity. Recently, our group identified LINC (LIN complex), a human multiprotein complex that is required for transcriptional activation of G2/M genes (Schmit et al., 2007).

1.2.1 LINC characterization in vitro

LINC consists of a stable core module including the four LIN proteins LIN9, LIN54, LIN52, LIN37 and the chromatin associated protein RbAp48. This five-protein core module dynamically associates with repressor proteins p130 and E2F4 and the transcription factor B-MYB in a cell cycle dependent manner. In quiescent cells, association of LINC with p130/E2F4 targets LINC to the promoters of G1/S genes. Notably, siRNA experiments demonstrated that this promoter binding is not essential for G1/S gene repression. Binding to B-MYB in S phase targets LINC to a large set of G2/M regulated genes. In vitro knock down experiments of different LINC core module proteins inhibited G2/M gene expression, suggesting a direct role for LINC/B-MYB as a transcriptional activator of those G2/M genes. Furthermore, chromatin immunoprecipitation (ChIP) experiments confirmed a direct binding of LINC/B-MYB to gene promoters (Osterloh et al., 2007; Schmit et al., 2007).

Important LINC/B-MYB regulated G2/M genes are amongst others the M phase cyclin/CDK genes cyclin B1, *CDK1* and cyclin A2. Corresponding to their fundamental role in cell cycle progression, depletion of different LINC components strongly impaired cell proliferation with an accumulation of cells in G2 followed by delayed entry into mitosis. Other LINC activated genes are for example mitotic genes like survivin, *BUB1*, *CENP-E* and *PLK1* (Schmit et al., 2007). Deregulation of mitotic genes is widely accepted to be implicated in tumorigenesis by promoting genetic instability.

1.2.2 LINC characterization in vivo

To investigate the physiological role of LINC in vivo, our group generated constitutive as well as conditional knockout mouse models by targeting LIN9, a protein of the stable core module (Reichert et al., 2010). With those two mouse models it was possible to investigate the role of LIN9 in development and, by generating inducible knockout MEFs, in gene regulation.

Heterozygous *Lin9*^{+/-} mice developed normally and showed no obvious defects. However, the complete loss of *Lin9* resulted in early embryonic lethality. Genotyping of embryos dissected from the deciduae at embryonic days 7.5 to 13.5 revealed that none of the embryos

was homozygous *Lin9*^{-/-}, suggesting that embryos die shortly after implantation (Reichert et al., 2010). Dramatically, also the loss of *Lin9* in adult mice resulted in death within seven days due to a complete atrophy of the small intestine, an organ renewing in the mouse every 3 to 5 days. Histological analysis of the remaining tissue revealed large and irregular nuclei as well as binucleated cells, indicating that LIN9 regulates mitosis and cytokinesis *in vivo* (Reichert et al., 2010).

Analysis of *Lin9* knockout MEFs confirmed the role of LIN9 as a regulator of mitosis and cytokinesis. *Lin9* knockout MEFs showed an abnormal cell cycle profile with an accumulation of tetraploid and polyploid cells. Single cell morphology, examined by fluorescence and time lapse microscopy, revealed that *Lin9* knockout resulted in a high amount of cells with aberrant nuclei morphology, aberrant number and distribution of centrosomes and a strong increase in binucleated cells. All in all, these phenotypes suggested a role for LIN9 in the transcriptional regulation of mitotic genes in mice (Reichert et al., 2010).

1.2.2.1 LINC target genes in mice

To identify LINC target genes in mice, genome wide microarray analysis of *Lin9* mutant MEFs was performed (Reichert et al., 2010). As suggested from the observed phenotype upon *Lin9* knockout in MEFs, 28 % of downregulated genes could be identified as known players in mitosis and cytokinesis. Beside this, 62 % of downregulated genes were implicated in other functions and the remaining 10 % have not been characterized so far. An overview of genes downregulated more than 1.8-fold is shown in table 1.1.

The top hit of downregulated genes upon *Lin9* depletion was *Gas2l3* (growth arrest specific 2 like 3), belonging to the 10 % of target genes that have not been characterized so far. However, the fact that *Gas2l3* belongs to a family of genes implicated in maintaining growth arrest, the Gas family of genes, attracted attention, since LIN9 has never been linked to growth arrest.

Fold Change	Gene Symbol	Function	Reference
3.19	<i>Gas2l3</i>	uncharacterized	
3.08	<i>Nusap1</i>	mitosis	(Raemaekers et al., 2003) (Ribbeck et al., 2007)
3.00	C230078M08	uncharacterized	
2.78	1190002F15I	uncharacterized	
2.76	<i>C9orf140</i>	other function	
2.68	<i>Aspm</i>	mitosis / cytokinesis	(Kouprina et al., 2005) (Zhong et al., 2005)
2.64	<i>CenpF</i>	mitosis / cytokinesis	(Feng et al., 2006) (Varis et al., 2006)
2.33	E130306D19	uncharacterized	
2.23	<i>Mxd3 (Mad3)</i>	other function	
2.22	<i>Phf19</i>	other function	
2.10	<i>Mki67</i>	other function	
1.94	D17H6S56E-5	uncharacterized	
1.94	<i>Plk1</i>	mitosis / cytokinesis	(Petronczki et al., 2008)
1.94	<i>Tnfaip8l1</i>	other function	
1.91	<i>Cdkn3</i>	other function	
1.89	<i>CenpE</i>	mitosis	(Rao et al., 2009)
1.85	<i>Top2a</i>	mitosis	(Cobb et al., 1999)
1.84	<i>Cdkn2c</i>	other function	
1.83	<i>Kif20a (Mklp2)</i>	mitosis / cytokinesis	(Fontijn et al., 2001) (Neef et al., 2006)
1.81	AK047015	uncharacterized	
1.81	<i>Kif23 (Mklp1)</i>	mitosis / cytokinesis	(Zhu et al., 2005a) (Zhu et al., 2005b)
1.81	<i>CenpA</i>	mitosis	(Torras-Llort et al., 2009) (Kalitsis et al., 2003)

Table 1.1. Genes downregulated upon *Lin9* depletion

Genome wide microarray analysis of *Lin9* knockout MEFs was performed. Listed are all genes downregulated more than 1.8-fold. (Data Reichert et al. 2010)

1.3 The family of growth arrest specific genes

The state of growth arrest, alternatively called G0 or quiescence, is a cell cycle phase characterized by a stop of cell proliferation. Reentry into the cell cycle is positively regulated through the transcriptional activation of growth promoting genes induced by exogenous growth factor signaling. Already in the early 1980s, numerous growth promoting genes have been identified, for example the today well characterized transcription factors c-fos and c-myc (Coughlin et al., 1985; Greenberg and Ziff, 1984). To identify genes that define the G0 phase and do not promote the G0/G1 transition, Schneider et al. performed a screen in murine fibroblasts looking for genes negatively regulated by serum or growth factor addition. The identified set of genes was termed the *Gas* genes (growth arrest specific genes). Transcriptional expression of one gene, the so called *Gas2* gene, was strictly arrest specific irrespective how the quiescence state was induced (Schneider et al., 1988). In humans, following research identified highly homologous genes and all together they represent the GAS2 family.

1.3.1 The GAS2 family

The GAS2 family is composed of the four family members GAS2, GAS2L1 (GAR22), GAS2L2 (GAR17) and GAS2L3. All family members share two highly conserved domains; a putative actin binding calponin homology (CH) domain and a putative microtubule binding growth arrest specific 2 (GAS2/GAR) domain. Proteins having both an actin binding and a microtubule binding domain, are proposed to function as cytoskeletal linker proteins, connecting and coordinating microfilaments and microtubules.

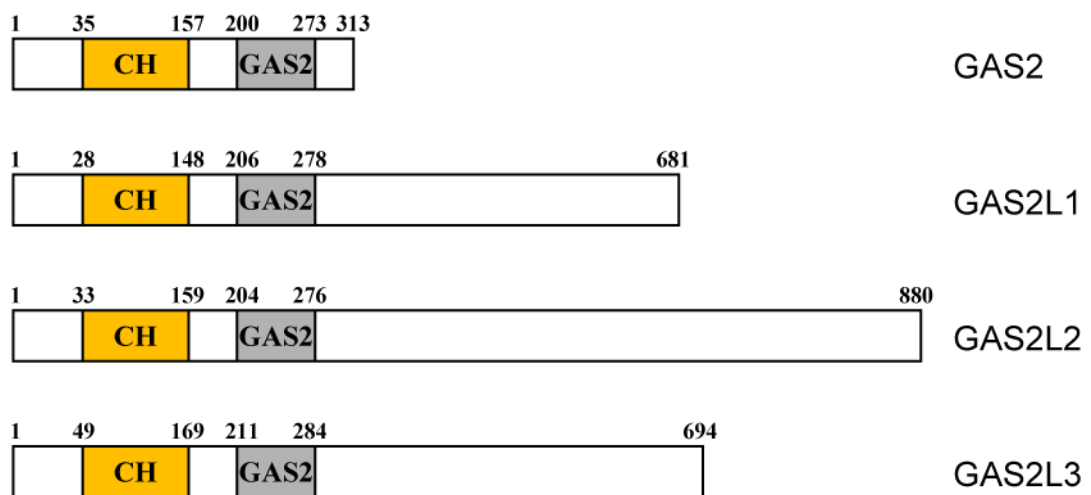


Fig. 1.4. Schematic illustration of the human GAS2 family members

For all proteins the same highly conserved CH and GAS2 domains have been predicted. CH: calponin homology domain; GAS2: growth arrest specific 2 domain

1.3.1.1 The highly conserved CH and GAS2 domains

The calponin homology (CH) domain, a sequence motif of about 120 amino acids originally identified in the protein calponin, has been suggested to confer actin binding to a variety of cytoskeletal and signaling proteins. Detailed analysis of all known CH domain containing proteins led to the classification into three different groups. Firstly proteins containing two tandem repeats of the CH domain, a domain designated as ABD (actin binding domain), secondly proteins containing two ABDs and thirdly, proteins containing only a single amino terminal CH domain (Stradal et al., 1998). Deeper investigation also revealed that single CH domains clearly function differently from ABDs containing two CH domains in tandem. CH domains within an ABD exhibit significant higher affinities for actin, whereas a single CH domain is neither sufficient nor necessary for actin binding (Gimona and Mital, 1998; Gimona and Winder, 1998; Stradal et al., 1998).

The GAS2-related (GAR/GAS2) domain was named after the GAS2 (growth arrest specific 2) protein. Only a few proteins have been found to possess this domain, including

microtubule–actin crosslinking factor (MACF), some members of the plakin family and the GAS2 family members. The GAS2 domain comprises about 57 amino acids and has been shown to bind to microtubules (Sun et al., 2001).

1.3.1.2 GAS2

Beside the fact that the GAS2 expression is highly restricted to growth arrested mouse and human fibroblasts, GAS2 has been shown to colocalize with actin fibers, thus being a component of the microfilament network (Brancolini et al., 1992; Schneider et al., 1988). The GAS2 protein has a quite long half-life time, but hyperphosphorylation of GAS2 upon the induction of the G0/G1 transition seems to be responsible for regulating its activity and specifically correlates with the reorganization of the actin cytoskeleton (Brancolini and Schneider, 1994). GAS2 has also been shown to be a caspase 3 substrate, thereby playing a role in regulating cell shape changes during apoptosis (Brancolini et al., 1995). Additionally, by interaction with m-calpain, GAS2 inhibits calpain-dependent processing of p53 thereby increasing p53 stability and the susceptibility to p53-dependent apoptosis (Benetti et al., 2005; Benetti et al., 2001). Consistent with its role in apoptosis, GAS2 expression and cleavage are induced during mouse embryonic development in the developing mouse limb, a region undergoing extensive apoptosis (Lee et al., 1999).

1.3.1.3 GAS2L1 (GAR22)

The human GAS2-related gene (*GAR22*) is located on chromosome 22q12 and exhibits loss of heterozygosity in many human tumor types (Zucman-Rossi et al., 1996). Alternative splicing of the primary transcript results in two GAS2L1 proteins, the short protein GAS2L1 α (36 kDa) and the longer protein GAS2L1 β (73 kDa) (Zucman-Rossi et al., 1996). Although human and mouse *GAS2L1* mRNAs are expressed nearly ubiquitously, mouse GAS2L1 protein can only be detected in testis and brain. Furthermore, only GAS2L1 β isoform is present in these tissues and the absolute amounts of expressed protein are extremely low. Whether posttranscriptional inhibition of gene expression or enhanced protein degradation account for the apparent lack of GAS2L1 proteins in *Gas2l1* mRNA containing tissues is not known so far (Goriounov et al., 2003). Overexpressed human GAS2L1 β is able to crosslink microtubules and microfilaments, suggesting that endogenous protein may involve integration of these two components of the cytoskeleton (Goriounov et al., 2003).

1.3.1.4 GAS2L2 (GAR17)

The human GAS2-related gene on chromosome 17 (*GAR17*) also encodes for two protein isoforms, GAS2L2 α and GAS2L2 β . Human *GAS2L2* mRNA expression is limited to skeletal

muscle, whereas the β transcript is the predominant mRNA. As well as GAS2L1 β , also the β isoform of GAS2L2 appears to be able to crosslink microtubules and microfilaments in transfected cells (Goriounov et al., 2003).

1.3.1.5 GAS2L3

The LINC target gene *GAS2L3* is located on chromosome 12 in human and chromosome 10 in mouse cells. Human *GAS2L3* mRNA encodes for 2085 bp and the estimated protein size is 75 kDa. An alignment of the human and mouse *GAS2L3* amino acid sequence results in 76 % identity. To date, nothing is known about the biological function or biochemical properties of the *GAS2L3* gene and the corresponding *GAS2L3* protein product.

1.4 Aim of this study

Failure during mitosis and cytokinesis can result in aneuploid cells. To date, the hypothesis that aneuploidy promotes tumorigenesis is widely accepted. Therefore, research on the identification of new mitotic regulators still attracts great attention.

The human LIN complex is a transcriptional activator of a set of G2/M specific genes and therefore essential for proper mitosis and cytokinesis. To identify so far unknown LINC target genes and consequently putative new mitotic regulators, our lab performed genome wide microarray analysis from *Lin9* knockout MEFs. The top hit of downregulated genes upon LIN9 depletion was *Gas2l3*, a member of the family of growth arrest specific 2 genes (Gas2 family). The fact that *Gas2l3* was completely uncharacterized made this gene a useful subject of investigation. Hence, the aim of this thesis was the biochemical as well as biological characterization of *GAS2L3* in the human system.

The biochemical characterization included the investigation of the transcriptional regulation of *GAS2L3* gene expression during the cell cycle. Also the identification of *GAS2L3* localization during the cell cycle was analyzed by immunofluorescence microscopy. To analyze in detail the domains responsible for the specific localization pattern, different *GAS2L3* deletion mutants were cloned. By using protein analytical methods, properties of *GAS2L3* full length protein and *GAS2L3* deletion mutants were monitored.

To analyze if *GAS2L3* has any biological function during the cell cycle, different siRNA approaches were used. For example, cell cycle behavior upon *GAS2L3* depletion was monitored by classical PI FACS analysis. To specifically monitor the fraction of mitotic cells upon *GAS2L3* depletion, pH3 FACS analysis was performed either with or without the induction of mitotic stress by treatment with microtubule poisons. Additionally, nuclei morphology of *GAS2L3* depleted cells was analyzed by microscopic single cell examination.

2 MATERIAL & METHODS

2.1 Materials

2.1.1 Chemical Stocks & Reagents

Unless otherwise indicated, commonly used chemicals were purchased from AppliChem, Roth, Invitrogen, Invivogen or Sigma with analysis quality.

Chemicals	Stock concentration
Ammonium Persulfate (APS)	10 % in H ₂ O
Ampicillin	100 mg/ml in H ₂ O
Blasticidin	10 mg/ml in 10 mM Hepes, pH 7.4
Bovine serum albumin (BSA)	20 mg/ml
dNTPs	2 mM dATP, dCTP, dGTP, dTTP each
DMSO	Ready to use
DTT	1 M in H ₂ O
Ethidium bromide	10 mg/ml in H ₂ O
ImmuMount (Shandon)	Ready to use
Isopropyl- β -D-1-thiogalactopyranoside (IPTG)	1M in H ₂ O
Luminol	250 mM in DMSO
MG132 (proteasome inhibitor)	20 mM in DMSO
Neomycin (G418)	200 mg/ml in H ₂ O
Nocodazole	1mg/ml in DMSO
p-Coumaric acid	90 mM in DMSO
Phalloidin	Ready to use
PMSF (Phenylmethylsulphonyl-fluoride) (Roche)	10 mg/ml in isopropanol
Polybrene (Hexadimethrine bromide)	4 mg/ml in H ₂ O
Ponceau S solution	0.1 % Ponceau S in 5 % acetic acid
Propidium Iodide (PI)	1 mg/ml in H ₂ O
Protease Inhibitor (PI) Mix	0.1 mg/ml Aprotinin 10 mg/ml AEBSF 0.5 mg/ml Bestatin 0.5 mg/ml E64

	1 mg/ml Leupeptin 0.1 mg/ml Pepstatin
Protease Inhibitor Cocktail Sigma	Ready to use
Proteinase K	10 mg/ml in 50 mM Tris-HCl pH 8.0 / 1 mM CaCl ₂
ProtoGel 30 % (Biozym)	Ready to use
Random primer (Roche)	0.5 mg/ml in H ₂ O
RNase A	10 mg/ml in 10 mM Tris-HCl pH 7.4 / 150 mM NaCl
RO-3306 (CDK1 Inhibitor)	10 mM in DMSO
Sodium dodecyl sulfate (SDS)	10 % in H ₂ O
Taxol	10mM in methanol 100 %
Temed 99 %	Ready to use
Trizol /Trifast (total RNA isolation reagent) (Peqlab / Thermo)	Ready to use
Thymidine	200 mM in DMSO

2.1.2 Enzymes

Enzymes	Company
Absolute QPCR SYBR Green Mix	ThermoFisher
Lysozyme (from chicken)	Sigma-Aldrich
M-MLV-RT Transcriptase (200U/μl)	Promega / Thermo Fisher
Phusion High-Fidelity-DNA Polymerase (2U/μl)	Finnzymes
Proteinase K (10 mg/ml)	AppliChem
Restriction Endonucleases	New England Biolabs (NEB), Fermentas
RNase A (10mg/ml)	Sigma-Aldrich®
RiboLock RNase-Inhibitor (40U/μl)	Fermentas
T4-DNA-Ligase (400U/μl)	New England Biolabs (NEB)

2.1.3 Antibiotics

Antibiotic	Stock concentration	Final concentration	Use for Cell line:
Ampicillin	100 mg/ml	100 μg/ml in LB-Medium	DH5α (E-coli)
Neomycin	200 mg/ml	400 μg/ml in DMEM	BJ-ET Eco ^R Neo
Blasticidin	10 mg/ml	5 μg/ml in DMEM	BJ-ET shGas2l3

2.1.4 Buffers

2.1.4.1 General buffers

<u>5X DNA Loading Buffer</u>	15 % Ficoll 0.05 % Bromphenol blue 0.05 % Xylene Cyanol 0.05 M EDTA in 1X TAE
<u>2X HBS</u>	280 mM NaCl 1.5 mM Na ₂ HPO ₄ 50 mM HEPES-KOH, pH 7.05
<u>Luria Bertani (LB) Agar</u>	40 g powder in 1 l H ₂ O, autoclave
<u>Luria Bertani (LB) Medium</u>	25 g powder in 1 l H ₂ O, autoclave
<u>Miniprep-Solution S1</u>	25 mM Tris-HCl pH 8.0 10 mM EDTA
<u>Miniprep-Solution S2</u>	200 mM NaOH 1 % SDS
<u>Miniprep-Solution S3</u>	29.44 g potassium acetate 11.5 ml acetic acid 28.5 ml H ₂ O
<u>Phosphate buffered saline (PBS) (1x)</u>	13.7 mM NaCl 0.3 mM KCl 0.64 mM Na ₂ HPO ₄ 0.15 mM KH ₂ PO ₄ adjust pH to 7.4 with HCl
<u>TAE buffer (1X)</u>	40 mM Tris base 5 mM glacial acetic acid 10 mM EDTA, pH 8.0
<u>TBS (1X)</u>	50 mM Tris-HCl, pH 7.4 150 mM NaCl
<u>TE</u>	10 mM Tris-HCl, pH 7.5 1 mM EDTA

2.1.4.2 Buffers for whole protein lysates

<u>TNN buffer</u>	50 mM Tris-HCl, pH 7.5 120 mM NaCl 5 mM EDTA 0.5 % NP-40 10 mM Na ₄ P ₂ O ₇ 2 mM Na ₃ VO ₄ 100 mM NaF ad 500 ml H ₂ O PI 1:100 / 1:1000 Sigma (add freshly) PMSF 1:200 (add freshly)
<u>Bradford Solution</u>	50 mg Coomassie Brilliant Blue G250 23.75 ml Ethanol 50 ml 85 % (v/v) ortho-phosphoric acid ad 500 ml H ₂ O filter twice

2.1.4.3 Buffers for immunoprecipitation and immunoblot

<u>Coomassie blue stain</u>	250 ml methanol 35 ml acetic acid 1 g Coomassie blue R-250 ad 500 ml H ₂ O
<u>Coomassie destain</u>	250 ml methanol 35 ml acetic acid ad 500 ml H ₂ O
<u>Acrylamidbuffer for SDS-Gels</u>	30 % (w/v) Acrylamide 0.8 % (w/v) N,N'-Methylenbisacrylamide
<u>Blotting buffer (1x)</u>	0.6 g Tris base 2.258 g Glycine 150 ml Methanol ad 1 l H ₂ O
<u>Blocking solution</u>	5 % (w/v) milk powder in TBST
<u>3X Electrophoresis Sample Buffer (3X ESB)</u>	300 mM Tris-HCl pH 6.8 15 mM EDTA 150 mM DTT 12 % (w/v) SDS 15 % (w/v) glycerol 0.03 % (w/v) bromphenol blue

<u>Ponceau S</u>	0.1 % Ponceau S 5 % glacial acetic acid
<u>TBS (1x)</u>	50 mM Tris-HCl pH 7.4 150 mM NaCl
<u>TBST</u>	0.05 % Tween in 1x TBS
<u>Substrate Solution</u>	10 ml 100 mM Tris-HCl pH 8.5 50 µl 250 mM Luminol 22 µl 90 mM p-coumaric acid 3 µl 30 % H ₂ O ₂

2.1.4.4 Buffers for inclusion body purification

<u>Lysis Buffer</u>	50 mM Tris-HCl pH 8.0 0.25 % (w/v) Sucrose 1mM EDTA pH 8.0
<u>Detergent Buffer</u>	20mM Tris-Cl pH 7.5 2 mM EDTA pH 8.0 200mM NaCl 1 % (w/v) deoxycholic acid 1 % (v/v) Nonidet P-40
<u>Washing Buffer</u>	0.5 % Triton X-100 1mM EDTA pH 8.0

2.1.4.5 Buffers for flow cytometry (FACS)

<u>Sodium Citrate</u>	38 mM in H ₂ O
<u>1x Binding Buffer</u>	10 mM HEPES, pH 7.4 0.14 M NaCl 2.5 mM CaCl ₂
<u>Incubation Buffer</u>	0,5 g BSA ad 100 ml 1x PBS

2.1.4.6 Buffers for immunofluorescence

<u>PSP</u>	15 g paraformaldehyde 10 g sucrose ad 500 ml 1x PBS, store at -20 °C
------------	--

<u>Mes Buffer</u>	100 mM MeS pH 6.9 1mM EGTA 1 mM MgCl ₂ ad 100 ml H ₂ O, store at 4 °C
<u>Methanol Fixative</u>	10 ml Mes Buffer 90 ml methanol, store at -20 °C
<u>10 % TCA</u>	10 g Trichloroacetic acid (TCA) in 100 ml PBS, store at 4 °C
<u>PBST</u>	0.5 ml triton 100 % 500 ml PBS, store at 4 °C
<u>Blocking Solution</u>	5 g BSA in 100 ml PBS, store at 4 °C or 10 ml FCS / 1 g Albumin ad 100 ml PBS, store at 4°C or 5 % goat serum in PBST, fresh made

2.1.5 Antibodies

2.1.5.1 Primary antibodies

Internal Number	Antibody against	Company	Origin	Application and Dilution	
# 99	GFP	Santa Cruz SC-9996	mouse monoclonal	IP	1:100
				WB	1:1000
# 158	A-tubulin	Sigma Aldrich T 6074	mouse monoclonal	WB	1:2500
				IF	1:100
# 196	B-actin	Santa Cruz	mouse monoclonal	WB	1:10000
# 194	Aurora B	Abcam® ab 2254	rabbit polyclonal	WB	1:1000
				IF	1:500
# 171	RhoA	Santa Cruz SC-418	mouse monoclonal	IF	1:100
# 115	Survivin	Novus (Acris) NB-500-201217	rabbit polyclonal	IF	1:100
# 193	GAS2L3	self made by Immunoglobe	rabbit polyclonal	WB	1:1000
# 195	GAS2L3	Abnova	mouse monoclonal	IP	1:50
				WB	1:250
				IF	1:50

# 40	Cyclin B1	Santa Cruz SC-245	mouse monoclonal	WB	1:1000
# 199	Securin	Pds-1 K0090-3	rabbit polyclonal	WB	1:100
# 203	MAD2	Covance	rabbit polyclonal	IF	1:100
# 198	MAD2	Bethyl Laboratories	rabbit polyclonal	WB	1:500
# 197	CDC20 (p55)	Santa Cruz	mouse monoclonal	IP	1:100
				WB	1:1000
# 205	BUBR1	requested from Stephen Taylor	sheep polyclonal	WB	1:1000
				IF	1:100
# 92	HA	Covance HA.11	mouse monoclonal	IF	1:100
# 90	HA	Santa Cruz SC-805	rabbit polyclonal	IF	1:100
# 206	phospho histone H3	Cell Signaling #9708	mouse monoclonal	FACS	1:10

2.1.5.2 Secondary antibodies

Antibody	Company	Application and dilution
anti-mouse HRP linked	GE-Healthcare	WB 1:5000
anti-protein A HRP linked	GE-Healthcare	WB 1:5000
anti-mouse Alexa 488	Invitrogen	IF 1:500
anti-mouse Alexa 594	Invitrogen	IF 1:500
anti-rabbit Alexa 594	Invitrogen	IF 1:500
anti-sheep Alexa 594	Invitrogen	IF 1:500
Phalloidin (Alexa 594 linked)	Invitrogen	IF 1:40

2.1.6 Plasmids

2.1.6.1 Plasmids for overexpression

Unless otherwise indicated, all plasmids encode for human sequences.

Internal number	Plasmid name	Description
# 170	pCDNA3-EGFP	vector backbone for cloning
# 174	pEGFP-N1	EGFP overexpression control
# 212	pCDNA3-HA	empty vector control for overexpression
# 1019	pCDNA3-HA-mouse Gas2l3	mammalian overexpression
#1033	pCDNA3-GFP-Gas2l3	mammalian overexpression
#1056	pCDNA3-GFP-Gas2l3 DelMut 3	mammalian overexpression
#1057	pCDNA3-GFP-Gas2l3 DelMut 4	mammalian overexpression
#1064	pCDNA3-GFP-Gas2l3 DelMut 1	mammalian overexpression
#1065	pCDNA3-GFP-Gas2l3 DelMut2	mammalian overexpression
#1068	pCDNA3-GFP-Gas2l3 DelMut 5	mammalian overexpression

2.1.6.2 Plasmids for recombinant proteins

Internal number	Plasmid name	Description
# 397	pGEX-4T2-GST	Recombinant expression of GST
# 1067	pGEX-4T2-GST Gas2l3 DelMut 2	Recombinant expression of GST-Gas2l3 DelMut 2

2.1.6.3 Plasmids for retroviral knock down

Internal number	Plasmid name	Description
# 746	pMSCV-H2B GFP	GFP control for knock down constructs
# 652	pMSCV-Blastcidin	empty vector control for knock down constructs

#1100 pMSCV-shGas2l3 #2 Blastcidin Retroviral expression vector for shGas2l3

2.1.7 Primers

Primer oligonucleotids were synthesized by Metabion International AG, Martinsried. Unless otherwise indicated, all primers were intended for human sequences.

2.1.7.1 Primers for cloning

Primer number	Sequence	Application	
SG 1075	<u>GCGGATCC</u> ATGCAGCCTGCAATTCAAGTATGGTTTG	hGas2l3	sense
SG 1076	GCT <u>CTAGAG</u> AGTATGTATTTATTTTCTAGGTTTCTTAC TTCCAG	hGas2l3	antisense
SG 1106	<u>GCGGATCC</u> AGATACGGGGTTGAGCCACCAG	DelMut1	sense
SG 1076	GCT <u>CTAGAG</u> AGTATGTATTTATTTTCTAGGTTTCTTAC TTCCAG	DelMut1	antisense
SG 1107	<u>GCGGATCC</u> AGTGTACCTGATTCGCCTGCCAG	DelMut2	sense
SG 1076	GCT <u>CTAGAG</u> AGTATGTATTTATTTTCTAGGTTTCTTAC TTCCAG	DelMut2	antisense
SG 1075	<u>GCGGATCC</u> ATGCAGCCTGCAATTCAAGTATGGTTTG	DelMut3	sense
SG 1108	GCT <u>CTAGACT</u> ATGGTGGCTCAACCCCGTATCT	DelMut3	antisense
SG 1075	<u>GCGGATCC</u> ATGCAGCCTGCAATTCAAGTATGGTTTG	DelMut4	sense
SG 1109	GCT <u>CTAGACT</u> ACTGGCAGGCGAATCAGGTACT	DelMut4	antisense
SG 1106	<u>GCGGATCC</u> AGATACGGGGTTGAGCCACCAG	DelMut5	sense
SG 1109	GCT <u>CTAGACT</u> ACTGGCAGGCGAATCAGGTACT	DelMut5	antisense
SG 1102	<u>GCCTCGAGG</u> AGTATGTATTTATTTTCTAGGTTTCTTAC TTCCAG	Delmut2	antisense

Restriction sites (BamHI GGATCC / XbaI TCTAGA / XhoI CTCGAG) are underlined. Primer stock solution was 100 pmol/μl in TE-buffer. Primer working solution was 10pmol/μl in ddH₂O.

2.1.7.2 Primer for shRNA design

Primers for shRNA design were HPLC purified.

Primer number	Sequence	Appli-cation	
SG 1155	gatcccCTATGTCAGTCCGTTCTAAttcaagagaTTAGAACGG ACTGACATAGtttta	shGas2l3	sense
SG 1156	agcttaaaaaCTATGTCAGTCCGTTCTAAtctcttgaaTTAGAAC GGACTGACATAGgg	shGas2l3	anti-sense

2.1.7.3 Primers for quantitative RT-PCR

Primer number	Sequence	Application	
SG 645	GCCCAATACGACCAAATCC	GAPDH	sense
SG 646	AGCCACATCGCTCAGACAC		antisense
SG 580	CCCCACCACGGTTACATTAT	Lin9	sense
SG 581	CGGCGACTGTCCTAATAAAGG		antisense
SG 787	GCCACATCAGCCAGTAGCTC	Lin54	sense
SG 788	TAACAACCACTGGCTTTGCTT		antisense
SG 690	TTGCTTGTA ACTACTGATCTTGAGC	Mad2	sense
SG 691	TTCTGAACTGAACACTTGTATAACCA		antisense
SG 1058	GCTGTCGGCATGAAGAGC	Gas2l3	sense
SG 1059	AATCGATGAGAACA ACTACAAGGA		antisense
SG 1098	CATTACCTGGACAAGCACGA	Gas2l1	sense
SG 1099	GTGGAGAAAAGGTGCAGACC		antisense
SG 1100	GGTGACTCCAACACCCTCAT	Gas2l2	sense
SG 1101	CCAGGTAATGGCCCAGTG		antisense
SG 1096	AAGAAGATCTGGCCTTGTGG	Gas2	sense
SG 1097	CAACTTCTCCATAAAAGTTTCTGCT		antisense

2.1.8 siRNA sequences

Unless otherwise indicated, siRNA Oligos were purchased from MWG or Dharmacon.

siRNA against	Sequence 5' to 3'	Target
ctrl.	UAGCGACUAAACACAUCAA	non trageting
Gas2l3 #1	GGGAUACUCUUCAAGGAUUTT	new designed
Gas2l3 #2	CUAUGUCAGUCCGUUCUAA	new designed
Gas2l3 #3	CAUUAAAUCCAGUAGGUAAT	new designed
Lin9 #4	GGAAGAGAGAUCAGCAUUAAU	Schmit et al. 2007
Lin54 #3	GCAAGCAACUCUACCUUUA	Schmit et al 2007

2.1.9 Cell lines / Cell culture media / Transfection reagents

DMEM (4.5 g Glucose/L-Glutamine)	Gibco®, Invitrogen
Penicillin/Streptomycin (10 U/µl each)	Cambrex / Lonza
Trypsin (EDTA) (200 mg/l)	Gibco®, Invitrogen
Foetal Bovine Serum (FCS)	Gibco®, Invitrogen
Serum Supreme	Cambrex
HeLa	DMEM 10 % FCS / 1 % PenStrep
BJ-ET	DMEM 10 % FCS / 1 % PenStrep
BJ-ET Eco ^R Neo	DMEM 10 % FCS / 1 % PenStrep / Neomycin
T98G	DMEM 10 % FCS / 1 % PenStrep
HCT 116	DMEM 10 % FCS / 1 % PenStrep
Phoenix	DMEM 10 % Serum Supreme / 1 % PenStrep
HeLa / T98G	Lipofectamine (Invitrogen)
BJ-ET	Metafecten Pro (Biontex)
Phoenix / HeLa	Calcium Phosphate

2.1.10 Markers

1 Kb DNA Ladder	Fermentas
SDS Page Ruler Mix	Fermentas

2.1.11 Kits

Jetstar Gel Extraction Kit	Genomed
Jetstar Plasmid Purification Midi/Maxi Kit	Genomed
Plasmid Mini/Midi/Maxi Kit	Promega / Invitrogen
QIAquick PCR Purification Kit	Qiagen
Absolute QPCR SYBR Green Mix	Thermo Fisher

2.1.12 Beads

Protein A Sepharose (Pierce)
Protein G Sepharose (Pierce)
Glutathione Sepharose (Amersham)

2.2 Methods

2.2.1 Cell culture

2.2.1.1 Passageing of cells

Eukaryotic cells were cultivated in a tissue culture incubator at 37 °C and with 5 % carbon dioxide (CO₂). For passageing, cells were washed once with PBS and incubated with Trypsin/EDTA for a few minutes at 37 °C. The detached cells were plated on new culture dishes.

2.2.1.2 Freezing of cells

To freeze cells, cells on 10 cm dishes were trypsinized and transferred into a 15 ml falcon with 10 ml fresh media. Next, they were centrifuged for 3 min at 1000 rpm, the supernatant was discarded and 1 ml ice cold freeze medium (DMEM media containing 10 % DMSO) was added. Pellets were resuspended and transferred into cooled cryotubes. Cells were stored at -80 °C for short term or in liquid nitrogen for long term.

2.2.1.3 Thawing of cells

Cells were quickly thawed in a 37 °C water bath. The cell suspension was mixed with 10 ml fresh medium and centrifuged for 3 min at 1000 rpm. The supernatant was discarded and pellets were resuspended in 10 ml fresh medium and seeded into 10 cm dishes.

2.2.1.4 Counting of cells

Cell counting was performed using a Neubauer Chamber. The number of cells per ml in suspension was calculated using the following formula:

$$\text{Cells/ml} = (\text{Cells counted} / \text{number of counted large squares}) \times 10^4$$

2.2.1.5 Transient transfection

2.2.1.5.1 Calcium phosphate transfection

HeLa and Phoenix cells were transfected using calcium phosphate. 15-30 µg of plasmid DNA was mixed with 50 µl of 2.5 M CaCl₂ and with H₂O to a final amount of 500 µl. 500 µl of 2x HBS

were continuously bubbled while DNA/CaCl₂ mixture was added drop wise. This solution was slowly added to the cells. After 14 – 18 h incubation, cells were washed with PBS and fed with fresh medium. Cells were harvested after 48 h post transfection for the desired procedure.

2.2.1.5.2 Lipofectamine / Metafectene transfection

T98G and HeLa cells were transfected with Lipofectamine 2000 (Invitrogen), HCT 116 and BJ-ET cells were transfected with Metafectene Pro (Biontix), according to the manufacturer's instructions.

2.2.1.6 Infection of BJ-ET cells

For the production of ecotrophic virus supernatants, Phoenix cells carrying the ecotrophic receptor were transiently transfected with the plasmid of interest using calcium phosphate (s. 2.2.1.5.1). 48 h after transfection, the virus supernatants were harvested and used immediately or were frozen in liquid nitrogen and stored at -80 °C.

BJ-ET cells were splitted 1:4 the day before infection. For the infection, the viral supernatant was mixed with 8 µg/ml polybrene, filtered (0.45 µm) and added to the cells. 14 – 18 h after infection, the cells were fed with fresh medium and selection was started 48h after infection.

2.2.1.7 Growth curve of BJ-ET cells

1x10⁵ of the infected and selected BJ-ET cells were plated on a 6-well-plate in triplicates. Every 4 days, cells were counted and 1x10⁵ cells replated. Mean values of the cumulative cell numbers were plotted against the time.

2.2.1.8 Synchronization of T98G cells by serum starvation

For synchronization in G₀, 60 % confluent T98G cells were washed twice with PBS and fed with DMEM without FCS for 72 h. Release into the cell cycle was achieved by adding 20 % FCS.

2.2.1.9 Synchronization of HeLa cells by thymidine

For synchronization at the G₁/S border, 60 % confluent HeLa cells were treated with 2.5 mM thymidine for 24 h. Afterwards cells were released into the cell cycle by washing twice with PBS and adding 10 % FCS medium.

2.2.1.10 Cell treatment with different reagents

To block asynchronously HeLa cells in metaphase, 150 ng/ml nocodazole or 33 nM taxol were directly added into fresh cell medium after siRNA transfection (s. 2.2.1.5.2). When cells were additionally synchronized by thymidine at the G1/S border (s. 2.2.1.9), 33 nM taxol was added into the medium directly after the cell cycle release.

For protein stabilization assays, calcium phosphate transfected HeLa cells (s. 2.2.1.5.1) were incubated for 7 – 10 h with 20 μ M MG132 40 h post transfection.

2.2.1.11 Determination of cell cycle phases by flow cytometry

For flow cytometry (FACS) measurement, cells were harvested by trypsinization, washed with cold PBS and fixed with 1 ml ice cold 80 % ethanol. After fixation at -20 °C for at least one night, cells were again washed with cold PBS and the cell pellet was resuspended in 500 μ l 38 mM NaCitrate and 25 μ l RNase A [10 mg/ml]. Cells were incubated for 1-2 h at 37 °C and stained with 30 μ l propidium iodide (PI) [1 mg/ml] directly before FACS measurement.

In order to determine the fraction of cells in early M phase, cells were stained with propidium iodide and an antibody specific for phosphorylated histone H3 at serine10 (phospho H3). Cells were harvested by trypsinization, washed in PBS and fixed in 2 % paraformaldehyde in PBS for 10 min at 37 °C. After 1 min on ice, cells were permeabilized for 30 min at 4 °C by adding 90 % ice cold methanol and afterwards stored at -20 °C over night. 5×10^5 cells were washed with 3 ml incubation buffer, resuspended in 90 μ l incubation buffer and blocked for 10 min at room temperature (RT). By addition of 10 μ l phospho H3 antibody the cells were stained for 1.5 – 2 h at RT in the dark. After a second washing step with incubation buffer, cells were incubated with 50 μ g/ml PI and 0.7 mg/ml RNaseA for 30 min at 37°C and analyzed by FACS to determine the fraction of phosphorylated histone H3 positive cells.

2.2.1.12 Immunofluorescence

For immunofluorescence studies, cells were plated on coverslips in 6-well plates, fixed with an adequate fixative and stained by direct or indirect immunofluorescence.

2.2.1.12.1 PSP fixation

For PSP fixation, cells plated on coverslips were washed once with PBS followed by fixation in 1.5 ml prewarmed PSP for 10 min at RT. After washing for 5 min with PBS, cells were

permeabilized in 2 ml PBS / 0,2 % triton for 5 min at RT. Cells were washed again twice in PBS / 0,1 % triton (PBST) before used for further staining procedure.

2.2.1.12.2 PSP / 0.3 % triton fixation

For PSP fixation with 0.3 % triton, cells plated on coverslips were washed once with PBS followed by fixation in 1.5 ml prewarmed PSP and additional 0.3 % triton for 10 min at RT. After washing for 5 min with PBS, cells were permeabilized in 2 ml PBS / 0,2 % triton for 5 min at RT. Cells were washed again twice in PBS / 0,1 % triton (PBST) before used for further staining procedure.

2.2.1.12.3 MesMetOh fixation

For MesMetOH fixation, cells plated on coverslips were washed once with PBS followed by fixation in 1.5 ml ice cold methanol fixative for 5 min at RT. Before further staining procedure, cells were thoroughly washed for 3 times in PBS.

2.2.1.12.4 TCA fixation

For TCA fixation, cells plated on coverslips were directly fixed in 1.5 ml ice cold 10 % TCA for 15 min at RT. After washing for 5 min with PBS, cells were permeabilized in 2 ml PBS / 0,2 % triton for 5 min at RT. Cells were washed again twice in PBS / 0,1 % triton (PBST) before used for further staining procedure.

2.2.1.12.5 Indirect immunofluorescence (standard procedure)

For indirect immunofluorescence staining, fixed cells were first incubated in blocking solution for minimal 20 min to avoid unspecific binding of the antibodies. After blocking, cells on cover slips were directly transferred to a dark humid chamber and incubated with 80 µl diluted primary antibody (standard dilution 1:100 in PBS) for 1 h at RT. Afterwards, the cover slips were washed 3 times with PBST and incubated with 75 µl of the appropriate fluorescence labelled secondary antibody (standard dilution 1:500 in PBS) and bisbenzamide (1:5000 in PBS) for nuclei staining. After 30 min incubation, cells were thoroughly washed with PBS and mounted with ImmuMount.

2.2.1.12.6 Direct immunofluorescence of actin filaments

For staining of actin filaments, direct immunofluorescence with fluorescence labelled phalloidin was performed. Cells were first fixed with PSP (s. 2.2.1.12.1), washed twice with PBS for 5 min and then incubated in blocking solution for 20 min at RT to minimize unspecific staining. Afterwards, cells were incubated with 80 µl diluted fluorescence labelled phalloidin (1:40 in PBS) for 30 min at RT in a dark humid chamber. Cells were washed 3 times for 5 min in PBST

following nuclei staining with bisbenzamide 1:2500 in PBS for 1 min at RT. Finally, cells were thoroughly washed with PBS and mounted with ImmuMount.

2.2.1.12.7 Fixation method for specific immunofluorescence stainings

Staining	Fixation Method
EGFP-GAS2L3	PSP + /- 0.3 % triton
endogenous GAS2L3	PSP + /- 0.3 % triton
A-tubulin	PSP + /- 0.3 % triton / MesMetOH
Aurora B	PSP + /- 0.3 % triton
Survivin	PSP + /- 0.3 % triton
RhoA	10 % TCA
MAD2	PSP + 0.3 % triton
BUBR1	PSP + 0.3 % triton
Actin filaments with Phalloidin	PSP - 0.3 % triton

2.2.2 Expression analysis

2.2.2.1 RNA isolation

Total RNA was isolated from cell culture cells by using the RNA isolation reagent Trifast from Peqlab. After removing the medium, 1 ml Trifast was added onto the cell culture plate and cells were scraped into a reaction tube. After 5 min incubation, 200 µl chloroform was added and thoroughly vortexed for 15 sec. The tubes were centrifuged at 11400 rpm and 4 °C for 10 minutes and the upper aqueous phase was transferred to a new reaction tube. RNA was precipitated with 500 µl isopropanol at RT for 10 minutes and centrifuged for 10 minutes at 11400 rpm and 4 °C. The pellet was washed with 80 % ethanol and resuspended with 25 -40 µl RNase free water.

2.2.2.2 Reverse transcription

To transcribe RNA into cDNA, 2.5 µg RNA were mixed with 0.5 µl random primer [0.5 µg/µl] and brought to 10 µl with water. After incubation at 70 °C for 5 min, the samples were left for 1 min at 4 °C and then mixed with 5 µl M-MLV 5 x reaction buffer, 6.25 µl dNTPs [2mM], 0.5 µl Ribolock RNase inhibitor [40 U/µl], 0.5 µl M-MLV-RT [200U] and 2.75 µl H₂O. For cDNA synthesis, the samples were incubated at 37 °C for 60 min and then inactivated for 15 min at 70 °C.

2.2.2.3 Quantitative real-time PCR (qRT-PCR)

To determine the amount of a specific mRNA compared to a housekeeping gene, the following reaction was prepared:

Standard reaction mix:

12.5 μ l absolute qRT-PCR Sybr Green Mix
 10.5 μ l H₂O
 1 μ l fw / rev primer mix (10 pmol/ μ l each)
 1 μ l cDNA

Standard PCR program (40 cycles):

95 °C 15 min
 95 °C 15 s
 60 °C 1 min

The relative expression of a gene compared to a housekeeping gene was calculated with this formula:

$$2^{-\Delta\Delta Ct}$$

with $\Delta\Delta Ct = \Delta Ct$ (sample) – ΔCt (reference)

and $\Delta Ct = Ct$ (gene of interest) – Ct (housekeeping gene)

The standard deviation of $\Delta\Delta Ct$ was calculated with:

$$s = \sqrt{(s_1^2 + s_2^2)}$$

with s_1 = standard deviation (gene of interest)

and s_2 = standard deviation (housekeeping gene)

The margin of error for $2^{-\Delta\Delta Ct}$ was determined by this formula:

$$2^{-\Delta\Delta Ct \pm s}$$

and the error used for the error bars was calculated with:

$$2^{-\Delta\Delta Ct + s} - 2^{-\Delta\Delta Ct - s}$$

2.2.3 Biochemical methods

2.2.3.1 Whole cell lysates

HeLa cells were scraped with cold PBS and centrifuged for 5 min at 3000 rpm and 4 °C. The pellet was resuspended with 10 times its amount of TNN buffer (with freshly added PI [1:100 / 1:1000 Sigma] and PMSF [1:200]) by vortexing and incubation on ice for at least 20 min. The lysates were spun at 14000 rpm for 10 min at 4 °C to remove the cell debris. The

supernatant was transferred in a new reaction tube and immediately used for immunoprecipitation or boiled in 3x ESB for 5 minutes and frozen at -20 °C.

2.2.3.2 Determination of protein concentration (Bradford)

The protein concentration was determined with the method described by Bradford (Bradford, 1976). 1 µl of whole cell lysate was mixed with 100 µl 0.15 M NaCl and 1 ml of Bradford solution. Extinction at 595 nm was measured and compared to a standard BSA dilution series.

2.2.3.3 Immunoprecipitation

For immunoprecipitation, between 0.5 and 1 mg of whole cell lysate was incubated for 4 hours or overnight with the desired antibodies on a rotating wheel at 4 °C. 40 µl of protein A- (polyclonal antibodies) or protein G-sepharose (monoclonal antibodies) were added and left incubated for additional 1 h at 4 °C on the rotating wheel. The beads were washed 5 times with TNN and spinned in between for 1 minute at 3000 rpm and 4 °C. After the last wash, the supernatant was removed completely with a Hamilton syringe and the beads were resuspended in 40 µl 3x ESB and boiled for 5 minutes at 95 °C. Samples were stored at -20°C or directly used for electrophoresis.

In parallel, 20 % of the protein amount used for immunoprecipitation was boiled with 3 x ESB at 95 °C for 5 min and used as input samples.

2.2.3.4 SDS polyacrylamide gel electrophoresis (SDS-PAGE)

SDS-PAGE analysis was performed using the discontinuous method (Laemmli, 1970). A 8 - 14 % separating gel was prepared and after polymerization, the stacking gel was poured on the top. The gels were prepared as follows:

Separating gel (10 %)

6.1 ml H₂O
3.7 ml 1.5 M Tris pH 8.8
5 ml Acrylamid/Bisacrylamid
75 µl 20 % SDS
100 µl 10 % APS
20 µl TEMED

Stacking gel

6.9 ml H₂O
1.4 ml 0.5 M Tris pH 6.8
1.6 ml Acrylamid/Bisacrylamid
50 µl 20 % SDS
50 µl 10 % APS
20 µl TEMED

Electrophoresis was carried out in 1X SDS running buffer for about 1 h at 35 mA/gel. The gels were either used for immunoblotting or stained for 30 minutes with Coomassie blue to visualize the proteins.

2.2.3.5 Immunoblotting

The transfer of proteins onto PVDF membranes was done via electroblotting using a BioRad Wet Blot gadget. The PVDF membrane was preincubated for 1 min with 100 % methanol and rinsed with blotting buffer. The membrane was laid onto a layer of Whatman filter paper and the SDS-polyacrylamide gel was placed on the membrane, followed by a second layer of filter paper. This “sandwich” was clasped on both sides by sponges and placed in a cooled wet blotting tank (Biorad). The transfer occurred for 60 min at 300 mA in 1X Blotting Buffer. Successful and equal transfer of proteins was visualized by staining of the membrane with a Ponceau S solution and destaining with H₂O.

To detect specific proteins with their respective antibodies, the membranes were blocked with 3 % milk powder in TBST (Blocking solution) for 2 - 4 h, and then incubated overnight at 4°C with the primary antibody diluted in blocking solution. Afterwards, the membrane was washed 3 times for 10 min in TBST and incubated with the secondary HRP-conjugated antibody for 1 h at RT. After 3 wash steps of 10 min in TBST, specific bands were detected using a Luminol-substrate-solution. The membrane was wrapped in plastic foil and exposed to an ECL-film.

2.2.3.6 Purification of inclusion bodies from recombinant bacteria for antibody production

Chemocompetent bacteria were transformed with the desired GST construct with heat-shock (s. 2.2.4.4.6).

50 ml over night culture of one single bacterial colony was diluted 1:10 in LB media and grown for 1 h at 37 °C. Then the recombinant protein expression was induced for 4 h with 1 mM IPTG. For fusion protein recovery, bacterial cultures were pelleted by centrifugation at 4000 rpm for 10 minutes at 4 °C and pellets resuspended in 30 ml ice cold lysis buffer. To completely lyse the bacteria, additional 7 ml lysis buffer together with 70 mg lysozyme was added to the bacteria and incubated for 30 min on ice followed by sonification (10 times for 30 seconds, 50 % intensity). After adding 70 ml detergent buffer, lysates were centrifuged 10 min for 7000 rpm at 4 °C. Afterwards the slightly orange supernatant was carefully removed and the remaining pellet was resuspended in 85 ml washing buffer followed by centrifugation for 10 min at 7000 rpm at 4°C. Washing was repeated as long as a tight pellet was obtained. This pellet was finally

washed with 85 ml 70 % ethanol and resuspended in a small volume of sterile PBS followed by sonification until a clear white suspension was obtained.

For estimation of protein concentration, an aliquot was boiled in 3x ESB and loaded onto a SDS-polyacrylamide gel. Proteins were visualized by Coomassie blue stain.

For antibody production, aliquots with 0.25 – 1 mg protein / 250 µl were frozen at -20°C and collected from immunoGlobe (Antikörpertechnik GmbH) for rabbit injection.

2.2.4 Molecular biology

2.2.4.1 Isolation of plasmid DNA from bacteria

2.2.4.1.1 Mini preparation

Single colonies were picked from an LB agar plate after transformation and incubated in 4 ml LB medium containing ampicillin over night in a shaker at 37 °C. 1.5 ml bacterial solution was pelleted and resuspended in 300 µl S1. The bacteria were lysed by adding 300 µl S2 for 5 minutes. This reaction was neutralized with 300 µl S3. The bacterial debris were pelleted for 10 minutes at full speed and plasmid DNA in the supernatant was precipitated with 700 µl isopropanol. After centrifugation for 60 minutes at room temperature, the pellet was washed with 1 ml 70 % ethanol. The pellet was air dried and resuspended in 30 µl H₂O. Correct bacterial clones were identified by restriction (s. 2.2.4.4.4).

2.2.4.1.2 Midi and Maxi preparation

A single colony was picked from a LB agar plate after transformation and cultured in 4 ml LB medium containing ampicillin at 37 °C for 4 - 8 h. This culture was transferred into either 50 – 100 ml (Midi preparation) or 200 – 400 ml (Maxi preparation) LB medium containing ampicillin and left growing over night in a shaker at 37 °C. Plasmids were purified with Midi- or Maxi-Kits from Genomed, Qiagen, Promega or Invitrogen according to the manufacturer's instructions.

2.2.4.2 Isolation of plasmid DNA fragments from agarose gels

Plasmid DNA was digested with the desired restriction enzymes and incubated at 37 °C for more than 2 h. The restriction was loaded on a 0.8 – 1.4 % agarose gel and fragments were separated by electrophoresis at 100 – 130 V for 1 h. The desired bands were cut out and isolated with the JetStar gel extraction kit (Genomed) according to the manufacturer's instructions.

2.2.4.3 Isolation of PCR products after restriction

To purify PCR products after restriction, the QIAquick PCR purification kit from Qiagen was used according to the manufacturer's protocol.

2.2.4.4 Standard cloning methods

2.2.4.4.1 *Primer design*

The use of perfect designed primers is essential for the specific amplification of the desired DNA. Optimal primers have a CG content of 50-60 % and a melting temperature higher than 54°C to ensure highly specific amplification products. A "C" or "G" at the 3'-end can result in an improved binding and elongation. Of course the primer sequences should be highly specific for the amplified product and the primer should not build up any secondary structures like hairpins. Furthermore both primers should not be able to interact with each other, as well as a primer should not be able to interact with itself.

Primers for cloning a DNA fragment additionally contained the desired restriction enzyme site. To calculate the melting temperature of new designed primers, the "Oligo Calculator" from the Dana-Farber Cancer Institute was used. Primer specificity was analyzed with the help of "Basic Local Alignment Search Tool" (BLAST) on NCBI.

2.2.4.4.2 *PCR for cloning of DNA fragments*

To amplify DNA fragments for cloning, the Phusion™ High Fidelity polymerase (Finnzymes) was used, which is a special proof reading polymerase and has a 3' - 5' proof reading / exonuclease activity.

Standard reaction mix:

template DNA	2-5 µl
Polymerase buffer	10 µl
Phusion polymerase	0,5 µl
dNTPs (2mM)	5 µl
primer fw (10µM)	3 µl
primer rev (10µM)	3 µl
ddH ₂ O	add to 50 µl

Standard PCR conditions:

1) initial denaturation	30 sec,	98 °C
2) denaturation	10 sec,	98 °C
3) annealing	30 sec,	45-59 °C primer dependent
4) elongation	30 sec / 1 kb,	72 °C → back to step 2, 30 cycles
5) final elongation	10min,	72 °C
6) store at	4 °C	

For primer annealing, temperature should be 3 °C above the temperature of the lower primer melting temperature.

For further cloning, PCR products were separated on a 0.8 - 1.4 % agarose gel by electrophoresis (s. 2.2.4.4.3), excised and then eluted from the gel. Afterwards they were digested with the appropriate restriction enzymes (s. 2.2.4.4.4).

2.2.4.4.3 Agarose gelelectrophoresis

DNA fragments from restrictions (s. 2.2.4.4.4) or cloning PCRs (s. 2.2.4.4.2) were separated for analytical or preparative purpose via agarose gelelectrophoresis. The desired amount of agarose (0.8 – 1.4 %) was added to 1xTAE buffer and then heated in a microwave until it was completely dissolved. Ethidiumbromide was added in the concentration of 1 µg/100ml TAE to enable the visibility of the DNA fragments under UV light. DNA samples were mixed with 6xDNA-Loading buffer and loaded into the pockets of the gel. As a marker, the 1kb DNA ladder of Fermentas was used. Electrophoresis was performed at 90 - 120V for about 1 h. DNA bands were visualized under UV light and then photographed and/or excised (s. 2.2.4.3).

2.2.4.4.4 Restriction

Restriction from plasmid DNA and PCR fragments was performed with an adequate restriction endonuclease and the recommended buffer for approximately 3 h at 37°C.

Standard reaction mix:

DNA	0,5-5 µg
10xbuffer	5 µl
Enzyme	0,5 µl
ddH ₂ O	add to 50µl

Digested DNA fragments from a vector were separated and analyzed by agarose gelelectrophoresis (s. 2.2.4.4.3). Digested PCR products were purified with the QIAquick PCR purification kit.

2.2.4.4.5 Ligation

Classical ligation was performed with T4-DNA-ligase (NEB) in a molar ratio of 1:3 (vector to insert). The mixture was set up in a 10 µl volume, with 1 Unit T4-ligase and ~50 ng vector DNA. The samples were incubated at RT over night.

2.2.4.4.6 Transformation (heat shock)

For transformation, chemical competent bacteria cells (DH5α) were used. These cells (stored at -80 °C) were first thawed on ice for 10 min. Then 200ng of plasmid DNA or the 10 µl ligation reaction were mixed with 100 µl of the bacteria in a reaction tube and the mixture was set on ice for 30 min. Next, the tube was heat shocked for 2 min at 42 °C and cooled on ice. After addition of 250 µl cold LB media (without ampicillin), the sample was incubated for 40 min at 37 °C. The bacterial cells were centrifuged for 1 min at 7000 rpm and the supernatant was discarded. The pellet was plated on LB agar plates and incubated at 37 °C o/n. The colonies were picked for plasmid isolation (s. 2.2.4.1.1).

2.2.4.4.7 Sequencing

All sequencing work was done by SeqLab (Göttingen).

2.2.4.4.8 Cloning of hGAS2L3 WT and Delmut 1-5

For cloning human *GAS2L3*, the *GAS2L3* mRNA sequence NM_174942 from NCBI was used as template for primer design. As template for PCR reaction, cDNA from G2/M synchronized T98G cells was used. *GAS2L3* was cloned into the mammalian overexpression vector pCDNA3 carrying the EGFP sequence in front of the N-terminus. For cloning *GAS2L3* Delmut 1-5, pCDNA3-EGFP h*GAS2L3* was used as template for PCR reaction. All forward primers carried a BamHI restriction site, the reverse primers a XbaI restriction site (primer list s. 2.1.7.1).

3 RESULTS

3.1 The uncharacterized LINC target gene *GAS2L3*

Gene expression analysis after LIN9 depletion in MEFs identified *GAS2L3* as the top hit of regulated genes by LINC (Reichert et al., 2010) (s. 1.2.2.1). So far, *GAS2L3* is a completely uncharacterized member of the GAS2 family of genes. In contrast to the well known G2/M target genes of LINC, the GAS2 family was originally identified in a screen looking for genes upregulated in growth arrested MEFs (Schneider et al., 1988) (s. 1.3.1).

3.2 *GAS2L3* is a LINC target gene in the human system

To verify that *GAS2L3* is also regulated by LINC in human cells, I depleted the LINC core proteins LIN9 and LIN54 by RNAi in HeLa cells (Fig. 3.1 A and 3.1 B). Gene expression analysis by quantitative real-time PCR (qRT-PCR) revealed that depletion of LIN9 (Fig. 3.1 A) and also LIN54 (Fig. 3.1 B) led to a significant downregulation of *GAS2L3* gene expression. I also validated these data in the human immortalized non transformed fibroblast cell line BJ-ET (Fig. 3.1 C). Depletion of LIN9 in BJ-ET cells by siRNA transfection again showed a specific downregulation of *GAS2L3* gene expression. Altogether, these data confirm that *GAS2L3* is also in human cells a bona fide LINC target gene.

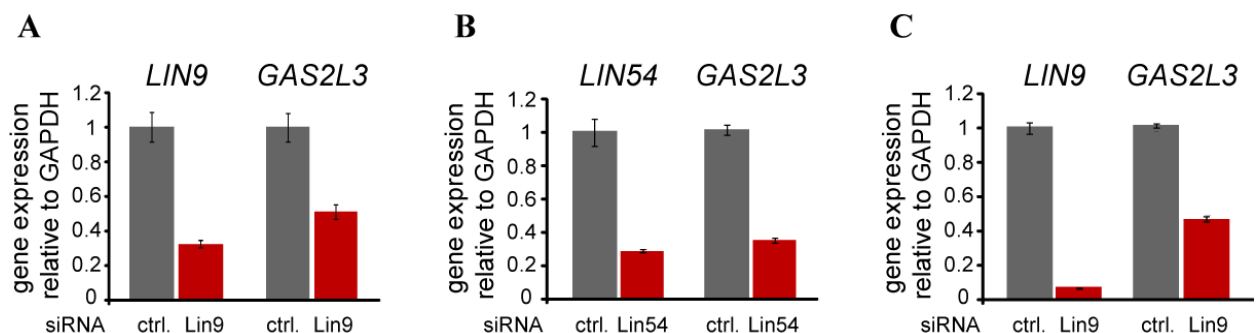


Fig. 3.1. *GAS2L3* is a LINC target gene in human cells

Gene expression analysis of *GAS2L3* was analyzed by qRT-PCR after siRNA transfection against LIN9 and LIN54. (A) LIN9 and (B) LIN54 were depleted in HeLa cells. Loss of *LIN9* to 70 % reduced *GAS2L3* mRNA levels to 60 %. Loss of *LIN54* to 80 % reduced *GAS2L3* mRNA levels to 70 %. (C) LIN9 was depleted in non transformed BJ-ET cells. Loss of *LIN9* to 90 % reduced *GAS2L3* mRNA levels to 60 %.

3.2.1 Transcriptional regulation during the cell cycle

Since it is well known that LINC regulates the expression of G2/M genes, I next analyzed the transcriptional expression of *GAS2L3* during the cell cycle. Therefore, I made use of the glioblastoma cell line T98G as these cells can be simply synchronized by serum starvation (Stein, 1979).

I washed T98G cells twice with PBS to remove the remaining serum following feeding with DMEM without serum. After 72 hours, cells were released from G0 cell cycle block by adding 20 % serum and started to progress synchronously through the cell cycle (Fig. 3.2 A). To check the efficiency of cell cycle synchronization, I harvested FACS samples for the indicated time points. FACS profiles in Figure 3.2 B show that cells nicely progressed synchronously through the cell cycle. Between 6 and 12 hours after release, cells started to enter G1 phase, progressed into S phase after 18 hours and reached G2/M phase after 24 hours. After mitotic progression they entered the next cell cycle between 29 and 34 hours. In parallel, I harvested RNA for the same time points and performed gene expression analysis by qRT-PCR for *GAS2L3* and the other *GAS2* family members *GAS2*, *GAS2L1* and *GAS2L2* (Fig. 3.2 C). *GAS2L3* gene expression was highest between 24 and 29 hours after serum addition when cells had entered G2/M phase. In contrast, *GAS2* gene expression peaked at 6 hours after serum addition when cells were still in G0/G1. *GAS2L1* gene expression did not significantly change during the cell cycle and *GAS2L2* gene expression could not be detected over the whole cell cycle at all (Fig. 3.2 C). Thus, in contrast to the well known *GAS2* family members *GAS2*, *GAS2L1* and *GAS2L2*, *GAS2L3* is unique in its G2/M specific expression pattern.

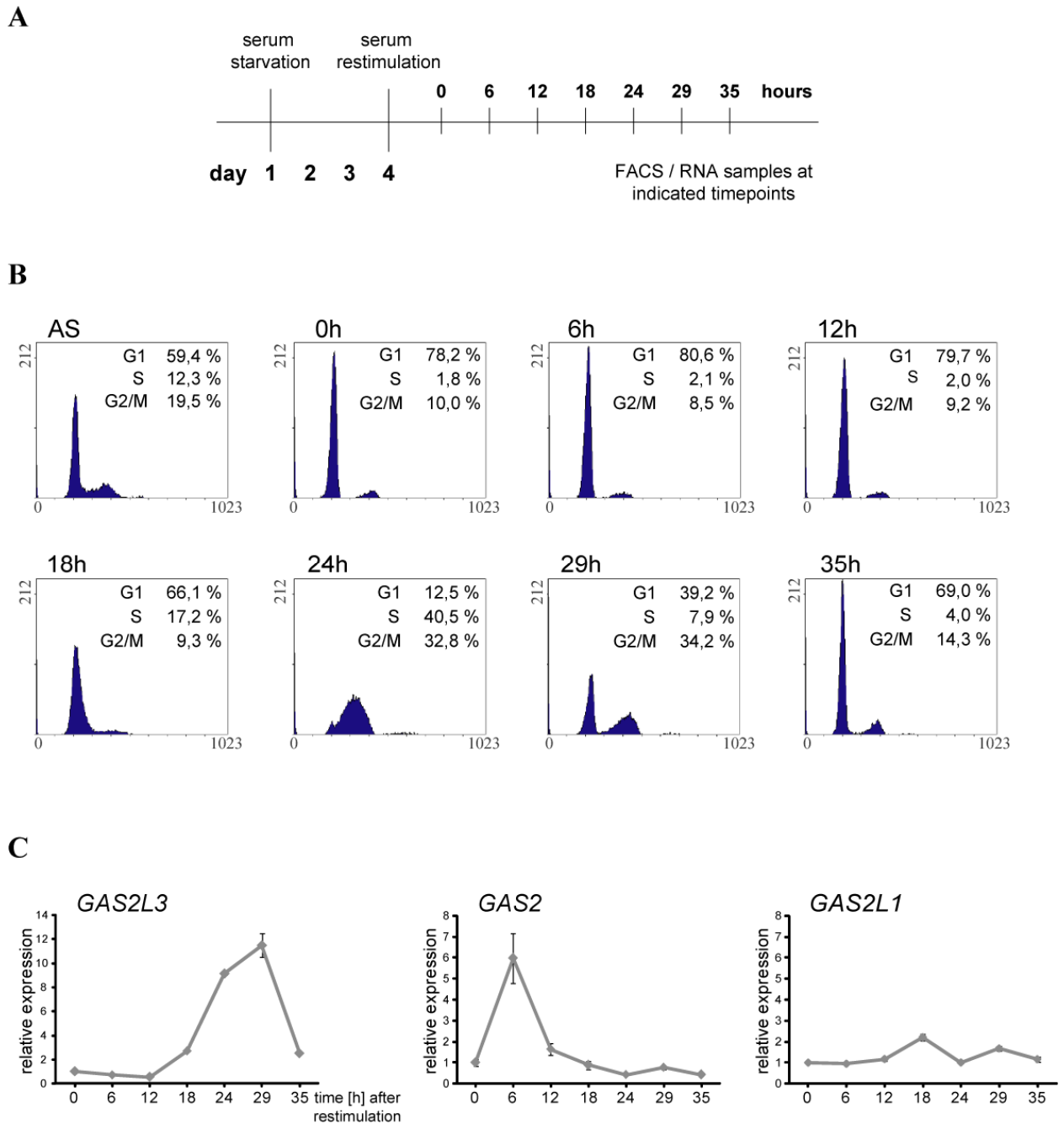


Fig. 3.2. *GAS2L3* is a G2/M regulated gene

Gene expression analysis of *GAS2L3* and the other *GAS2* family members was performed in synchronized T98G cells by qRT-PCR. (A) Scheme of the experimental set up. (B) T98G cell synchronization was confirmed by FACS analysis at the indicated time points. (C) *GAS2L3* is transcriptionally activated during G2/M phase. *GAS2* gene expression peaks in G0/G1 phase. *GAS2L1* gene expression is not regulated at all during the cell cycle.

3.2.2 G2/M specific expression pattern is LINC dependent

To test, if LINC is required for cell cycle dependent expression of *GAS2L3*, I additionally depleted LIN9 in three days serum starved T98G cells and waited again 24 hours before starting serum restimulation. At indicated time points, I harvested RNA for gene expression analysis (Fig.3.3 A). In LIN9 depleted T98G cells, cell cycle dependent *GAS2L3* gene expression was strongly inhibited, whereas control transfected cells showed the G2/M specific expression pattern (Fig. 3.3 B). For transfection control, I also investigated cell cycle dependent *LIN9* gene expression, which was inhibited in LIN9 depleted cells, respectively (Fig. 3.3 B).

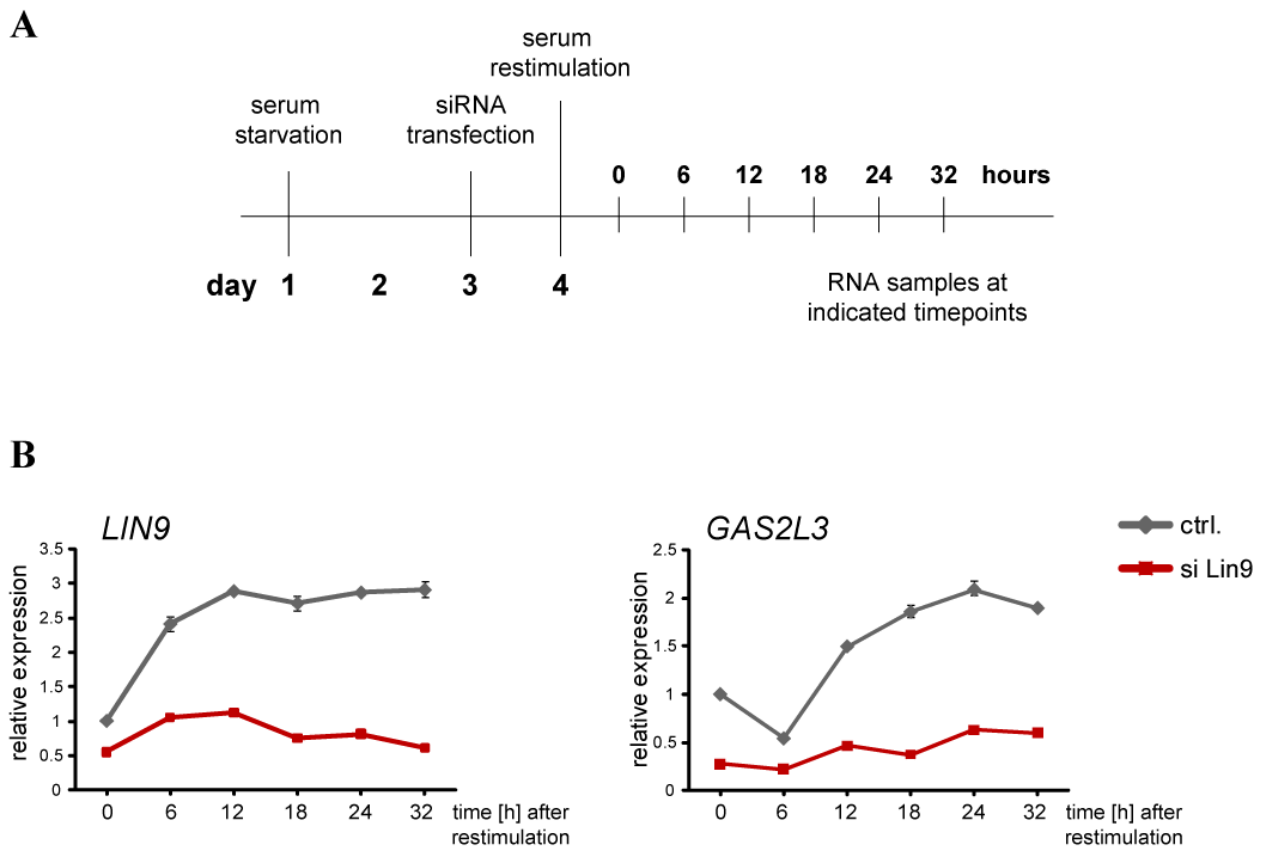


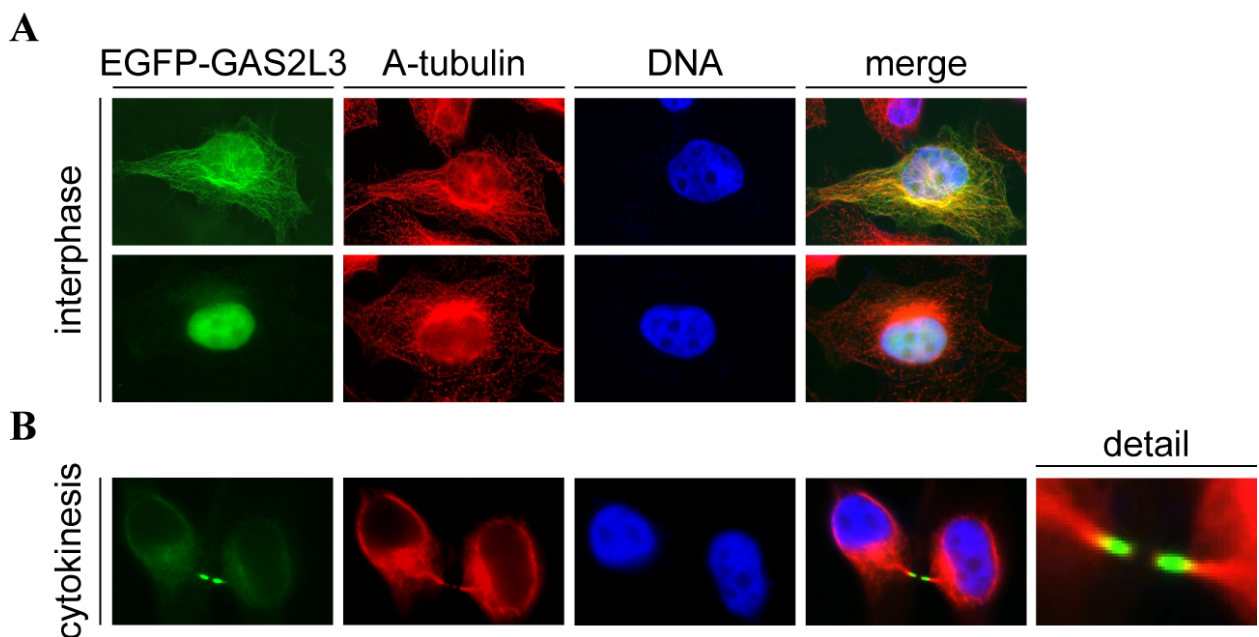
Fig. 3.3. *GAS2L3* G2/M specific gene expression is LINC dependent

Gene expression analysis of *GAS2L3* was performed in LIN9 depleted synchronized T98G cells by qRT-PCR. (A) Scheme of the experimental set up. (B) Cell cycle dependent *LIN9* and *GAS2L3* gene expression is inhibited in LIN9 depleted cells (red line) compared to control cells (grey line).

3.3 Localization pattern of overexpressed GAS2L3

To determine the subcellular localization of GAS2L3, I amplified the human *GAS2L3* sequence by PCR and cloned it behind an EGFP tag in the mammalian overexpression vector pCDNA3. I transfected asynchronously HeLa cells growing on coverslips with the EGFP-GAS2L3 fusion protein and fixed the cells with 3 % paraformaldehyde / 2 % sucrose in PBS (PSP) 18 hours after transfection. As a cytoskeleton marker, I counterstained the cells for A-tubulin in red and the cell nuclei were stained with Hoechst in blue. Immunofluorescence microscopy of these cells revealed distinct localization of GAS2L3 (Fig. 3.4). In interphase cells, GAS2L3 expression was mostly cytoplasmatic and colocalized with the microtubule network. A small fraction of interphase cells also showed nuclear GAS2L3 localization (Fig. 3.4 A). Strikingly, during cytokinesis, GAS2L3 was exclusively detected at the midbody (MB) (Fig. 3.4 B).

It is well known that the overexpression of some microtubule binding proteins can stabilize the microtubule network. For example MACF (microtubule actin crosslinking factor), a large protein also containing the GAS2 domain, is able to prevent microtubules from depolymerization upon drug treatment (Sun et al., 2001). To analyze, if this is also the case for EGFP-GAS2L3 overexpressing cells, I treated those cells, in comparison to control cells, with a low dose of the microtubule depolymerization drug nocodazole. Whereas the microtubules were completely depolymerized in control cells, the microtubule network was not disturbed in EGFP-GAS2L3 overexpressing cells upon nocodazole treatment (Fig. 3.4 C).



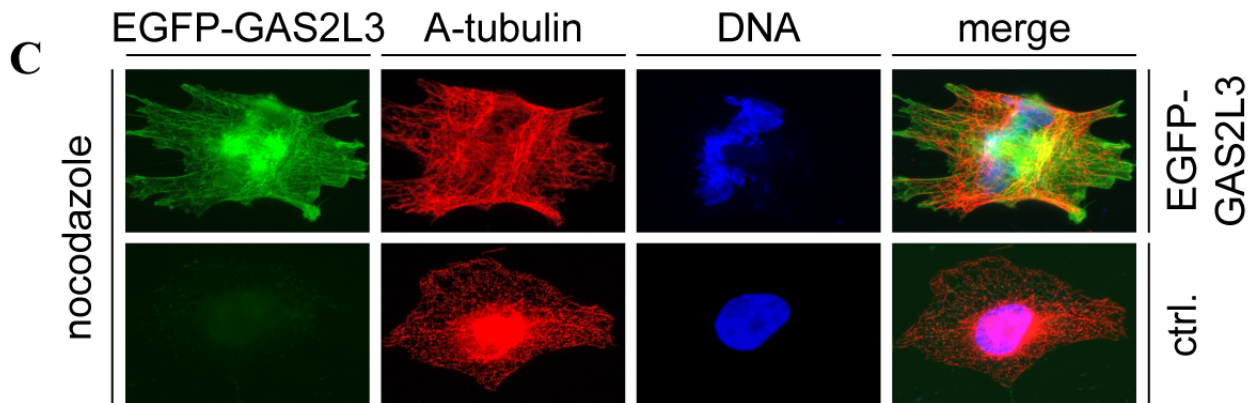


Fig. 3.4. GAS2L3 shows distinct subcellular localization during the cell cycle

HeLa cells were transfected with 2 μ g EGFP-GAS2L3 plasmid DNA and fixed 18 hours after transfection with PSP. The cytoskeleton was counterstained with A-tubulin in red. Nuclei were visualized in blue by Hoechst staining. For microtubule depolymerization, cells were treated with 100 ng/ml nocodazole for 14 hours. (A) In interphase cells, EGFP-GAS2L3 either colocalizes with the microtubule network or is present in the nuclei. (B) During cytokinesis EGFP-GAS2L3 localizes exclusively to two distinct spots at the midbody. (C) Cytoplasmatic EGFP-GAS2L3 overexpression stabilizes the microtubule network upon nocodazole treatment.

3.3.1 Validation of the midbody localization

The midbody (MB), the final bridge between dividing cells, is a microtubule and protein rich region formed at the end of mitosis right before abscission. The outer arms of the MB embrace the so called midbody ring (MBR) or Flemming body, a characteristic ring-like arrangement in the center of the dividing cells (Pohl and Jentsch, 2008). Proteins of the MB, for example Aurora B, RhoA and Survivin are known to be master regulators of cytokinesis (Glotzer, 2009a) (s. 1.1.2.2.2).

To validate distinct MB localization of overexpressed GAS2L3, I used the well known MB components RhoA and Survivin as MB markers. To do so, I overexpressed HA-tagged mouse GAS2L3 in HeLa cells. Even though mouse GAS2L3 shows high homology to the human GAS2L3 sequence it can be more easily overexpressed (data not shown). After cell fixation, the HA-tag was detected with a red-fluorescent secondary antibody and either counterstained for Survivin or RhoA, detected with a green-fluorescent secondary antibody. Nuclei were visualized in blue by Hoechst staining (Fig. 3.5). In cytokinesis, HA-GAS2L3 and Survivin showed perfect colocalization at the outer arms of the MB (Fig. 3.5 A). RhoA and GAS2L3 showed no overlap but were in closest proximity (Fig. 3.5 B). Since RhoA is known to localize exclusively to the midbody ring (MBR), this again proves that GAS2L3 localizes to the MB, but not to the MBR.

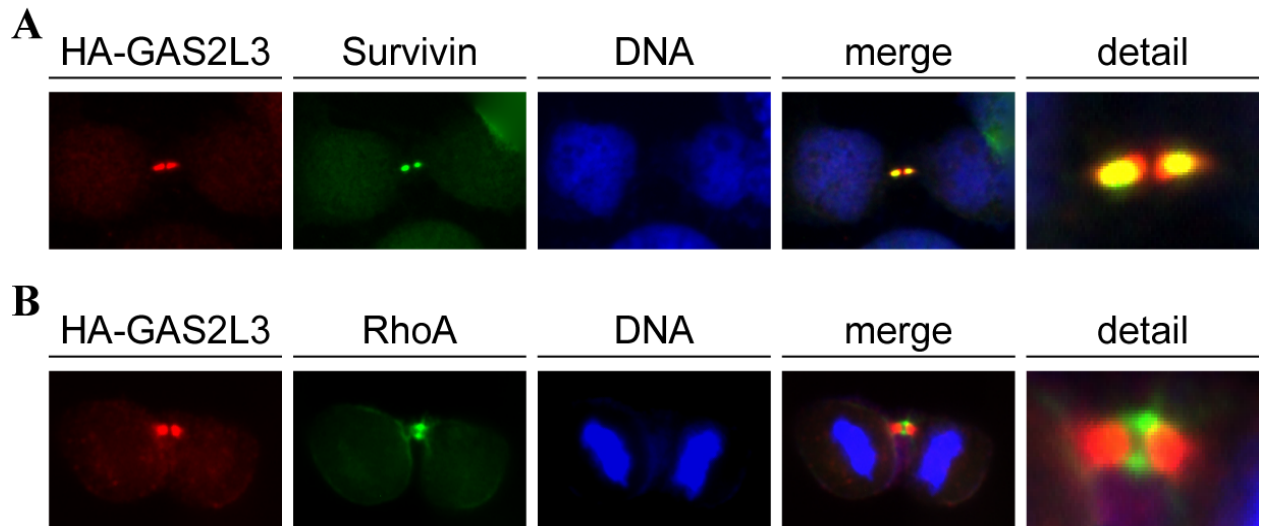


Fig. 3.5. GAS2L3 localizes to the midbody during cytokinesis

HeLa cells were transfected with 2 μ g HA-GAS2L3 plasmid DNA and fixed 48 hours after transfection with PSP. GAS2L3 was stained with a HA antibody in red, endogenous Survivin or RhoA were counterstained in green with specific antibodies. Nuclei were visualized by Hoechst staining. (A) HA-GAS2L3 and Survivin perfectly colocalize at the outer arms of the MB. (B) HA-GAS2L3 and RhoA show no overlap at the MBR.

To exclude that MB localization is specific to HeLa cells, I also investigated HA-GAS2L3 localization in two other cancer cell lines; T98G cells and the colon carcinoma cell line HCT 116. I again stained overexpressed HA-GAS2L3 in red, A-tubulin in green and nuclei in blue (Fig. 3.6). T98G cells (Fig. 3.6 A) as well as HCT 116 cells (Fig. 3.6 B) confirmed the distinct MB localization of overexpressed GAS2L3.

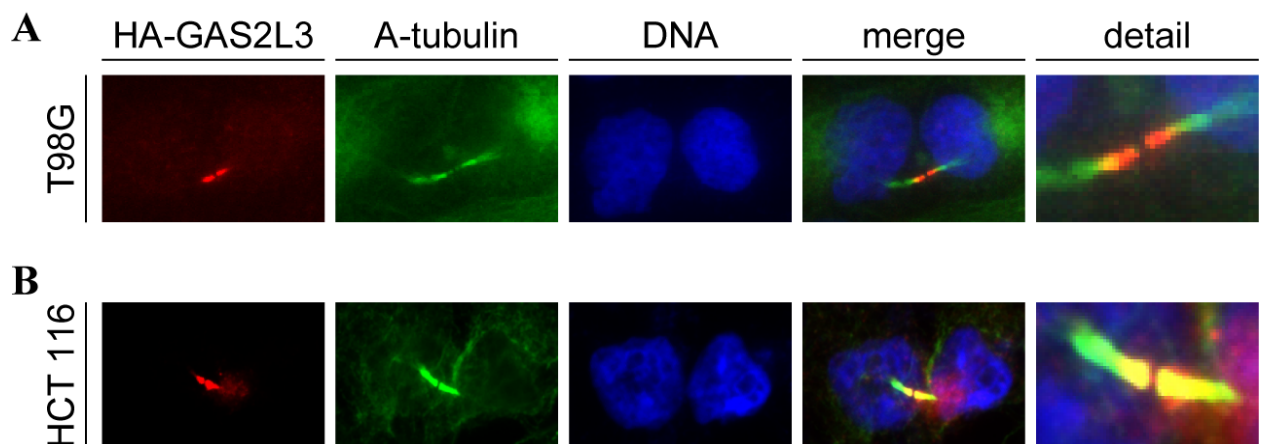


Fig. 3.6. MB localization of GAS2L3 is not HeLa cell specific

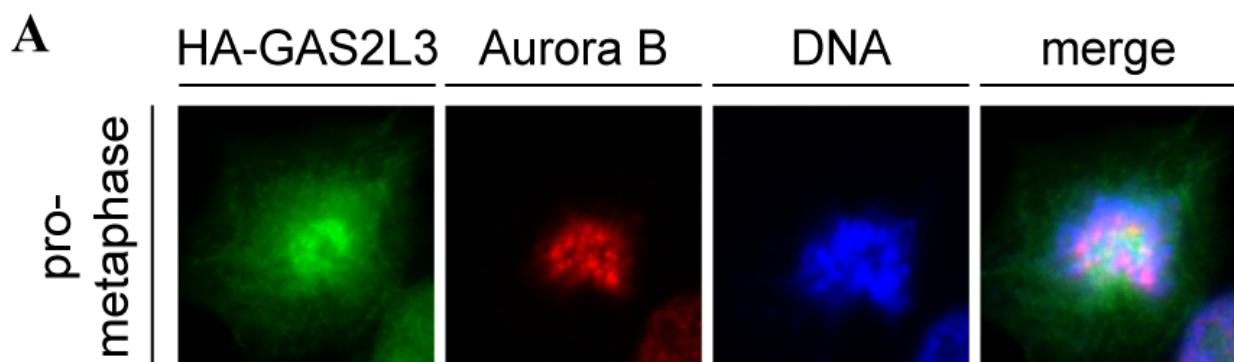
T98G and HCT 116 cells were transfected with 2 μ g HA-GAS2L3 plasmid DNA and fixed 48 hours after transfection with PSP. GAS2L3 was stained with an HA antibody in red, A-tubulin was counterstained in green. Nuclei were visualized by Hoechst staining. (A) HA-GAS2L3 localizes to the MB in T98G, as well as in (B) HCT 116 cells.

3.3.2 Mitotic distribution of GAS2L3

It is well known that many MB proteins also show a distinct localization pattern in earlier stages of mitosis. Aurora B for example, a so called chromosomal passenger protein, remains a part of centromeres from prometaphase to metaphase. After chromatids begin to separate in anaphase, Aurora B relocates to the midzone spindle and persists at the midbody from beginning of telophase until cytokinesis is completed. Corresponding to this distinct mitotic localization, Aurora B is not only essential for cytokinesis. Due to its centromere localization, Aurora B is an important component of the spindle assembly checkpoint and therefore indispensable for proper chromosomal segregation (Fu et al., 2007; Hauf et al., 2003).

To check if GAS2L3 is also present at distinct regions in earlier mitotic stages I transfected HeLa cells with HA-GAS2L3. After fixation, I stained HA-GAS2L3 in green and counterstained for Aurora B, as a mitotic marker, in red. Nuclei were stained in blue by Hoechst.

Interestingly, I could detect HA-GAS2L3 also in early mitotic stages (Fig. 3.7). In prometaphase, distinguishable by centromeric localization of Aurora B, HA-GAS2L3 was diffusely expressed in the whole cell and seemed to be enriched at microtubule spindle poles from where the mitotic spindle is built up (Fig. 3.7 A). In metaphase, when chromosomes have aligned at the metaphase plate and Aurora B is still present at the centromeres, HA-GAS2L3 clearly localized to the minus ends of the mitotic spindle microtubules (Fig. 3.7 B). In anaphase, when chromatids start to separate and Aurora B migrates to the spindle midzone, HA-GAS2L3 was still enriched at the minus ends of the mitotic spindle microtubules. In late anaphase, also HA-GAS2L3 seemed to relocate to some extent to midzone microtubules (Fig. 3.7 C). In contrast to Aurora B, which relocates to the central part of the spindle midzone, HA-GAS2L3 seemed to localize more diffusely to the complete microtubule network of the whole midzone (Fig. 3.7 C & D). The only colocalization of Aurora B and HA-GAS2L3 was detectable in the end of telophase, when both proteins relocated to the MB (Fig. 3.7 D).



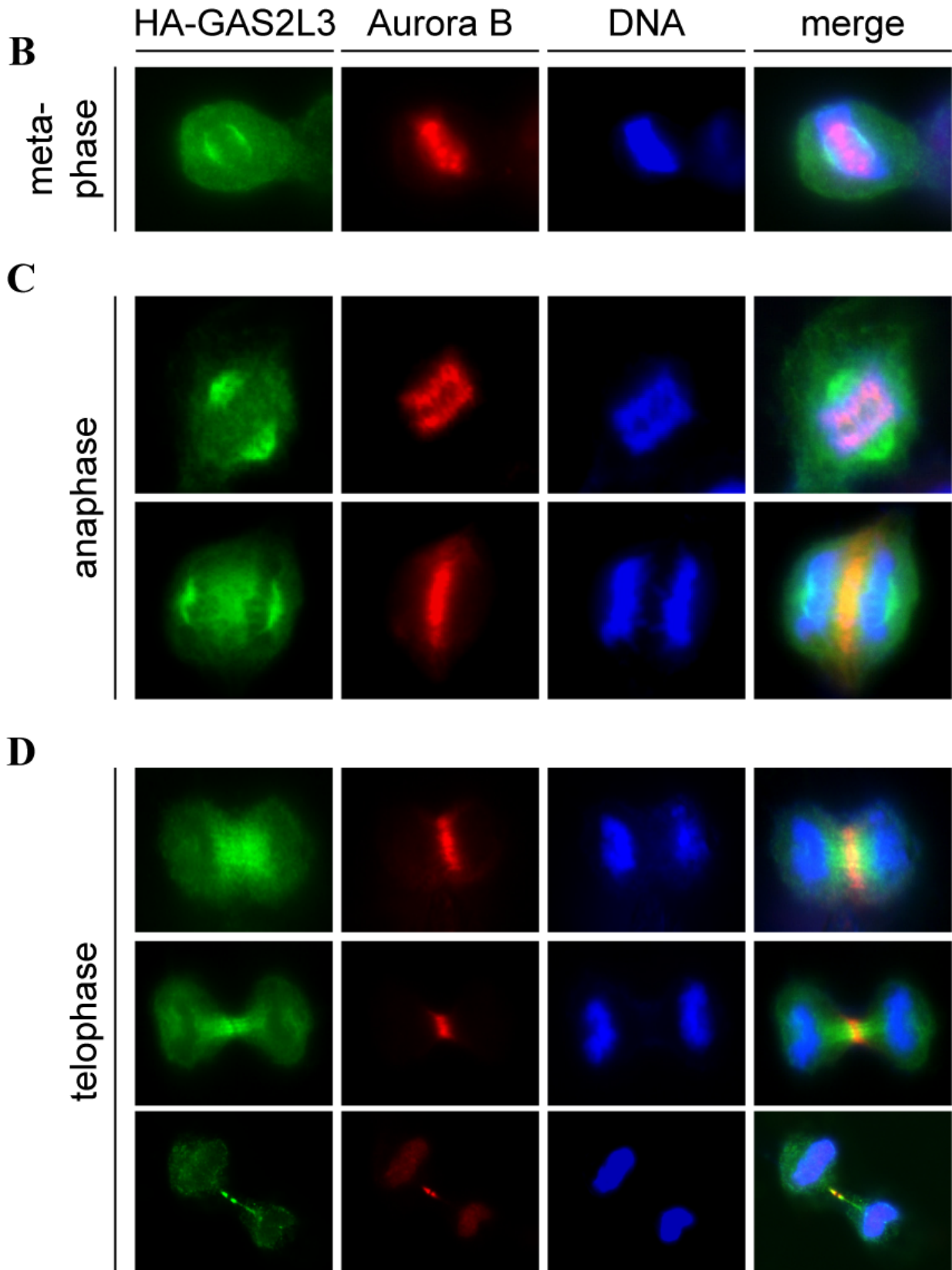
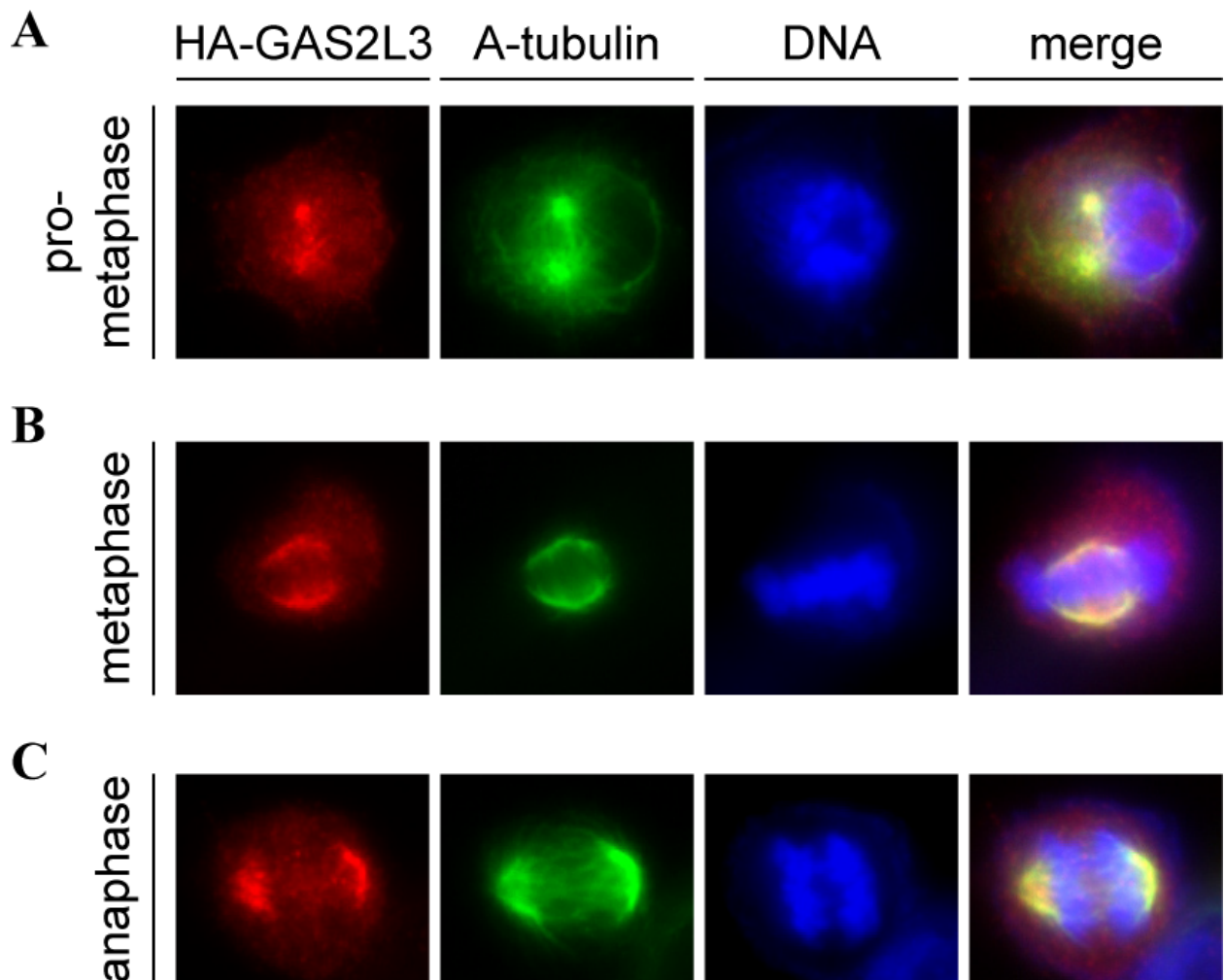


Fig. 3.7. GAS2L3 shows a distinct mitotic localization pattern

HeLa cells were transfected with 2 μ g HA-GAS2L3 plasmid DNA, fixed with PSP 40 hours after transfection and immunostained for HA in green and Aurora B in red. Nuclei were visualized by Hoechst staining in blue. GAS2L3 localization was monitored in different mitotic stages. (A) During prometaphase GAS2L3 is enriched at the spindle poles. (B) In metaphase, GAS2L3 localizes to the minus ends of the mitotic spindle and remains there until anaphase (C). In late anaphase, GAS2L3 starts to relocate to midzone microtubules (C), and migrates from there during telophase to the MB (D).

To validate microtubule colocalization during mitosis, I also counterstained HA-GAS2L3 overexpressing HeLa cells with an A-tubulin antibody and again focused on the same mitotic stages (Fig. 3.8).

Prometaphase cells showed a clear colocalization of HA-GAS2L3 with microtubule spindle poles from where the mitotic spindle is built up (Fig. 3.8 A). In metaphase, HA-GAS2L3 clearly colocalized with minus ends of the mitotic spindle microtubules (Fig. 3.8 B) and remained there until anaphase (Fig. 3.8 C). In early telophase, HA-GAS2L3 started to migrate from the spindle midzone microtubules to the MB (Fig. 3.8 D). The MB localization in late telophase was the first stage during mitosis, where GAS2L3 left the microtubule network.



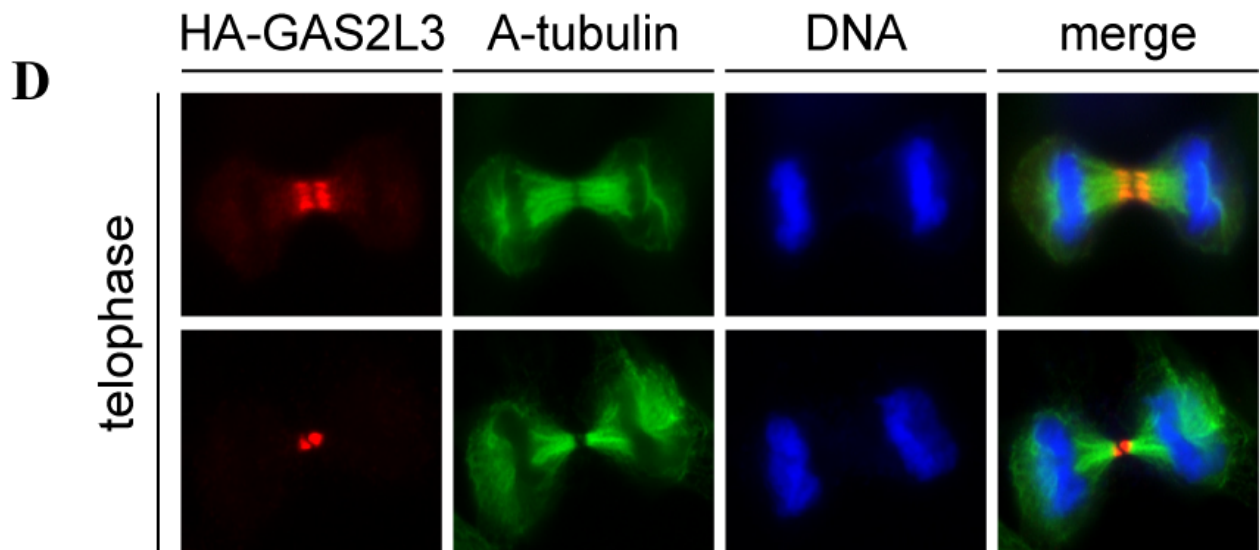


Fig. 3.8. GAS2L3 mainly colocalizes with the microtubule network during mitosis

HeLa cells were transfected with 2 μ g HA-GAS2L3 plasmid DNA, fixed with PSP 40 hours after transfection and immunostained for HA in red and A-tubulin in green. Nuclei were visualized by Hoechst staining in blue. GAS2L3 localization was monitored in different mitotic stages. (A) During prometaphase GAS2L3 colocalizes with microtubule spindle poles. (B) In metaphase, GAS2L3 localization overlaps with the minus ends of mitotic spindle microtubules and remains there until anaphase (C). (D) During telophase, GAS2L3 migrates from midzone microtubules to the MB.

3.4 Localization of endogenous GAS2L3

Since overexpression constructs, due to additional amino acids of the tag, can show different localization than the endogenous protein, I next analyzed endogenous GAS2L3 localization.

Therefore, I stained asynchronously growing HeLa cells with a commercial monoclonal GAS2L3 antibody in green and counterstained for Aurora B in red, as a well known MB component. To confirm specific GAS2L3 staining of the antibody I transfected cells before staining with either siRNA against GAS2L3 or control.

Endogenous GAS2L3 staining confirmed the MB localization during cytokinesis (Fig. 3.9). Importantly, this localization was completely abolished in GAS2L3 depleted cells, indicating a specific staining by the commercial antibody. No GAS2L3 signal could be detected in earlier mitotic stages and interphase cells, respectively. Whether this is due to the antibody or due to endogenous GAS2L3 protein levels cannot be clarified from these experiments.

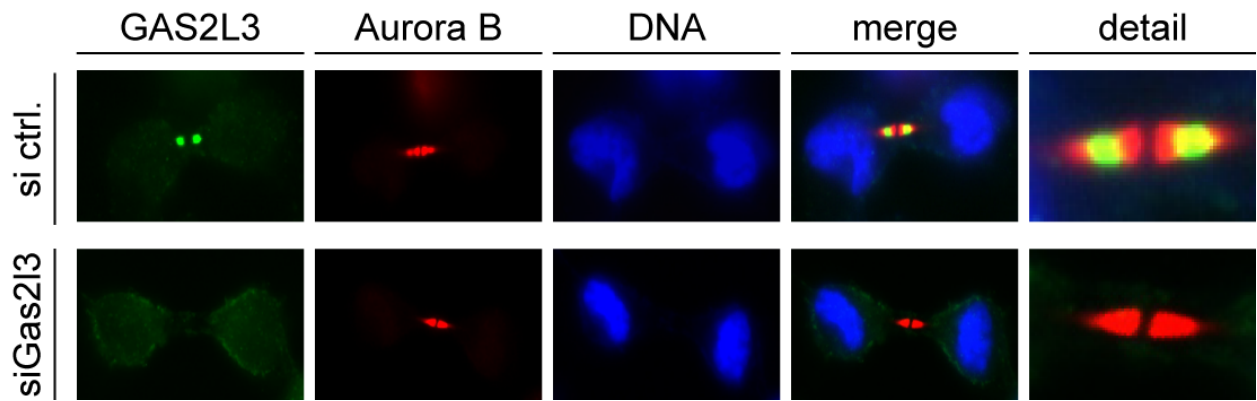


Fig. 3.9. Endogenous GAS2L3 localizes to the midbody during cytokinesis

HeLa cells were immunostained for GAS2L3 in green and Aurora B in red. Nuclei were visualized by Hoechst staining in blue. GAS2L3 is prominently visible at the outer arms of the MB, confirmed by Aurora B co-staining.

3.5 Characterizing GAS2L3 protein domains

All GAS2 family members share the highly conserved Calponin Homology (CH) and Growth Arrest Specific 2 (GAS2) domain (Fig. 1.4.). However, the distinct mitotic subcellular distribution of GAS2L3 has not been shown for any other family member. To get information about protein domains required for this specific localization, I cloned several deletion mutants of GAS2L3. All deletion mutants were cloned into the same mammalian overexpression vector pCDNA3 behind an EGFP tag. A summary of all mutants is illustrated in Fig. 3.10 A.

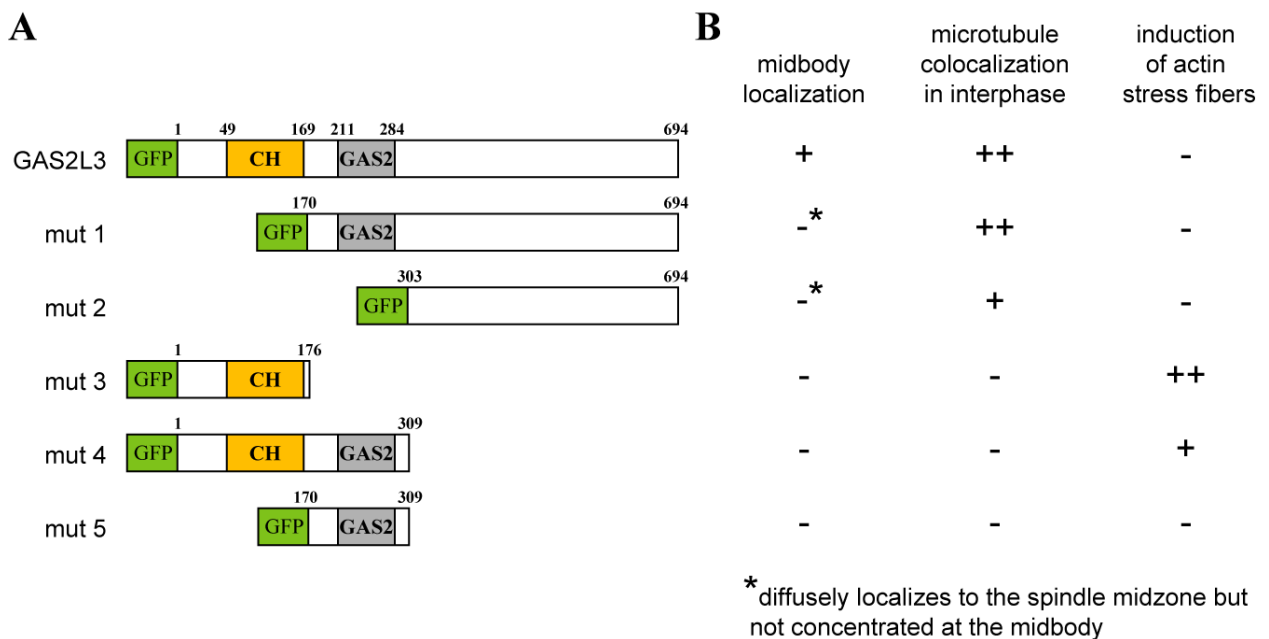


Fig. 3.10. (A) Diagram of GAS2L3 deletion mutants (B) Summary of the results obtained by microscopic examination in Fig. 3.11 – 13

3.5.1 Protein domains essential for specific localization pattern

To investigate the protein domains essential for the specific localization pattern of GAS2L3, I transfected asynchronously HeLa cells growing on coverslips with each of my deletion mutant constructs. I fixed cells 18 hours after transfection with PSP and counterstained the cytoskeleton in red with an A-tubulin antibody. Nuclei were stained in blue with Hoechst.

First, I investigated the ability of all constructs for MB localization (Fig.3.11). Full length EGFP-GAS2L3, serving as a positive control, located prominently at the MB. Deletion mutant 1 (mut 1), missing the first 170 amino acids of the N-terminal part containing the CH domain, still showed colocalization with the midzone microtubules, but not the distinct MB localization compared to full length GAS2L3. Also deletion mutant 2 (mut 2), missing additionally the GAS2 domain, could still colocalize with midzone microtubules, but not as prominent as mut 1 (Fig. 3.11). In contrast, deletion mutants 3 - 5 (mut 3 - 5), which all lack the whole C-terminal part, showed no midzone microtubule colocalization and MB localization (Fig. 3.11). Mut 3 and mut 4, containing either the CH domain of the N-terminus or additionally the GAS2 domain, seemed to localize to the microfilament network during cytokinesis. Mut 5, containing only the GAS2 domain was expressed diffusely all over the cell. In summary, only full length GAS2L3 shows the distinct MB localization during cytokinesis.

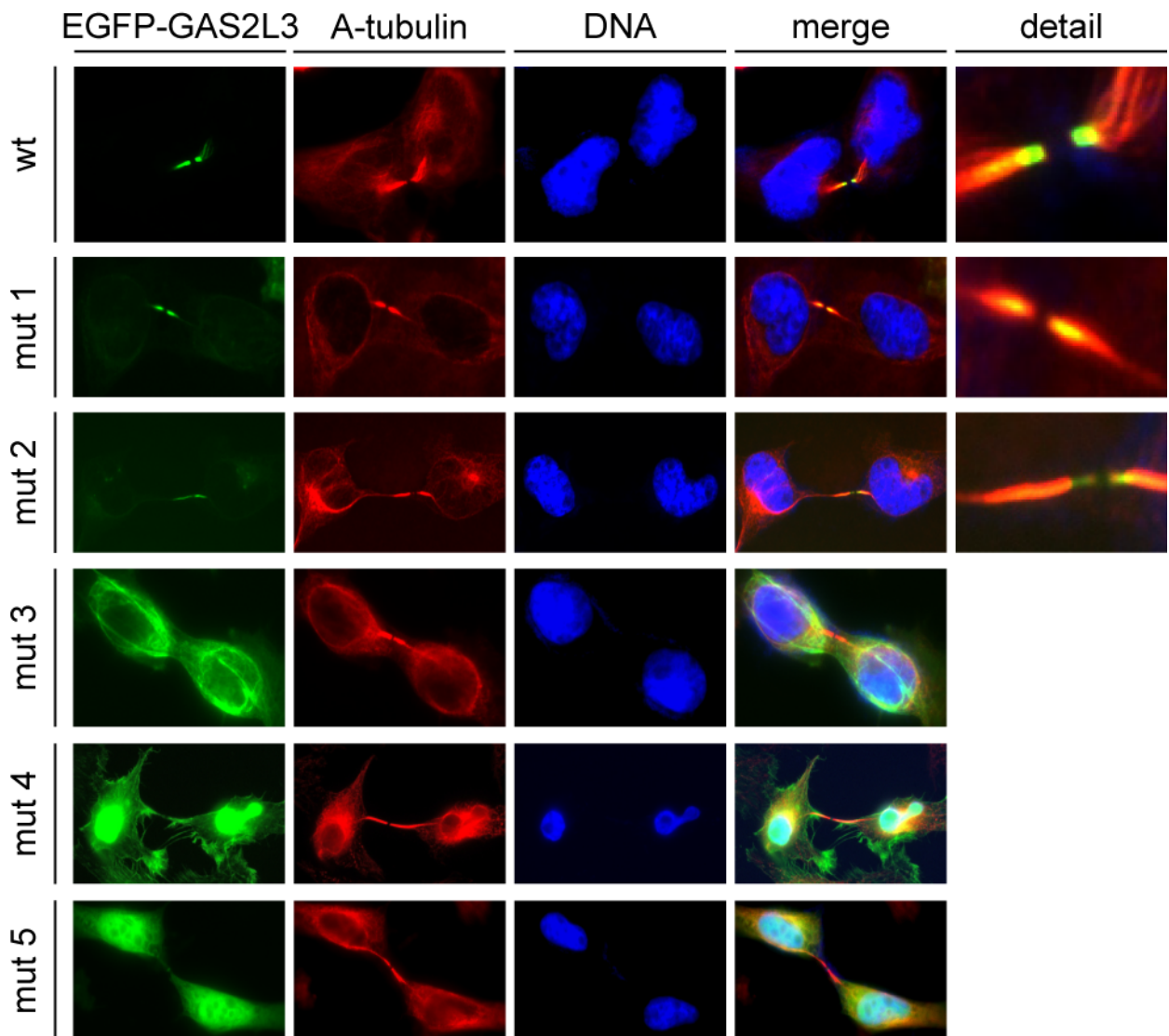


Fig. 3.11. Only full length GAS2L3 can localize to the MB

HeLa cells were transfected with 2 μ g of each construct. Cells were fixed with PSP 18 hours after transfection following immunostaining with A-tubulin in red. Nuclei were visualized by Hoechst staining in blue. Microscopic examination was performed for cells during cytokinesis. WT GAS2L3, mut 1 and mut 2, all containing the C-terminus, can colocalize with midzone microtubules, but only WT GAS2L3 shows distinct MB localization. Mut 3, 4 and 5, only consisting of the N-terminal part, cannot colocalize with midzone microtubules and are mainly expressed in the cytoplasm (mut 3 and 4) or in the nuclei (mut 4 and 5). A summary of the results is shown in Fig. 3.10 B.

Next, I analyzed interphase cells to investigate the ability of the different constructs to localize to microtubules (Fig. 3.12). As already shown in Fig. 3.4 A, full length EGFP-GAS2L3 prominently colocalized with microtubules (Fig. 3.12). Also mut 1 and mut 2, which already showed the midzone microtubule localization during cytokinesis (Fig. 3.11) not only colocalized with, but also bundled microtubules in interphase cells. In contrast, mut 3, 4 and 5 showed no

microtubule colocalization in interphase cells (Fig. 3.12). Mut 5 was again expressed diffusely all over the cell. Mut 3 and mut 4 seemed to colocalize with the microfilament network and even to induce the formation of actin stress fibers.

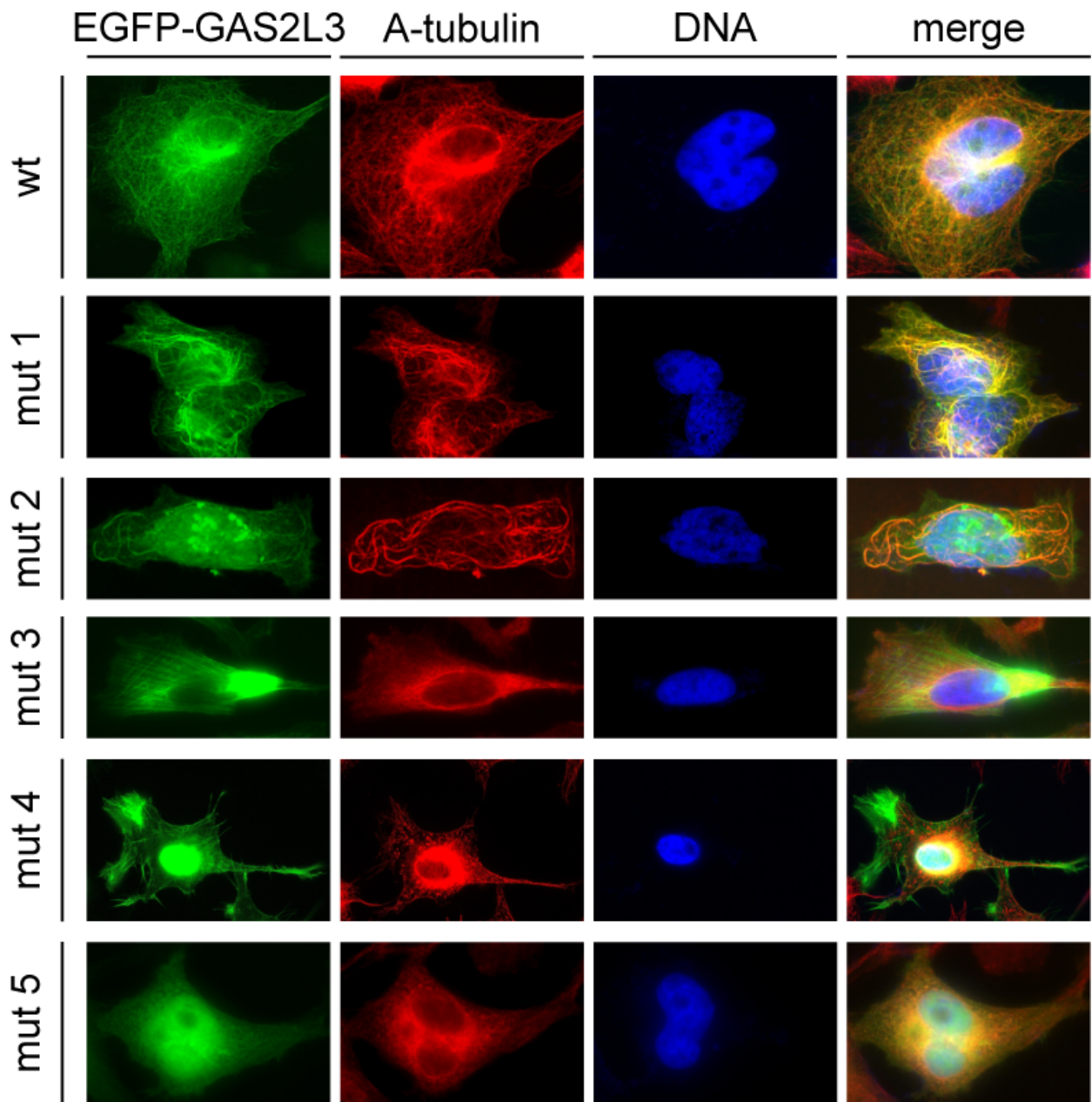


Fig. 3.12. GAS2L3 mutants show different localization pattern during interphase

HeLa cells were transfected with 2 μ g of each construct. Cells were fixed with PSP 18 hours after transfection following immunostaining with A-tubulin in red. Nuclei were visualized by Hoechst staining in blue. Only interphase cells were monitored for microtubule colocalization. WT GAS2L3, mut 1 and mut 2 can colocalize with microtubules, whereas mut 3, 4 and 5 cannot. A summary of the results is shown in Fig. 3.10 B.

To confirm the induction of actin stress fibers by overexpressing GAS2L3 mut 3 and mut 4, I also counterstained those mutants with phalloidin labeled with a fluorescent dye in red. Phalloidin is a poison from the fungus *Amanita phalloides* and specifically interacts with F-actin fibers of the cytoskeleton (Wulf et al., 1979). Figure 3.13 shows that the interphase expression of mut 3 and mut 4 perfectly overlapped with the actin cytoskeleton. Therefore, mut 3 and mut 4 not only induce the formation of actin stress fibers, they also colocalize with them.

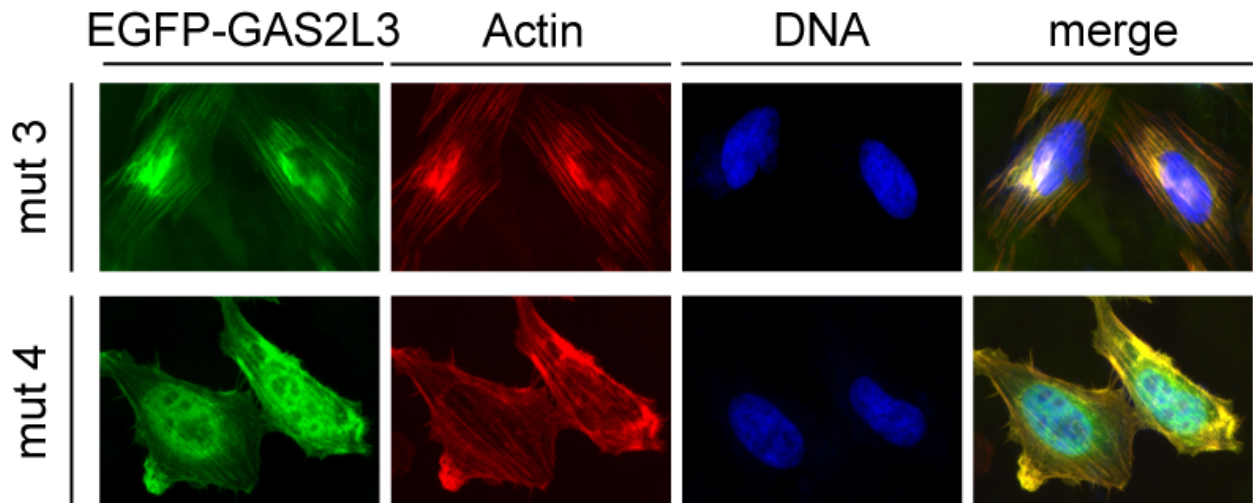


Fig. 3.13. GAS2L3 mut 3 and mut 4 induce the formation of actin stress fibers

HeLa cells were transfected with 2 μ g of each construct. Cells were fixed with PSP 18 hours after transfection followed by Actin staining with phalloidin in red. Nuclei were visualized by Hoechst staining in blue. Mut 3 and mut 4 also colocalize with the induced actin stress fibers. A summary of the results is shown in Fig. 3.10 B.

A summary of the results is shown in Figure 3.10 B.

3.5.2 Domains essential for GAS2L3 protein stability

Beside the different localization pattern of all GAS2L3 mutants, I noticed that the expression efficiency and time of stable overexpression after transfection were remarkably different between single mutants. Therefore, I decided to analyze the protein levels of the different mutants.

To compare the protein levels of GAS2L3 mutants I transfected HeLa cells growing on 10 cm dishes with 30 μ g plasmid DNA of each construct. Since it is well known that many proteins are specifically degraded by the proteasomal pathway, I additionally treated the cells 40 hours after transfection either with or without MG132, a proteasome inhibitor (Lee and Goldberg, 1998). After 48 hours I harvested the cells, made whole cell lysates and performed Western Blot analysis.

Immunoblot analysis with an antibody against GFP revealed large differences in protein levels between the different mutants (Fig. 3.14). Whereas full length GAS2L3, mut 1 and mut 2 were not detectable at all after short exposure, mut 3, mut 4 and mut 5 were highly expressed. Also it was obvious that treatment with the proteasome inhibitor MG132 did not significantly alter the protein levels of mutants 3 to 5. After longer exposure, full length GAS2L3, mut 1 and mut 2 were also detectable, but compared to the other mutants much weaker. For those three proteins MG132 treatment led to a slight enrichment of total protein amount (Fig. 3.14).

Immunoblot analysis with a polyclonal antibody against GAS2L3 confirmed the protein stabilization after MG132 treatment of full length GAS2L3, mut 1 and mut 2 (Fig. 3.14). Since the polyclonal GAS2L3 antibody was raised against the N-terminal part of the protein, mut 3, mut 4 and mut 5 cannot be detected by this antiserum. Immunoblotting against A-tubulin served as a loading control.

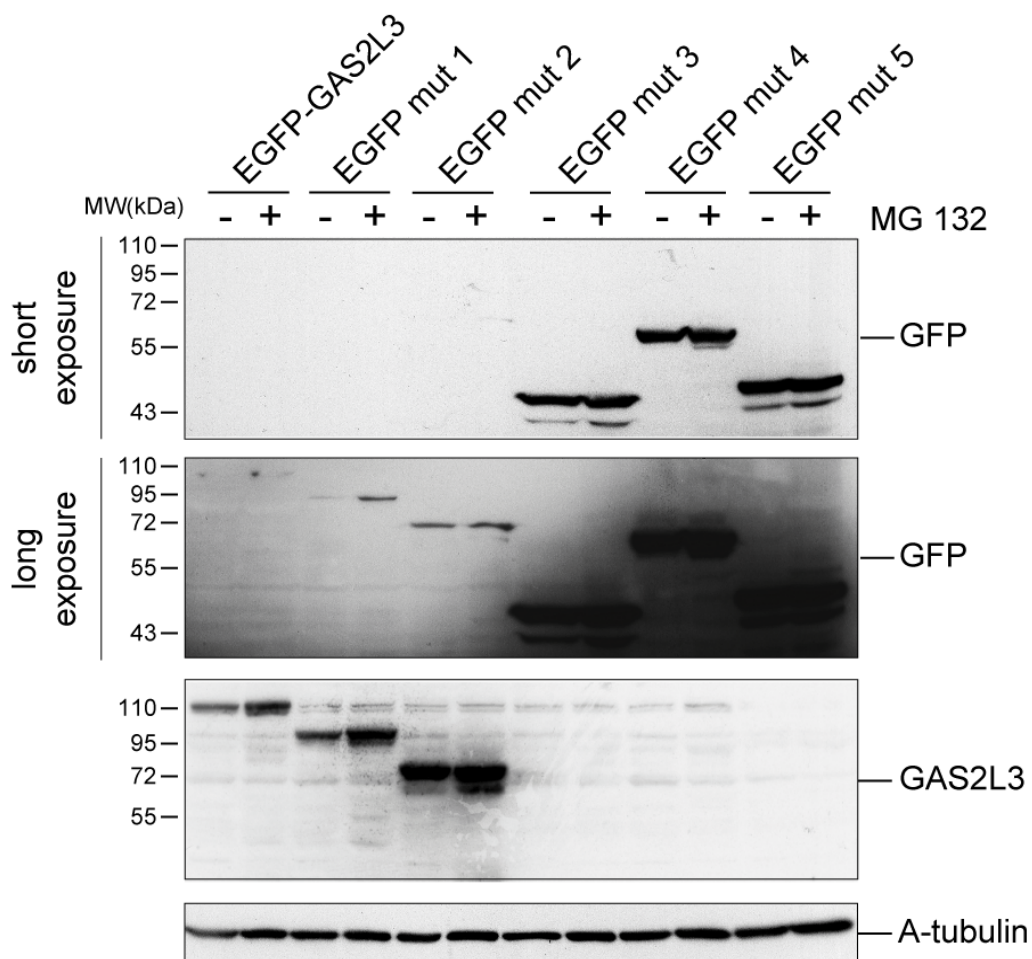


Fig. 3.14. Protein characteristics of GAS2L3 mutants are remarkably different

HeLa cells were transfected with 30 μ g of each construct. After 40 hours, cells were treated either with or without 20 μ M MG132 for 8 h. Whole cell lysates were performed and equal amounts of protein immunoblotted against GFP, GAS2L3 and A-tubulin as loading control. Mut 3, 4 and 5 can be easily overexpressed and are not degraded by the proteasome. WT GAS2L3, mut 1 and mut 2 show only a weak overexpression, but significantly elevated protein amounts can be detected after MG132 treatment.

3.6 Immunoblot analysis of endogenous GAS2L3 protein

To detect endogenous GAS2L3 protein I performed immunoprecipitation and immunoblot analysis. Since it is known from gene expression experiments that *GAS2L3* transcription is highly regulated during the cell cycle (Fig. 3.2 C), I synchronized HeLa cells in different cell stages. By adding thymidine, HeLa cells were synchronized at the G1/S border, RO 3306, a specific Cdk1 inhibitor, blocked cells in the late G2 phase and nocodazole treatment, a spindle poison, arrested cells in early mitosis due to an activated spindle assembly checkpoint. Additionally, I transfected cells with siRNA against GAS2L3 and control and treated one sample either with or without 20 μ M MG132 for 9 hours. As positive control, I overexpressed full length EGFP-GAS2L3 and treated those cells also with MG132.

I performed whole cell lysates 48 hours after transfection and immunoprecipitated all samples with a monoclonal GAS2L3 antibody followed by immunoblotting with the same antibody. Figure 3.15 clearly shows the successful overexpression of full length EGFP-GAS2L3. Additionally, two EGFP-GAS2L3 degradation products were visible at the size of approx. 50 and 40 kDa. Unfortunately, no endogenous GAS2L3 could be detected in any of the samples. Immunoblotting against Actin served as a loading control.

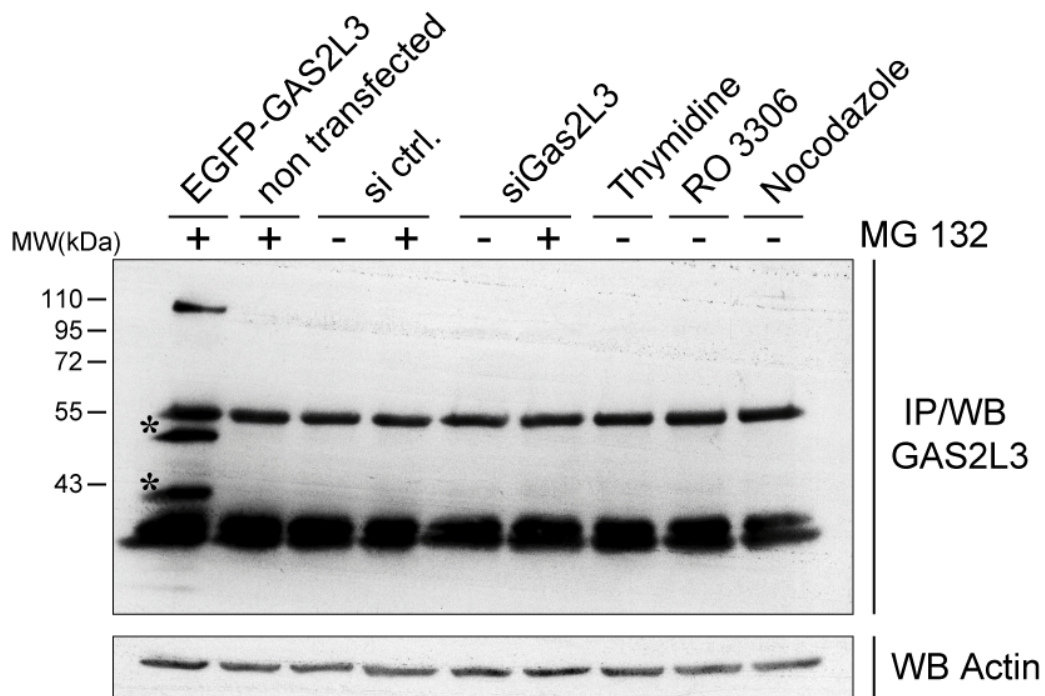


Fig. 3.15. Endogenous GAS2L3 protein cannot be detected by immunoblot analysis

After indicated treatment of HeLa cells, whole cell lysates were immunoprecipitated with a monoclonal GAS2L3 antibody followed by immunoblotting with the same antibody. Successful overexpression of 30 μ g EGFP-GAS2L3 is shown in the first lane. Endogenous GAS2L3 is not detectable in any of the other lanes. * EGFP-GAS2L3 degradation products

3.7 Biological relevance

Subcellular localization of GAS2L3 suggested that it might be a regulator of mitosis and cytokinesis (Fig. 3.8). A possible function in mitosis and cytokinesis can be tested by depleting the protein followed by cell cycle distribution analysis. For example, depletion of master regulators of cytokinesis leads to an enrichment of binucleated cells, which can be easily observed by either FACS analysis or microscopic examination of single cells.

3.8 GAS2L3 depletion under physiological conditions

To address this question, I designed three different short interfering RNAs (siRNA) to specifically deplete *GAS2L3*. First, I tested the efficiency of *GAS2L3* depletion by the designed siRNAs. HeLa cells were transfected with the three siRNAs against *GAS2L3* and a control siRNA. After 48 hours, I harvested RNA and quantified *GAS2L3* mRNA levels of *GAS2L3* depleted cells compared to control cells by qRT-PCR. Since *GAS2L1* shows high homology to *GAS2L3*, I additionally compared *GAS2L1* mRNA levels to exclude any off target effect.

All three siRNAs against *GAS2L3* (Gas2l3 si #1, #2, #3) were highly efficient and reduced *GAS2L3* mRNA levels between 80 % and 90 % compared to control cells (Fig. 3.16). Depletion of *GAS2L3* with si #1 and si #2 had no off target effect on *GAS2L1* RNA levels, whereas depletion with Gas2l3 si #3 slightly upregulated *GAS2L1* RNA levels (Fig. 3.16). Based on these results, I decided to use Gas2l3 si #2 for further experiments.

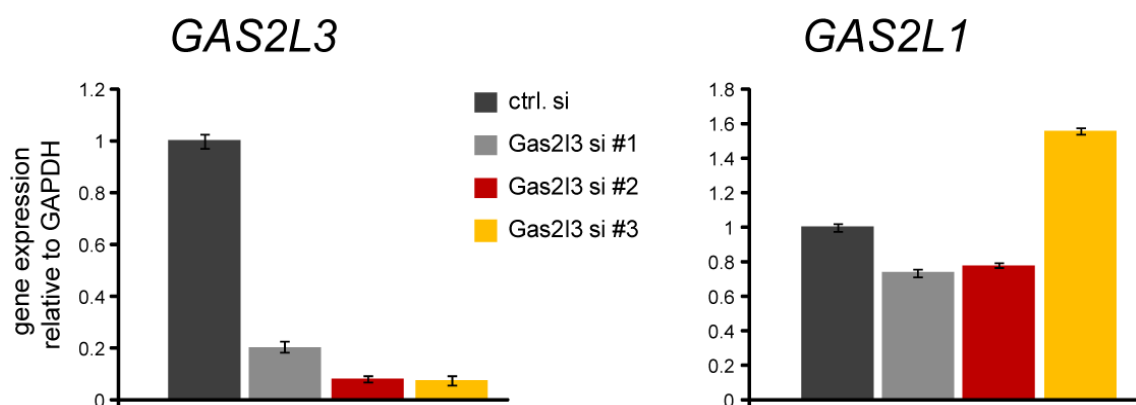


Fig. 3.16. Newly designed Gas2l3 siRNAs are highly efficient

HeLa cells were transfected with three different siRNAs against *GAS2L3* and control siRNA. After 48 h *GAS2L3* and *GAS2L1* mRNA levels were quantified by qRT-PCR.

Next, I depleted *GAS2L3* in asynchronously growing HeLa cells and also in the human non transformed fibroblast cell line BJ-ET to analyze the role of *GAS2L3* in cell division.

3.8.1 *GAS2L3* depletion in transformed cells

By siRNA transfection I depleted *GAS2L3* in asynchronously growing HeLa cells and investigated the cell cycle distribution by FACS analysis. There were no significant differences in cell cycle distribution 48 hours and 72 hours post transfection between control and *GAS2L3* depleted cells (Fig. 3.17 A). The efficiency of *GAS2L3* depletion was confirmed on RNA level by qRT-PCR (Fig.3.17 B).

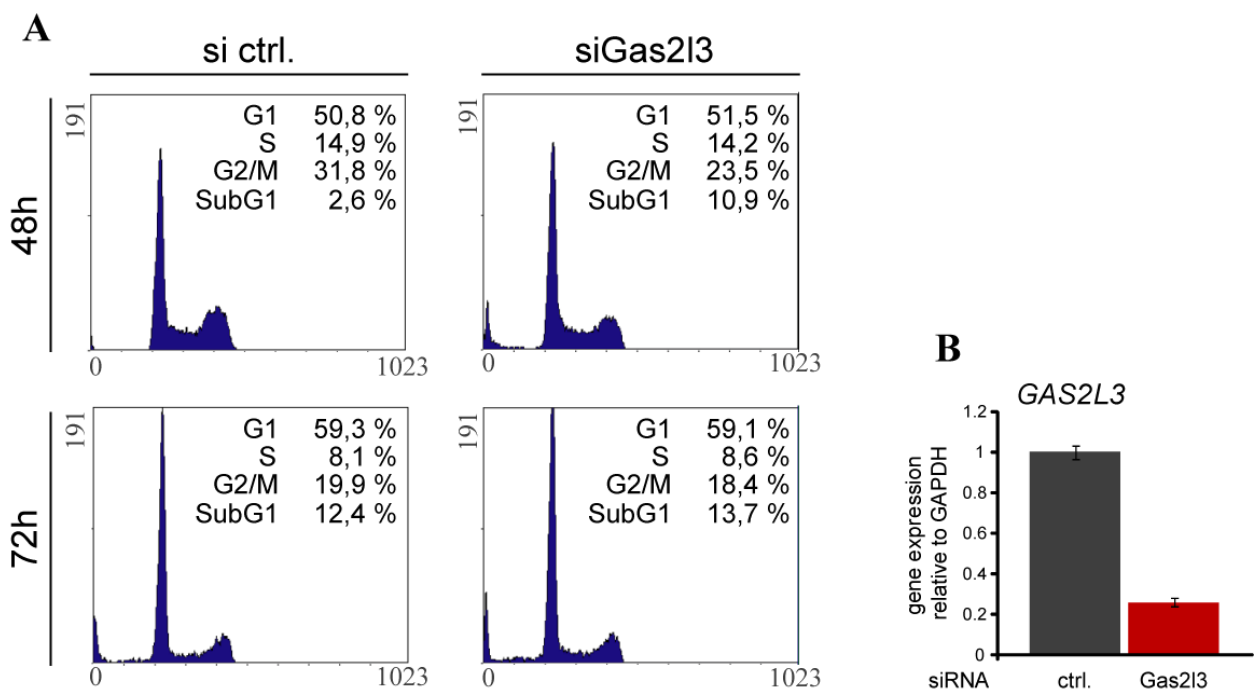


Fig. 3.17. *GAS2L3* depletion has no effect on cell cycle distribution in HeLa cells

HeLa cells were transfected with either siRNA control or siRNA Gas2l3. (A) FACS analysis was performed 48 h and 72 h post transfection. (B) *GAS2L3* knock down was confirmed on mRNA by qRT-PCR.

Since FACS analysis can only detect prominent differences in cell cycle distribution, I also investigated the phenotype of *GAS2L3* depleted cells by microscopic examination. I again transfected HeLa cells growing on coverslips with afore mentioned siRNAs, fixed the cells 24 hours after transfection and examined single cell morphology by staining with an A-tubulin antibody in green as a cytoskeleton marker and nuclei in blue with Hoechst. First, I counted cells in cytokinesis easily detectable by the A-tubulin staining. Figure 3.18 A shows a clear enrichment of cytokinesis in *GAS2L3* depleted cells (10 %) compared to control cells (4 %). The amount of multinucleated cells, i.e. cells with nuclei abnormalities like micronuclei or fragmented nuclei and binucleated cells was also quantified. Figure 3.18 B shows a clear enrichment of

multinucleated cells after GAS2L3 depletion (12 %) compared to control cells (4 %). Example photographs are shown in Figure 3.18 C.

Previous experiments in our lab demonstrated that the loss of LIN9 in MEFs leads to a significant enrichment in binucleated cells, suggesting that several LIN9 target genes are well known regulators of cytokinesis. To confirm this in human cells, I depleted LIN9 in HeLa cells and in parallel depleted GAS2L3. The fraction of micronucleated cells was counted 24 hours after transfection by microscopic examination. Additionally, I distinguished between micronucleated cells and binucleated cells. Both, the loss of LIN9 and the loss of GAS2L3 led to an increase in the fraction of abnormal nuclei compared to control transfected cells (Fig. 3.18 D). As expected, the loss of LIN9 led also in human cells to an increase in binucleated cells from under 1 % in control cells up to 8 %. In contrast, GAS2L3 depletion did not significantly alter the amount of binucleated cells (Fig. 3.18 D).

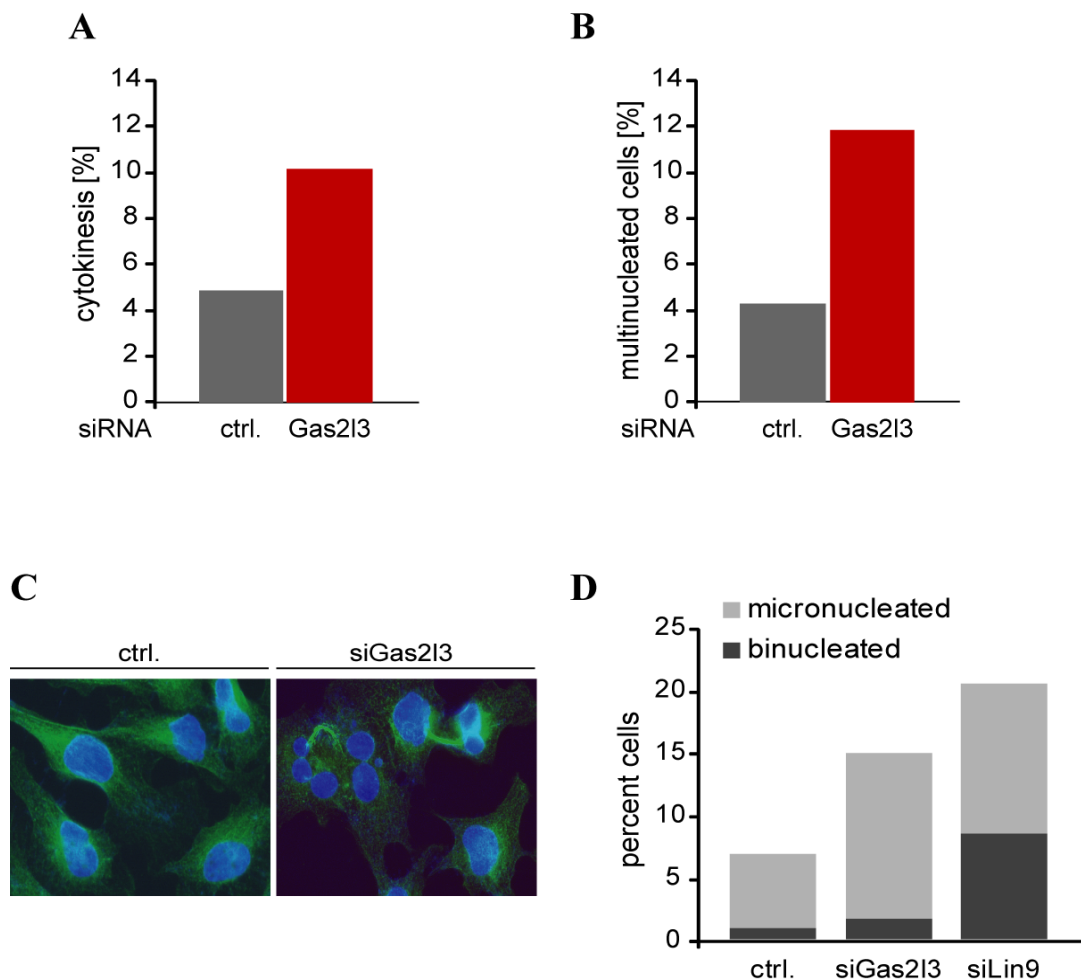


Fig. 3.18. GAS2L3 depletion induces enrichment of cytokinesis and multinucleated cells

HeLa cells were transfected with either siRNA control or siRNA Gas2l3 or Lin9. Cells were fixed with PFP 24 h after transfection followed by A-tubulin staining in green. Nuclei were visualized by Hoechst staining in blue. Amount of cytokinesis and multinucleated cells were calculated by microscopic examination of single cells. (A) GAS2L3 depletion increases the amount of cytokinesis and (B) multinucleated cells. (C) Example photographs showing fragmented nuclei and cytokinesis in GAS2L3 depleted cells. (D) LIN9 depletion leads to a significant enrichment of binucleated cells, whereas GAS2L3 depletion does not.

3.8.2 GAS2L3 depletion in untransformed cells

I next investigated the phenotype after GAS2L3 depletion in the human diploid foreskin fibroblast cell line BJ-ET. BJ-ET cells are not transformed and immortalized by overexpressing human telomerase (hTERT). Additionally the ecotropic receptor is stably integrated into their genome, which allows infection with murine viruses.

After depletion of GAS2L3 in asynchronously growing BJ-ET cells, I analyzed cell cycle distribution by FACS analysis. There were no significant differences in cell cycle distribution 48 hours and 72 hours post transfection between control and GAS2L3 depleted cells (Fig. 3.19 A). The efficiency of *GAS2L3* depletion was confirmed on RNA level by qRT-PCR (Fig 3.19 B).

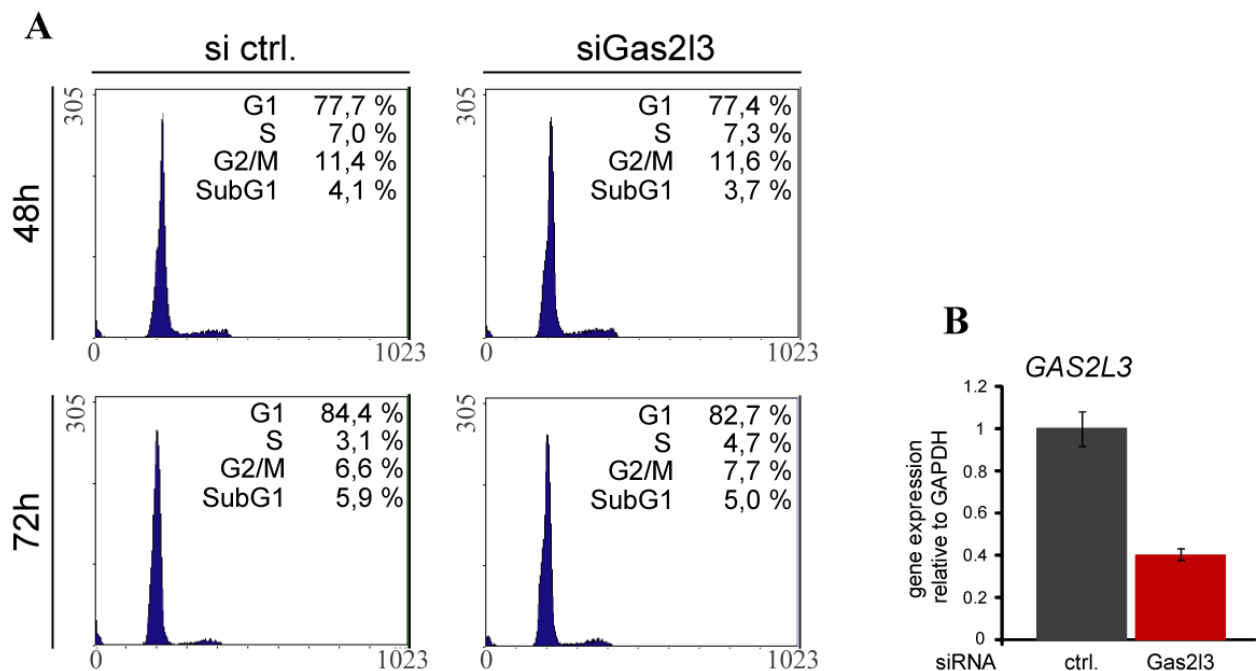


Fig. 3.19. GAS2L3 depletion has no effect on cell cycle distribution in BJ-ET cells

BJ-ET cells were transfected with either siRNA control or siRNA Gas2l3. (A) FACS analysis was performed 48 h and 72 h post transfection. (B) *GAS2L3* knock down was confirmed on mRNA by qRT-PCR.

FACS analysis of BJ-ET cells also revealed that most of the cells are in the G1 phase of the cell cycle due to a very slow proliferation rate of non transformed primary cells (Fig. 3.19 A). Hence, it is not possible to make any statement about the proliferation ability of BJ-ET cells by simple FACS analysis. To investigate, if GAS2L3 depletion has an effect on the proliferation rate of primary cells, I established a stable GAS2L3 depleted BJ-ET cell line.

To do so, I infected BJ-ET cells with retroviruses encoding for a short hairpin RNA (shRNA) against *GAS2L3* or an unspecific control sequence and a blasticidin resistance cassette. After infection I selected the cells for 7 days with 5 µg/ml blasticidin. Afterwards the efficiency of *GAS2L3* depletion was confirmed on RNA level by qRT-PCR. Stable *GAS2L3* depleted cells showed a reduction in *GAS2L3* mRNA of approximately 60 % (Fig. 3.20 A). To analyze the proliferation behavior of *GAS2L3* depleted cells (shGas2l3) compared to control cells (ctrl.), I performed a cumulative proliferation curve over 10 days. I plated 1×10^5 cells in triplicates, counted the cells every 3 days and replated again 1×10^5 cells. Total cell numbers were calculated and plotted against time. *GAS2L3* depleted cells showed a slight decrease in their proliferation rate compared to control cells (Fig. 3.20 B).

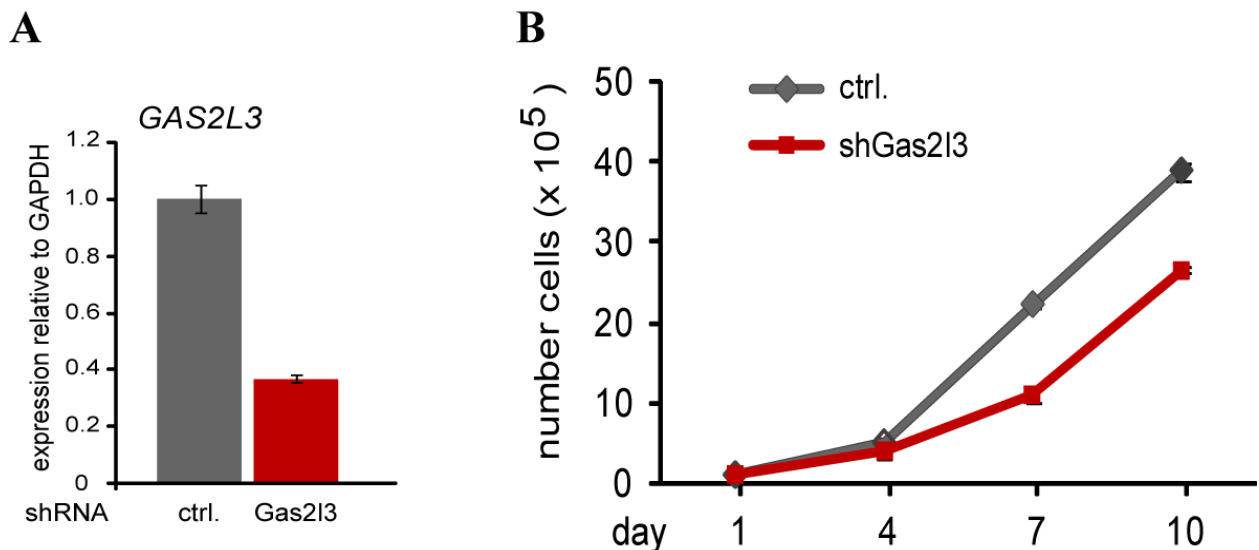


Fig. 3.20. Stable *GAS2L3* depletion leads to reduced proliferation of BJ-ET cells

BJ-ET cells were infected with control or shRNA-virus against *GAS2L3*. (A) *GAS2L3* knock down was confirmed on mRNA by qRT-PCR. (B) Cumulative growth curve of control cells and *GAS2L3* depleted cells.

3.9 *GAS2L3* depletion after induction of mitotic stress

Failure in chromosome segregation during mitosis can lead to aneuploidy which in turn is known to promote tumor formation. An indispensable checkpoint for proper chromosome segregation during early mitosis is the spindle assembly checkpoint (SAC) (s. 1.1.3). SAC components share distinct mitotic localizations in early mitosis, typically at the mitotic spindle, the centrosomes or the centromeres (Ciliberto and Shah, 2009). Since I could detect *GAS2L3* also at the mitotic spindle (Fig. 3.8) and the depletion of *GAS2L3* led to an increase of multinucleated cells (Fig. 3.18), I next wanted to analyze a possible role for *GAS2L3* in the SAC.

3.9.1 Spindle assembly checkpoint activation by nocodazole

The SAC consists of two arms, one arm monitoring correct attachment of spindle microtubules to single kinetochores, the other arm monitoring proper tension between the mitotic spindle apparatus and attached chromosomes (Skoufias et al., 2001; Taylor et al., 2001; Waters et al., 1998). The microtubule poison nocodazole completely abolishes mitotic spindle formation by depolymerization of microtubules and hence, activates the SAC by a complete loss of attachment (Peterson and Mitchison, 2002).

3.9.1.1 SAC activation over time

To investigate a possible role for GAS2L3 in the SAC, I treated GAS2L3 depleted or control HeLa cells with 150 ng/ml nocodazole for up to 30 hours. At indicated time points, I harvested cells for analysis of phosphorylated histone H3 (pH3) by FACS measurement and Western Blotting (Fig.3.21 A). Histone H3 gets specifically phosphorylated between late G2 phase and early mitosis and after cells bypass metaphase it is rapidly dephosphorylated. Therefore, it is a marker for cells arrested in metaphase due to an activated SAC (Wei et al., 1999).

As expected, after nocodazole treatment, control cells accumulated to a high percentage pH3 positive cells due to an activated SAC (Fig. 3.21 B). After 15 hour treatment the maximum of control cells had reached metaphase (between 60 % and 70 %) and persisted there until 24 hour treatment. Between 24 hour and 30 hour treatment control cells overcame the SAC, indicated by a decrease in pH3 positive cells to about 40 % (Fig. 3.21 B). Between 8 hour and 24 hour treatment GAS2L3 depleted cells first accumulated to the same extent in mitosis as control cells (Fig. 3.21 B). Strikingly, between 24 hour and 30 hour treatment GAS2L3 depleted cells overcame the SAC faster, indicated by a decrease in pH3 positive cells to 25 % compared to 40 % of control cells (Fig. 3.21 B). GAS2L3 depletion was confirmed on RNA level by qRT-PCR (Fig.3.21 C).

It is known that SAC slippage occurs due to a leaky inhibition of APC/C^{CDC20} by MAD2/BUBR1 complexes over time. APC/C^{CDC20}, as a specific mitotic E3 ubiquitin ligase, leads in turn to Cyclin B1 and Securin degradation following initiation of anaphase and chromosome segregation (Brito and Rieder, 2006). Therefore, I additionally investigated total amounts of Cyclin B1 and Securin protein levels by Western Blot analysis. Both proteins get faster degraded in GAS2L3 knock down cells compared to control cells (Fig. 3.21 D). The strongest effect was seen after 24 hour treatment (Fig. 3.21 D), the time point where also the SAC slippage occurred (Fig. 3.21 C). To exclude any off target effects by siRNA transfection against GAS2L3, I also analyzed total MAD2 protein levels. There was no difference in total MAD2 protein amount between control and GAS2L3 depleted cells (Fig. 3.21 D). Immunoblot against Actin served as a loading control.

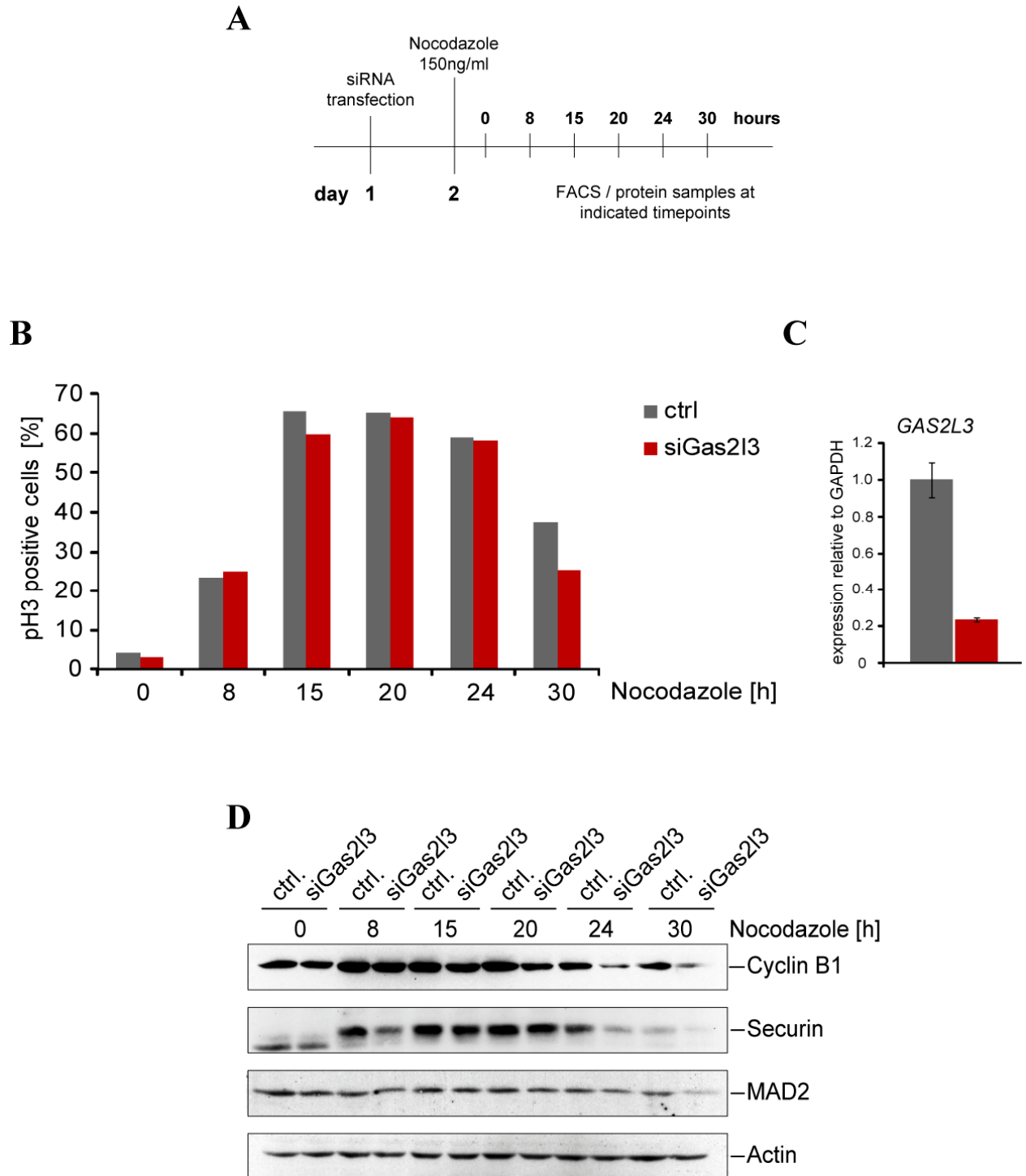


Fig. 3.21. GAS2L3 depletion leads to a weakened SAC after nocodazole treatment

GAS2L3 depleted and control HeLa cells were treated with 150 ng/ml nocodazole for the indicated time points followed by pH3 FACS analysis and Western Blot analysis. (A) Diagram of the experimental set up (B) pH3 FACS analysis shows faster SAC slippage of GAS2L3 depleted cells between 24 h and 30 h nocodazole treatment. (C) GAS2L3 knock down is confirmed on RNA level by qRT-PCR. (D) Immunoblot analysis of Cyclin B1 and Securin shows faster degradation of those proteins in GAS2L3 depleted cells. Total MAD2 protein levels are not affected by siRNA Gas2l3.

3.9.1.2 SAC recovery assay

To confirm aforementioned results of a weakened SAC after GAS2L3 depletion, I additionally performed a SAC recovery assay in HeLa cells. I treated GAS2L3 knock down cells with 100 ng/ml nocodazole. After 15 hours nocodazole treatment, I harvested mitotic cells by mechanical shake-off, thoroughly washed the cells and replated cells in fresh media without nocodazole. After indicated time points I harvested cells for pH3 FACS analysis (Fig.3.22 A).

GAS2L3 depleted cells, like control cells, initially accumulated to the same extent in mitosis indicated by 80 % pH3 positive cells at the 0 hour time point (Fig. 3.22 B). After replating, GAS2L3 depleted cells left early mitosis faster than control cells, confirming premature inactivation of the SAC in those cells (Fig. 3.22 B).

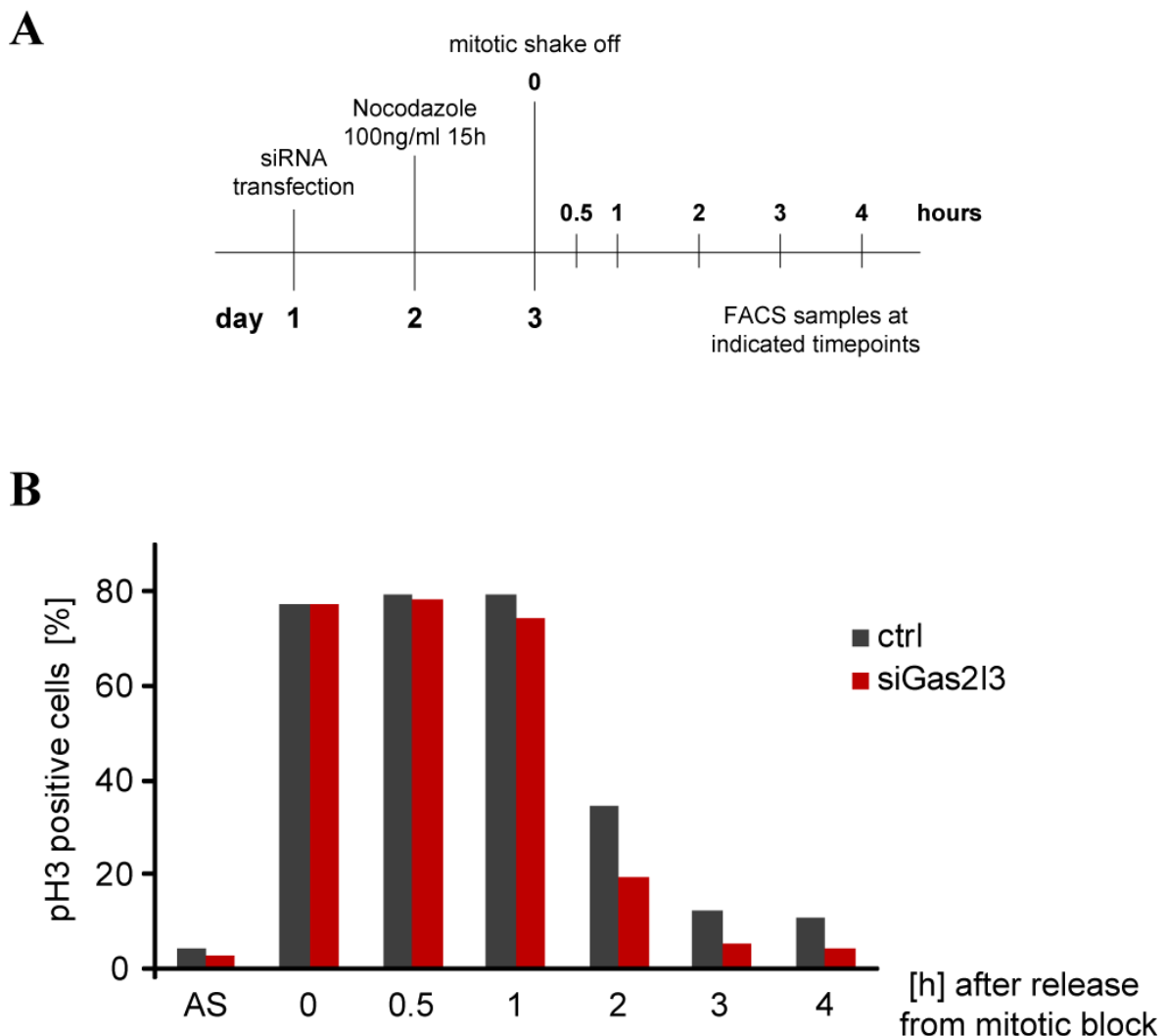


Fig. 3.22. GAS2L3 depleted cells show faster SAC recovery

GAS2L3 depleted and control HeLa cells were treated with 100 ng/ml nocodazole. After 15 h, mitotic cells were harvested by mechanical shake-off and replated in media without nocodazole. PH3 FACS analysis was performed for the indicated time points. (A) Diagram of the experimental set up (B) GAS2L3 depleted cells show faster SAC recovery indicated by a faster decrease in pH3 positive cells after replating.

3.9.2 Spindle assembly checkpoint activation by Taxol

The microtubule poison taxol leads to hyperstabilization of microtubules (Peterson and Mitchison, 2002). In that case, the mitotic spindle can properly develop, but the spindle dynamic is completely disturbed. This in turn activates the SAC by a loss of tension.

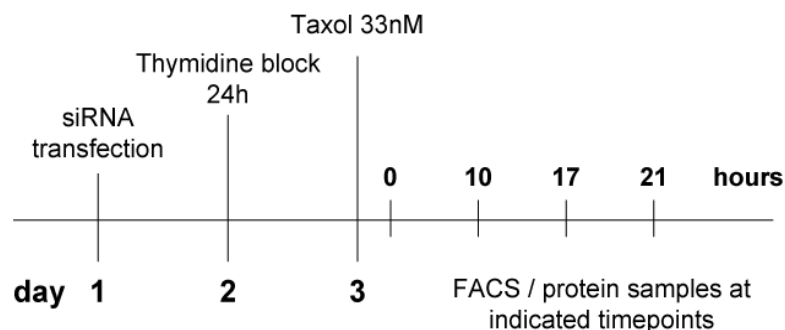
3.9.2.1 SAC activation over time

To monitor SAC activation induced by loss of tension in GAS2L3 deficient HeLa cells, I treated the cells with taxol. After GAS2L3 depletion, I first synchronized cells at the G1/S border by a single thymidine block for 24 hours. Afterwards I started with 33 nM taxol treatment for indicated time points and harvested cells for pH3 FACS analysis and Western Blot analysis (Fig. 3.23 A).

At no time point after taxol treatment, GAS2L3 deficient cells reached the amount of pH3 positive control cells (Fig. 3.23 B). Whereas control cells reached a maximum of 45 % pH3 positive cells after 17 hour treatment, only 25 % of cells were pH3 positive in GAS2L3 depleted cells at this time, indicating a weakened SAC upon depletion of GAS2L3 (Fig. 3.23 B).

Additionally, I investigated total protein amounts of Cyclin B1 and Securin by immunoblot analysis. As was observed after nocodazole treatment (Fig. 3.21 D), Securin and Cyclin B1 were degraded faster in GAS2L3 depleted cells compared to control cells (Fig. 3.23 C). Immunoblot analysis of MAD2 revealed no difference in total protein amount between control and GAS2L3 depleted cells, excluding an off target effect of siGas2l3 on *MAD2* RNA levels (Fig. 3.23 C). To validate this, I also investigated *MAD2* mRNA level by qRT-PCR, which was not affected upon GAS2L3 depletion (Fig. 3.23 D).

A



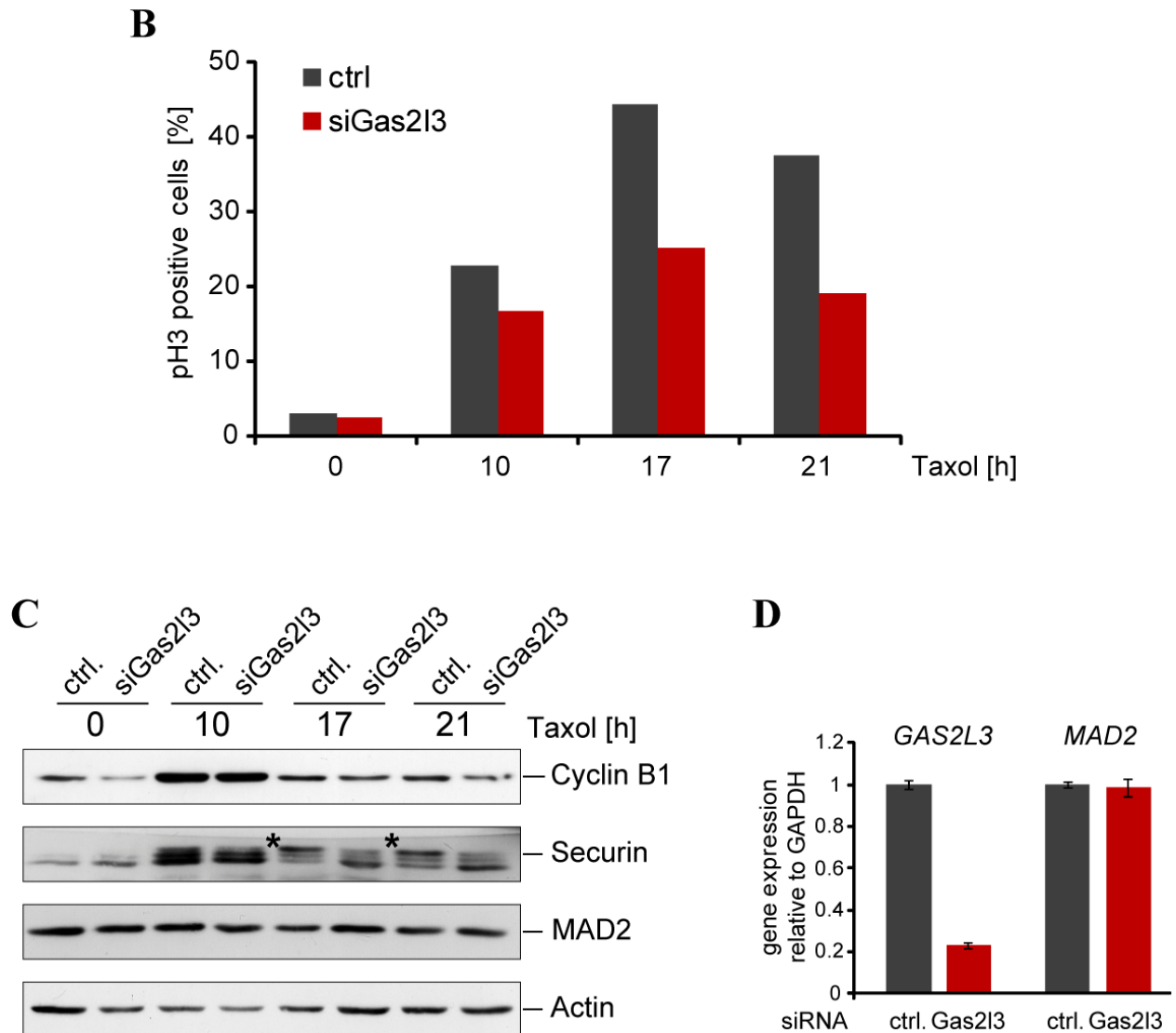


Fig. 3.23. GAS2L3 depletion leads to a highly weakened SAC after taxol treatment

GAS2L3 depleted and control HeLa cells were synchronized in G1/S by a single thymidine block for 24 h followed by 33 nM taxol treatment for the indicated time points. (A) Diagram of the experimental set up (B) GAS2L3 depleted cells do not reach the same amount of pH3 positive cells than control samples, indicating a highly weakened SAC. (C) Immunoblot analysis of Cyclin B1 and Securin shows faster degradation of those proteins in GAS2L3 depleted cells. Total MAD2 protein levels are not affected by siRNA Gas2L3. (D) qRT-PCR analysis of *GAS2L3* and *MAD2* RNA confirms specificity of siRNA against *GAS2L3*.

3.9.3 Mechanism behind a compromised SAC

Previous experiments demonstrated that GAS2L3 depleted cells, after nocodazole and taxol treatment, show a weakened SAC (Fig.3.21, 3.22, 3.23). An important question to answer is the upstream mechanism leading to the compromised SAC upon GAS2L3 depletion. Therefore, I next analyzed the protein characteristics of MAD2 and BUBR1 after GAS2L3 depletion, two important proteins regarding SAC functionality.

3.9.3.1 MAD2 protein characterization after GAS2L3 depletion

Ubiquitination of Securin and Cyclin B1 by the APC/C^{CDC20} complex leads to their degradation by the proteasome. After SAC activation, MAD2 binding to CDC20 inhibits APC/C^{CDC20} complex formation. A prerequisite for MAD2/CDC20 interaction is the relocalization of MAD2 to kinetochores after SAC activation. Hence, the SAC can be weakened due to a premature loss of MAD2/CDC20 interaction or due to an insufficient MAD2 kinetochore localization. Even though total protein amount of MAD2 was not affected by GAS2L3 depletion (Fig. 3.21, 3.23), differences in MAD2 kinetochore localization or in MAD2/CDC20 interaction potential are still possible.

3.9.3.1.1 MAD2 kinetochore localization after taxol treatment

To investigate if MAD2 is able to localize to kinetochores after SAC activation in GAS2L3 depleted cells, I synchronized HeLa cells in G1/S following treatment with 33 nM taxol for 8 hours. After fixation, GAS2L3 depleted and control cells were stained with an antibody against MAD2 in red and counterstained with an antibody against A-tubulin in green. Nuclei were visualized in blue by Hoechst staining.

Control cells, as well as GAS2L3 depleted cells showed a clear enrichment of MAD2 protein at the kinetochores in cells arrested in mitosis due to an activated SAC (Fig. 3.24). Notable, no conclusion can be made about possible quantitative differences in kinetochore bound MAD2 from this experiment.

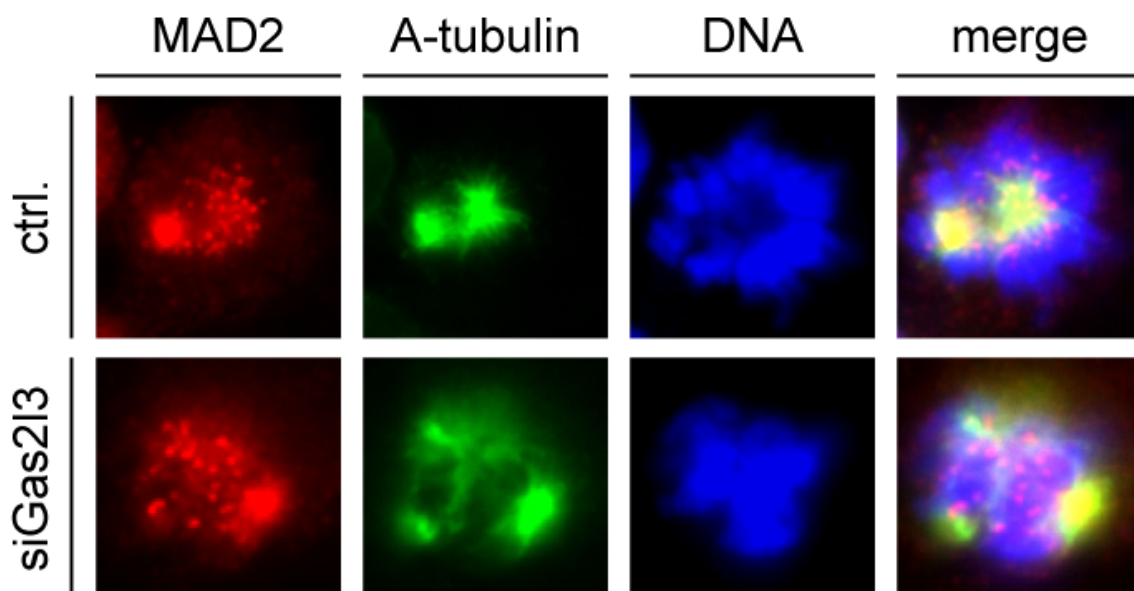


Fig. 3.24. MAD2 can still localize to kinetochores in GAS2L3 depleted cells

G1/S synchronized GAS2L3 depleted HeLa cells were treated with 33 nM taxol for 8 h, fixed with PSP and immunostained for MAD2 in red and A-tubulin in green. Nuclei were visualized in blue by Hoechst staining. Cells arrested in mitosis were analyzed for kinetochore bound MAD2.

3.9.3.1.2 *MAD2/CDC20 interaction after taxol treatment*

Next, I analyzed MAD2/CDC20 interaction after the loss of GAS2L3 in HeLa cells following SAC activation by taxol treatment. G1/S synchronized GAS2L3 depleted cells were treated with 33 nM taxol and protein samples were harvested at the indicated time points. Whole cell lysates were immunoprecipitated with a specific CDC20 antibody followed by immunoblotting against MAD2. Corresponding input samples were immunoblotted against MAD2 and CDC20 (Fig. 3.25).

Binding of MAD2 to CDC20 was indeed significantly reduced in GAS2L3 depleted cells 14 hours and 25 hours after taxol treatment, even though MAD2 input protein amounts were equal (Fig. 3.25). Importantly, the amount of immunoprecipitated and input CDC20 protein was not affected by GAS2L3 depletion (Fig. 3.25). Faster degradation of Cyclin B1 and Securin total protein amounts confirmed the premature SAC inactivation in GAS2L3 depleted cells (Fig.3.25).

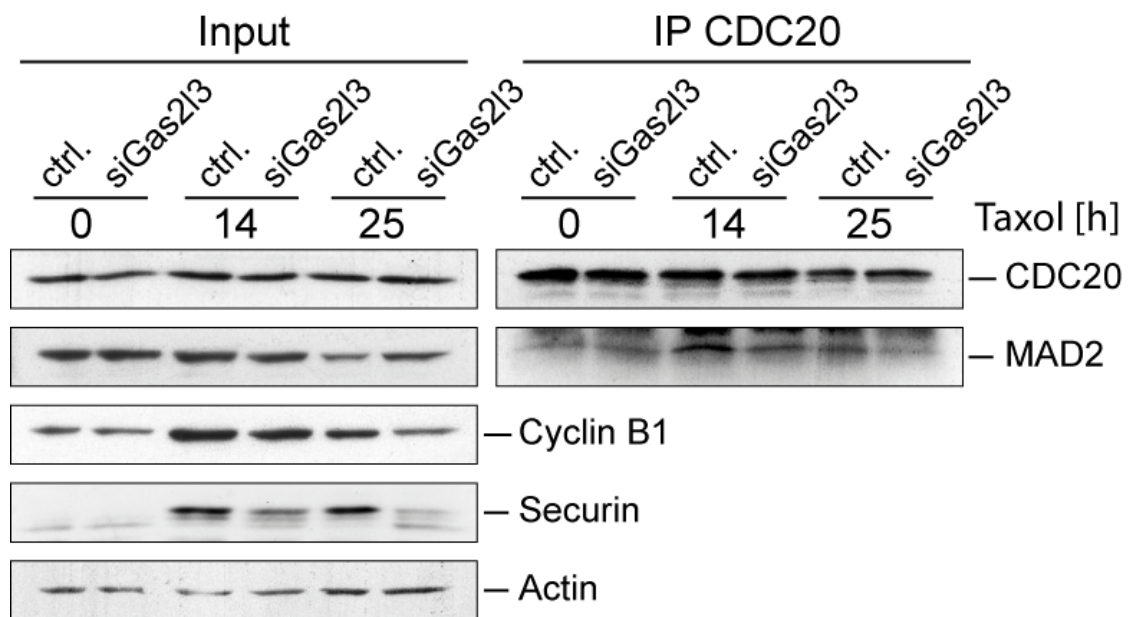


Fig. 3.25. MAD2/CDC20 interaction is compromised in GAS2L3 depleted cells

GAS2L3 depleted and control HeLa cells were synchronized in G1/S by a single thymidine block for 24 h followed by 33 nM taxol treatment for the indicated time points. Whole cell lysates were immunoprecipitated with a CDC20 antibody and bound MAD2 was detected by immunoblot. Corresponding input samples were immunoblotted against indicated proteins.

3.9.3.2 *BUBR1 protein characterization after GAS2L3 depletion*

The protein kinase BUBR1 gets extensively phosphorylated during mitosis which correlates with BUBR1 activity. On one hand, BUBR1 localizes to some extent to kinetochores during prometaphase and controls correct kinetochore microtubule attachment (Ditchfield et al., 2003; Lampson and Kapoor, 2005). On the other hand, direct binding to CDC20 makes this protein

also an important and indispensable inhibitor of APC/C^{CDC20} (Li et al., 1999; Wu et al., 2000). As well as for MAD2, I investigated total BUBR1 protein levels and also BUBR1/CDC20 interaction after taxol treatment in GAS2L3 depleted cells. Additionally, I checked for the possibility of BUBR1 kinetochore localization in GAS2L3 knock down cells.

3.9.3.2.1 *BUBR1 kinetochore localization*

To investigate if BUBR1 is still able to localize to kinetochores after GAS2L3 depletion, I stained GAS2L3 depleted asynchronously growing and G1/S synchronized taxol treated HeLa cells with an antibody against BUBR1 in red. Nuclei were visualized in blue by Hoechst staining. In asynchronously growing HeLa cells, I monitored different mitotic stages for kinetochore bound BUBR1. In taxol treated HeLa cells, I analyzed for the ability of BUBR1 kinetochore localization upon SAC activation.

No obvious differences in BUBR1 localization could be seen between control and GAS2L3 depleted cells (Fig. 3.26). BUBR1 localizes to kinetochores in the beginning of prometaphase and remains there during whole metaphase. As soon as the SAC is satisfied and cells enter anaphase to separate their chromatids, BUBR1 disappears from kinetochores (Fig. 3.26). Also GAS2L3 depleted cells showed a clear enrichment of BUBR1 at the kinetochores in cells arrested in mitosis due to an activated SAC (Fig. 3.26). Notable, no conclusion can be made about possible quantitative differences in kinetochore bound BUBR1 from this experiment.

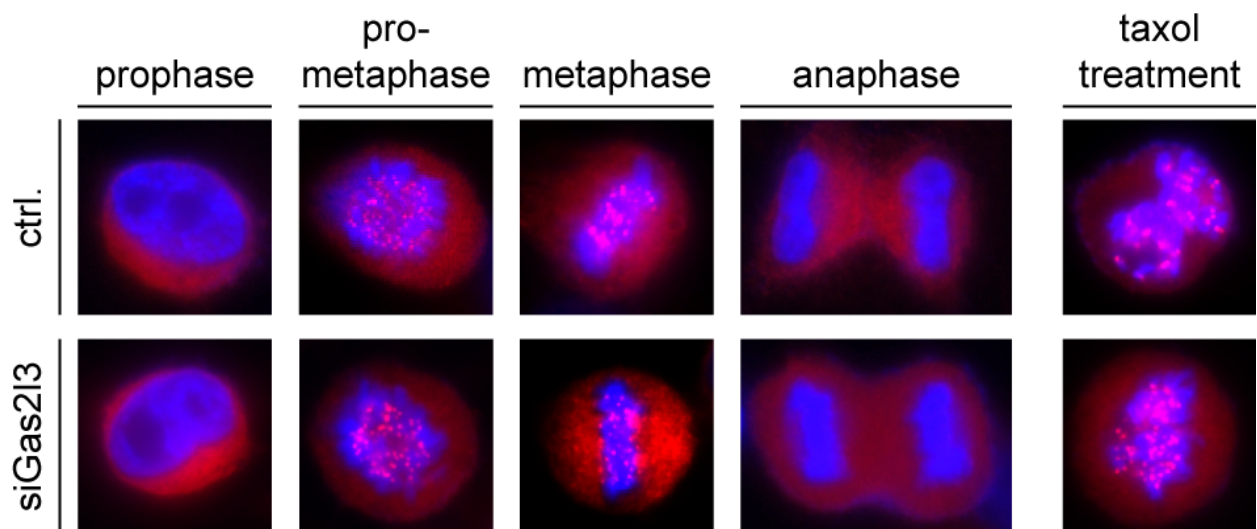


Fig. 3.26. BUBR1 can still localize to kinetochores in GAS2L3 depleted cells

Asynchronously and G1/S synchronized taxol (33 nM; 8 h) treated GAS2L3 depleted HeLa cells were fixed with PSP followed by immunostaining of BUBR1 in red. Nuclei were visualized in blue by Hoechst staining and different mitotic stages were examined for BUBR1 kinetochore localization.

3.9.3.2.2 *BUBR1* protein levels after taxol treatment

To analyze if BUBR1 protein is affected by GAS2L3 depletion, I treated G1/S synchronized HeLa cells with 33 nM taxol and harvested protein samples at indicated time points. Whole cell lysates were immunoprecipitated with a specific CDC20 antibody followed by immunoblotting against BUBR1. Corresponding input samples were immunoblotted against BUBR1 and CDC20 (Fig. 3.27).

The BUBR1 immunoblot clearly demonstrated changes in BUBR1 migration due to phosphorylation of BUBR1 after mitotic entry, visible by the upper band appearing after 12 hour taxol treatment (Fig.3.27). Strikingly, BUBR1 became less efficiently phosphorylated in GAS2L3 depleted cells compared to control cells between 12 hour and 16 hour treatment. Since already phosphorylated BUBR1 input levels varied between control and GAS2L3 knock down cells, differences in CDC20/BUBR1 interaction after GAS2L3 depletion were not due to a compromised binding potential (Fig. 3.27).

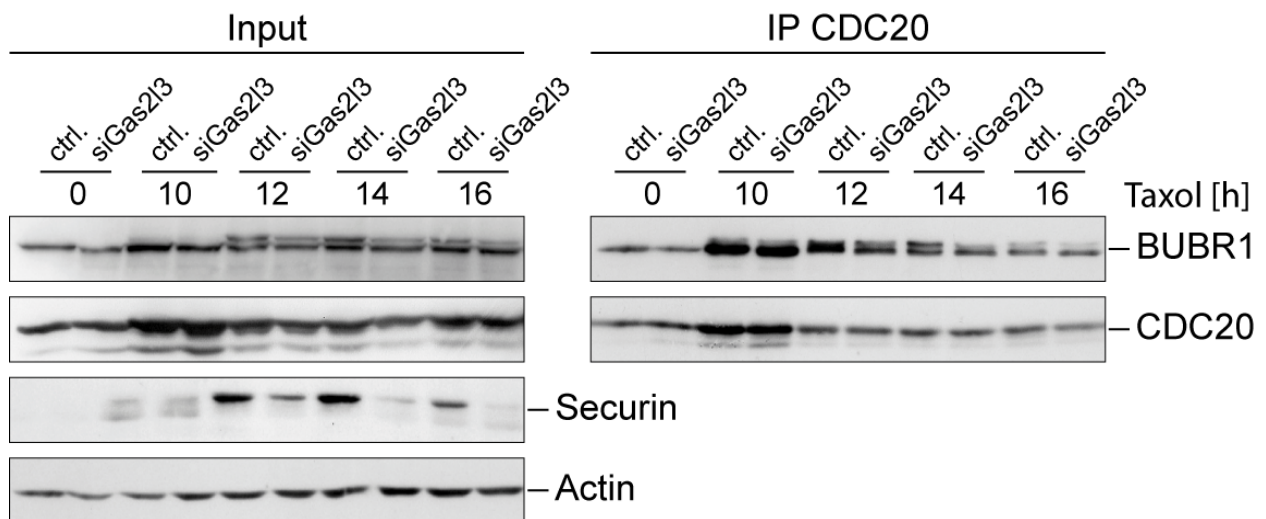


Fig. 3.27. BUBR1 phosphorylation is compromised after GAS2L3 depletion

GAS2L3 depleted and control HeLa cells were synchronized in G1/S by a single thymidine block for 24 h followed by 33 nM taxol treatment for the indicated time points. Whole cell lysates were immunoprecipitated with a CDC20 antibody and bound BUBR1 was detected by immunoblot. Corresponding input samples were immunoblotted against indicated proteins.

4 DISCUSSION

4.1 Characterization of GAS2L3

Failure during mitosis results in the loss of genomic integrity which is known to promote tumorigenesis. Hence, the identification of new G2/M regulatory genes still attracts great attention.

To identify putative new mitotic regulators our lab performed genome wide microarray analysis from *Lin9* depleted MEFs (Reichert et al., 2010). LIN9, a core protein of the LIN complex, is a transcriptional activator of G2/M specific genes (Osterloh et al., 2007; Schmit et al., 2007). The top hit of LIN9 activated genes in MEFs was *Gas2l3*, a so far completely uncharacterized member of the family of growth arrest specific 2 genes. This work addressed the biochemical as well as biological characterization of GAS2L3 in human cells.

4.2 *GAS2L3* is a G2/M regulated LINC target gene

GAS2L3 gene expression was strongly inhibited in LIN9 and LIN54 depleted HeLa cells (Fig. 3.1 A & B), indicating that *GAS2L3* is also a LINC target gene in human cells. The same result was obtained upon LIN9 depletion in the non transformed human fibroblast cell line BJ-ET (Fig. 3.1 C).

GAS2L3 belongs to the GAS2 family of genes, which were originally identified to be transcriptionally activated in growth arrested MEFs (Schneider et al., 1988). Therefore, the next important question was the transcriptional regulation of *GAS2L3* during the cell cycle in human cells. Strikingly, transcriptional activation of *GAS2L3* gene expression started in the S phase and reached its maximum when most of the cells were in G2/M (Fig. 3.2). This G2/M specific gene expression was completely inhibited in LIN9 depleted cells (Fig. 3.3). In contrast, none of the other GAS2 family members showed a similar gene expression profile (Fig. 3.2). All together, these data confirm that *GAS2L3*, unlike the other GAS2 family members, is a bona fide G2/M activated LINC target gene in human cells.

4.3 *GAS2L3* localization during the cell cycle

The G2/M specific expression pattern argued for a possible role of *GAS2L3* in mitosis. To get more information about a possible biological function of *GAS2L3*, I next investigated its localization during the cell cycle. The fact that *GAS2L3* contains the highly conserved CH and GAS2 domain (Fig. 1.4) raised suspicion that *GAS2L3* might function as a cytoskeletal linker protein, connecting and coordinating microfilaments and microtubules (s. 1.3.1.1).

4.3.1 GAS2L3 colocalizes with and stabilizes the interphase microtubule network

During interphase, in a small fraction of cells nuclear localization of EGFP-GAS2L3 was observed (Fig. 3.4 A). However, in most of the interphase cells GAS2L3 was cytoplasmatic and colocalized with the microtubule network (Fig. 3.4 A). Additionally, microtubules in EGFP-GAS2L3 expressing cells were more resistant to depolymerization than those in control cells. Therefore, overexpressed GAS2L3 is not only able to colocalize with, but also stabilizes microtubules (Fig. 3.4 C). These observations were the first hint that the GAS2 domain of GAS2L3 might indeed function as a microtubule binding domain.

4.3.2 GAS2L3 colocalizes with the mitotic microtubule network

During mitosis, overexpressed GAS2L3 also colocalized with the microtubule network. In prometaphase, GAS2L3 was diffusely expressed in the whole cell but slightly enriched at microtubule spindle poles from where the mitotic spindle is built up (Fig. 3.7 A & 3.8 A). In metaphase, GAS2L3 clearly localized to the minus ends of the mitotic spindle microtubules (Fig. 3.7 B & 3.8 B). In the beginning of anaphase, when Aurora B migrated to the spindle midzone, GAS2L3 was still enriched at the minus ends of the mitotic spindle microtubules. In late anaphase, also GAS2L3 relocated to some extent to spindle midzone microtubules (Fig. 3.7 C & 3.8 C). In contrast to Aurora B, which relocated to the central part of the spindle midzone, GAS2L3 was present more diffusely at the complete microtubule network of the whole spindle midzone. Interestingly, during telophase, GAS2L3 started to migrate from the spindle midzone microtubules to the midbody. The midbody in late telophase was the first structure where GAS2L3 and Aurora B showed a perfect colocalization (Fig. 3.7 D & 3.8 D). Also midbody localization was the first stage during mitosis, where GAS2L3 left the microtubule network.

4.3.3 GAS2L3 localizes to the midbody during cytokinesis

The midbody (MB) is a dense structure formed in telophase and derived from the central spindle and a massive number of recruited proteins (Fig. 1.3). Until the end of cytokinesis, the MB is the final bridge between the dividing cells. Many proteins of the MB, for example RhoA, Aurora B and Survivin, are well known master regulators of cytokinesis. Not surprisingly, disruption of those proteins leads to cytokinesis failure resulting in binucleated cells.

Co-staining of GAS2L3 with the well known MB component Survivin and the MBR (midbody ring) component RhoA validated GAS2L3 MB localization and defined GAS2L3 localization to the outer arms of the MB which embrace the MBR (Fig. 3.5). GAS2L3 MB localization was also confirmed in the two other cancer cell lines HCT 116 and T98G (Fig. 3.6).

Strikingly, also endogenous GAS2L3 was clearly detectable at the MB in HeLa cells (Fig. 3.9), confirming that GAS2L3 is indeed a member of the MB and a possible regulator of cytokinesis.

Even though overexpressed GAS2L3 localized to the mitotic microtubule network (Fig. 3.7 & 3.8), no endogenous GAS2L3 could be detected there. This might be due to a low antibody titer and / or a low concentration of GAS2L3 protein at those structures. As well, these results point out that high amounts of GAS2L3 protein seem to be present at the MB.

4.4 Characterization of GAS2L3 protein domains

To determine which protein domains are required for the specific localization pattern of GAS2L3, I overexpressed a series of EGFP-GAS2L3 deletion mutant constructs in HeLa cells and monitored their localization during the cell cycle (Fig. 3.10 A).

4.4.1 The GAS2 domain is neither needed nor sufficient for microtubule binding

Association of GAS2L3 to the cytoplasmic microtubule network was highly dependent on sequences in the C-terminus (Fig. 3.12). However, constructs containing additionally the GAS2 domain showed stronger overlap with the microtubule network, indicating that GAS2L3 has at least two microtubule binding domains (MBD): the GAS2 domain, which is already known as MBD, and a further domain in the C-terminus, so far not characterized. Both MBDs work cooperatively and are needed for proper microtubule colocalization.

Other experiments in our lab suggest that a second MBD is located between amino acids 455 and 535 (Kremling H, diploma thesis). However, predictive domain analysis with this amino acid sequence revealed no known MBD.

It is important to mention that the colocalization of proteins observed by immunofluorescence microscopy provides evidence but is not a proof for protein binding. To confirm that GAS2L3 binds to the microtubule network, other in vitro assays should be performed. For example, a simple assay is the microtubule (MT) spin down assay. This assay relies on the fact that MTs will pellet when centrifuged. Therefore, any protein that is associated with the MTs will pellet with them during centrifugation. A simple immunoblot analysis of the supernatant versus pellet fraction will identify if a protein is able to associate with MTs.

4.4.2 The CH domain is an actin binding domain

Overexpressing the mutants that contain only the CH domain or the CH and the GAS2 domain resulted in the prominent induction of and colocalization with actin stress fibers (Fig. 3.12 & 3.13 & 3.10 B). This indicates that the CH domain has the potential to function as an actin binding domain.

Remarkably, full length GAS2L3 protein never showed colocalization with the actin filament network. Therefore, it is possible that the CH domain of full length GAS2L3 is masked by an intramolecular interaction with the C-terminus. Even though such conformational regulation is poorly understood, it may have wide generality as it has been proposed for several proteins, for example for the cytoskeletal proteins vinculin and the ERM proteins (Johnson and Craig, 1994; Johnson and Craig, 1995; Pearson et al., 2000).

4.4.3 Only full length GAS2L3 localizes to the midbody

Interestingly, only full length GAS2L3 showed defined MB localization (Fig. 3.11 & 3.10 B). Deletion mutants lacking the CH domain or the CH and GAS2 domain could still diffusely localize to spindle midzone microtubules, whereas all mutants lacking the C-terminus even failed to localize to spindle midzone microtubules (Fig. 3.11 & 3.10 B). These results confirm that there must be at least one additional MBD in the C-terminus. The fact that only full length GAS2L3 shows defined MB localization argues for the importance of the actin binding CH domain. This is an interesting point, since I mentioned before that it is likely that the CH domain of GAS2L3 is masked by the C-terminus in interphase cells (s. 4.4.2). However, it might be possible that localization of GAS2L3 to the microtubule network during mitosis somehow leads to conformational changes which eventually unmask the CH domain during cytokinesis.

4.4.4 GAS2L3 is highly regulated on protein level

Protein levels of constructs containing the C-terminus were almost undetectable by immunoblot analysis (Fig. 3.14). However, treatment with the proteasome inhibitor MG132 significantly elevated their protein levels (Fig. 3.14). In contrast, constructs containing only parts of the N-terminus could be easily overexpressed and MG132 treatment had no effect on their protein levels (Fig. 3.14). All together these data indicate that GAS2L3 is highly regulated on protein level and this regulation is, at least partially, due to degradation by the proteasome. The signal for the proteasomal degradation must lie within the C-terminus. Experiments of Heidi Kremling (diploma thesis) suggest that the area responsible for proteasomal degradation is located between amino acids 375 and 455. However, predictive domain analysis with this amino acid sequence revealed no known degradation domains.

Full length GAS2L3 protein levels, even after MG132 treatment, never reached the amount of the stable N-terminus constructs (Fig. 3.14). Hence, it is likely that, beside the proteasomal degradation, other pathways affect GAS2L3 stability. Interestingly, in some experiments GAS2L3 degradation products or GAS2L3 cleaved fragments were visible, but only from constructs containing the C-terminus (Fig. 3.15 and data not shown). It might be possible that GAS2L3 is per se highly unstable and only stabilized by specific posttranslational modifications during particular cell cycle stages like mitosis. Well known posttranslational modifications which control many aspects of mitosis by regulating protein activity are protein phosphorylation and dephosphorylation. Recent work has highlighted the important role played by protein phosphatases in the regulation of mitosis and show that protein phosphatases are not merely silent partners to kinases (Trinkle-Mulcahy and Lamond, 2006). Master mitotic kinases are CDK1, PLK1 and Aurora B and the master phosphatases are PP1 and CDC25. Screening for predictive GAS2L3 mitotic phosphorylation sites identified four putative CDK1 sites in the C-terminus. However, site specific mutagenesis resulting in the disruption of those phosphorylation sites did neither alter protein stability nor protein localization to the midbody (data not shown).

Like phosphorylation, O-GlcNAc (O-linked-beta-N-acetylglucosamine) is a reversible modification of nuclear and cytoplasmic proteins and consists of the attachment of a single β -N-acetyl-glucosamine moiety to hydroxyl groups of serine or threonine residues. O-GlcNAc transferase (OGT) catalyzes the addition of the sugar moiety from the donor substrate to proteins (Hart et al., 2007). During M phase, OGT localizes to discrete structures, such as centrosomes in metaphase and the mitotic spindle in anaphase. During cytokinesis OGT localizes to the midbody along with O-GlcNAcase (OGA), the enzyme that removes the sugar. Interestingly, OGT overexpression in HeLa cells reduces the abundance of protein components of the chromosomal passenger complex at the midbody, resulting in an increase in polyploidy due to defective cytokinesis (Slawson et al., 2005; Wang et al., 2010). However, the identity of other OGT mitotic substrates is currently not known and it is tempting to speculate that GAS2L3 might be an OGT substrate.

To get information about the mechanism affecting GAS2L3 protein characteristics, posttranslational modification sites could be identified by mass spectrometry. However, one problem is that endogenous GAS2L3 could never be detected by IP/WB, even after cell synchronization in different cell cycle stages (Fig. 3.15). Given that immunofluorescence staining only detected endogenous GAS2L3 at the midbody (Fig. 3.9), it should be tested, if GAS2L3 could be detected by immunoblot analysis from purified midbodies.

4.5 Biological relevance: GAS2L3 is a regulator of mitosis and cytokinesis

Genes with mitotic functions such as Cyclin B, Aurora B and *PLK1* have similar transcriptional expression profiles during the cell cycle, as they are all induced in G2/M. In 2002 Whitfield et al. reported that 566 genes in the human transcriptome are induced in G2 or G2/M, and interestingly *GAS2L3* was found to be one of 30 novel genes with the best induction in G2/M (Whitfield et al., 2002).

Also in this work, *GAS2L3* gene expression profiles (Fig. 3.2 & 3.3) and subcellular localization of *GAS2L3* (Fig. 3.7 & 3.8) suggested that it might be a regulator of mitosis and cytokinesis.

4.5.1 GAS2L3 depletion results in mitosis and cytokinesis failure

Strikingly, *GAS2L3* depleted HeLa cells showed a significant enrichment in multinucleated cells, indicating failure during chromosome segregation in mitosis (Fig. 3.18 B). Additionally, I could observe an enrichment of cells in cytokinesis (Fig. 3.18 A). This might be an indicator for prolonged cytokinesis in *GAS2L3* depleted cells, perhaps due to failure during the last step of cytokinesis, the abscission.

Live cell imaging by time lapse microscopy (Kremling H, diploma thesis) showed that metaphase-anaphase transition was significantly shortened in *GAS2L3* depleted HeLa cells (16 min) compared to control cells (24 min). A shortened metaphase can result in chromosomal mis-segregation since cells have not enough time for correct alignment at the metaphase plate and bipolar kinetochore attachment. A high amount of *GAS2L3* depleted cells (22 % compared to 3.5 % of control cells) also showed defects in completing cytokinesis. Even though cells started cytokinesis properly, they could not complete cytokinesis and the already divided sister chromatids re-fused, often accompanied by nuclei de-fragmentation. Taken together, time lapse microscopy confirmed my results obtained by single cell examination, representing that *GAS2L3* is essential for proper M phase progression.

Depletion of master regulators of cytokinesis, for example Anillin or the chromosomal passenger protein INCENP (inner centromere protein), result typically in an increase of binucleated cells, which can be easily observed in elevated amounts of G2/M cells by FACS analysis (Oegema et al., 2000; Zhao and Fang, 2005; Zhu et al., 2005a). Binucleated cells arise from failure during the last step of cytokinesis, the abscission of the cytoplasmic membrane in two daughter cells.

Even though mitosis and cytokinesis failure induced by *GAS2L3* depletion in HeLa cells were detectable at the single cell stage (Fig. 3.18 A & B), they did not result in a severe phenotype detectable by FACS analysis (Fig. 3.17). Also single cell examination showed no

enrichment of binucleated cells upon GAS2L3 depletion compared to control cells (Fig. 3.18 D). In contrast, depletion of LIN9, a well known transcriptional regulator of many cytokinesis genes, enriched the amount of binucleated cells from under 1 % in control up to 8 % in LIN9 depleted cells (Fig. 3.18 D). Therefore, the mechanism how GAS2L3 depletion affects cytokinesis, resulting in a low but reproducible number of cells showing nuclei re-fusion accompanied by nuclei de-fragmentation, cannot be simply explained by GAS2L3 being a regulator of abscission.

Also for other midbody components it has been already shown that depletion in cell culture does not necessarily result in severe cytokinesis defects. A very good example is ASPM, the abnormal spindle-like microcephaly associated protein. Homozygous mutations in the ASPM gene are the leading cause of autosomal recessive primary microcephaly, a neurological disorder in which patients exhibit reduced occipital frontal head circumference and mild to severe mental retardation (Woods et al., 2005; Zhong et al., 2005). ASPM is the putative human ortholog of the *Drosophila melanogaster* abnormal spindle gene (*asp*), which is essential for mitotic spindle function. Larval neuroblasts in *Drosophila asp* mutants fail to complete asymmetric cell division (do Carmo Avides and Glover, 1999; Gonzalez et al., 1990). In human cells, ASPM has been shown to localize to the midbody ring in vitro (Paramasivam et al., 2007). Despite its midbody localization, depletion of ASPM in mammalian cell culture has never been described to result in cytokinesis failure (Fish et al., 2006; Horvath et al., 2006; Zhong et al., 2005).

It could be possible that GAS2L3 depletion, like ASPM, has in vivo a severe phenotype compared to the in vitro phenotype in cell culture. If GAS2L3 is for example essential during embryonic development or for the maintenance of genomic integrity, there would be no chance to identify such functions by using HeLa cells, an already highly transformed human breast cancer cell line. First evidence for a possible role in maintaining genomic integrity comes from experiments in the non transformed human foreskin fibroblast cell line BJ-ET. Even though transient depletion of GAS2L3 by siRNA transfection had no impact on cell cycle distribution (Fig. 3.19), stable GAS2L3 depleted BJ-ET cells by shRNA infection showed a slight decrease in their proliferation rate (Fig. 3.20). Strikingly, after longer passaging of those stable GAS2L3 depleted BJ-ET cells, karyogram analysis and FISH examination revealed a slight increase in aneuploidy (Wolter P, unpublished data).

The fact that more than 100 proteins have been identified to be midbody components should also attract interest. It could be possible that other midbody components are able to compensate for the decreased GAS2L3 expression. Therefore, the next important step should be the identification of direct GAS2L3 interacting partners. Unfortunately, the instability of GAS2L3 protein in human cells makes immunoprecipitation and immunoblot experiments very difficult (Fig. 3.14 & 3.15).

Another strategy to identify direct interacting partners is for example the yeast two hybrid screen. First experiments already showed that GAS2L3 is stable in yeast and can be used as bait for following screenings (Hauser S, unpublished data).

4.5.2 GAS2L3 depletion weakens the spindle assembly checkpoint

GAS2L3 localization to the mitotic spindle as well as the shortened metaphase-anaphase transition pointed out a possible role for GAS2L3 in the spindle assembly checkpoint (SAC), an indispensable checkpoint for proper chromosome segregation during early mitosis.

The SAC consists of two arms, one arm monitoring correct attachment of spindle microtubules to single kinetochores, the other arm monitoring proper tension between the mitotic spindle apparatus and attached chromosomes (Skoufias et al., 2001; Taylor et al., 2001; Waters et al., 1998) (detailed information s. 1.1.3). By using different microtubule poisons both arms can be activated separately. Treatment with the microtubule poison nocodazole completely abolishes mitotic spindle formation by depolymerization of microtubules and hence, activates the SAC by a complete loss of attachment. In contrast, the microtubule poison taxol leads to the hyperstabilization of microtubules (Peterson and Mitchison, 2002). In that case, the mitotic spindle can properly develop, but the spindle dynamic is completely disturbed. This in turn activates the SAC by a loss of tension.

At early time points of nocodazole treatment no differences were seen between control and GAS2L3 depleted cells in the amount of pH3 positive cells (Fig. 3.21 B). This indicates that the SAC, after the activation by nocodazole, is in GAS2L3 depleted cells initially as active as in control cells. However, between 24 hour and 30 hour treatment GAS2L3 depleted cells overcame the SAC faster, indicated by a decrease in pH3 positive cells to 25 % compared to 40 % of control cells (Fig. 3.21 B). SAC slippage came along with the faster degradation of Cyclin B and Securin (Fig. 3.21 D), another proof for premature SAC silencing (detailed information s. 1.1.3). These results were also confirmed in a SAC recovery assay. In this assay, mitotic cells, after 14 hours nocodazole treatment, were harvested by mechanical shake-off and replated in fresh media without nocodazole (Fig. 3.22 A). Again, GAS2L3 depleted cells initially arrested to the same amount in metaphase like control cells, but after replating showed premature SAC silencing (Fig. 3.22 B).

In contrast, by using taxol, the amount of pH3 positive GAS2L3 depleted cells never reached the amount of pH3 positive control cells (Fig. 3.23 B). Whereas control cells reached a maximum of 45 % pH3 positive cells after 17 hour treatment, only 25 % of cells were pH3 positive in GAS2L3 depleted cells at this time, indicating a highly weakened SAC (Fig. 3.23 B). Again SAC slippage came along with the faster degradation of Cyclin B and Securin (Fig. 3.23 C), confirming premature SAC silencing.

To conclude, in the absence of microtubules GAS2L3 is more or less dispensable for proper SAC function (Fig. 3.21 & 3.22), whereas in the presence of microtubules that do not create tension, GAS2L3 is necessary to generate and sustain SAC signaling (Fig. 3.23).

Interestingly, a similar phenotype has already been published for the chromosomal passenger proteins Aurora B and Survivin (Lens and Medema, 2003). It is proposed that Aurora B and Survivin are not direct effectors of the SAC, but that they render the cell capable to communicate a lack of tension back to the attached microtubules and the SAC. The localization of Aurora B and Survivin at the inner centromere, surrounded by two sister kinetochores, places them in an ideal location to do so. A predicted model is that Survivin recruits Aurora B to the inner centromere as cells enter mitosis accompanied by MAD2 and BUBR1 recruitment to the kinetochore. During prometaphase, microtubule attachment occurs randomly with a high chance of syntelic or merotelic attachments. Although these types of attachments can result in transient displacement of MAD2, tension fails to be generated on the kinetochore and displacement of the microtubules by the Survivin/Aurora B complex will result in renewed recruitment of MAD2 (Biggins and Murray, 2001; Hauf et al., 2003; Tanaka et al., 2002).

However, recent research demonstrated that treatment with the Aurora kinase inhibitor ZM447439 also impaired BUBR1 and BUB1 kinetochore localization upon nocodazole treatment. Even though those cells could initially arrest in metaphase, they exited mitosis precociously, indicating a direct role of Aurora B in sustained SAC signaling upon the loss of attachment (Hauf et al., 2003). Morrow et al. could also show that Aurora kinase activity cooperates with BUB1 to maintain SAC functionality. Whereas Aurora kinase inhibited or BUB1 depleted cells could initially undergo mitotic arrest when exposed to nocodazole, their combined loss had a synergistic effect resulting in a defective SAC response (Morrow et al., 2005).

It would be interesting to analyze, if the ability of BUB1 deficient cells to mount a robust SAC response following spindle destruction is also dependent on GAS2L3. If yes, this would argue for a role of GAS2L3 in the Aurora B pathway mainly essential for the communication of a lack of tension but probably also for the maintenance of SAC activity.

4.5.3 Role of GAS2L3 in the SAC

To elucidate the mechanism how GAS2L3 affects SAC functionality, I next investigated the behavior of the SAC master regulators MAD2 and BUBR1. As mentioned before, MAD2 and BUBR1 localization to kinetochores and their ability to bind and inhibit CDC20 are indispensable for proper SAC function (detailed information s. 1.1.3 & 3.9.3.1 & 3.9.3.2).

4.5.3.1 MAD2 can still localize to kinetochores but MAD2/CDC20 interaction is compromised

Even though MAD2 could still localize to kinetochores in GAS2L3 depleted HeLa cells upon taxol treatment (Fig. 3.24), MAD2/CDC20 interaction was compromised (Fig. 3.25).

Binding of MAD2 to CDC20 was significantly reduced in GAS2L3 depleted cells 14 hours and 25 hours after taxol treatment (Fig. 3.25). Premature SAC silencing was also confirmed by the faster degradation of Securin and Cyclin B (Fig. 3.25). Importantly, MAD2 input protein levels were not affected by GAS2L3 depletion (Fig. 3.25), indicating a specific reduced MAD2/CDC20 interaction in those cells. However, still the question remains, if the reduced interaction is a direct effect of GAS2L3 depletion or if it is only a secondary effect as a consequence of the premature SAC silencing resulting in faster progression through mitosis. To clarify this question, the same experiment should be performed again also with earlier time points of taxol treatment combined with MG132 treatment. MG132 treatment would arrest the cells in metaphase by blocking Securin and Cyclin B degradation and therefore a reduced MAD2/CDC20 interaction would definitely be a direct effect of GAS2L3 depletion.

Also it has to be mentioned that it is still possible that GAS2L3 quantitatively affects MAD2 localization to kinetochores. Even though MAD2 kinetochore localization after 8 hours of taxol treatment was unchanged in GAS2L3 depleted cells (Fig. 3.24), a quantification of MAD2 amounts at the kinetochores has still to be done. Therefore, a co-staining of MAD2 and a kinetochore protein that is not affected by taxol treatment, for example CENP-A or CREST, should be performed.

4.5.3.2 BUBR1 phosphorylation is affected in GAS2L3 depleted cells

The protein kinase BUBR1 is an important component of the SAC and also essential for kinetochores to establish microtubule attachments (Lampson and Kapoor, 2005; Mao et al., 2003). To fulfill those functions, BUBR1 has to become extensively phosphorylated during mitosis by multiple mitotic kinases.

Upon taxol treatment, BUBR1 phosphorylation was reduced in GAS2L3 depleted cells (Fig. 3.27). This reduced phosphorylation of BUBR1 was visible as soon as cells arrested in metaphase due to SAC activation by taxol treatment (Fig. 3.27). On the one hand, this argues for a direct effect of GAS2L3 in affecting the BUBR1 phosphorylation status. On the other hand, against a direct effect argues the Securin immunoblot which demonstrated that the SAC was never fully activated upon taxol treatment in GAS2L3 depleted cells (Fig. 3.27).

To elucidate, if the effect on the BUBR1 phosphorylation status is cause or consequence of the weakened SAC, cells should be synchronized in unperturbed mitosis without activating the SAC, for example with the specific CDK1 inhibitor RO-3306. Treatment

with RO-3306 reversibly arrests cells at the G2/M border and after release, cells progress synchronously through mitosis without failure (Vassilev, 2006; Vassilev et al., 2006). Cell release combined with MG132 treatment would arrest cells in mitosis and mitotic cells could be collected by mechanical shake-off. Immunoblot analysis from those mitotic cells should also reveal a compromised BUBR1 phosphorylation in GAS2L3 depleted cells.

Even though GAS2L3 depleted cells showed less efficient BUBR1 phosphorylation, BUBR1 was still able to localize to kinetochores in untreated as well as taxol treated cells (Fig. 3.26). However, as mentioned before (s. 4.5.3.1), if there are quantitative differences in BUBR1 protein amounts at the kinetochores is still an open question and should be clarified by co-staining with CENP-A or CREST.

An indispensable function of BUBR1 in inducing a stable metaphase arrest upon SAC activation is the inhibitory binding to CDC20 (Fang, 2002; Tang et al., 2001). However, less efficient binding of phosphorylated BUBR1 to CDC20 in GAS2L3 depleted cells exactly reflected reduced input BUBR1 levels and thus, are no indicator for a compromised BUBR1/CDC20 interaction (Fig. 3.27). Therefore, how the reduced BUBR1 phosphorylation upon GAS2L3 depletion might affect the SAC is still an open question.

An important step to elucidate a possible mechanism would be the identification of the affected phosphorylation sites by using specific BUBR1 phosphorylation antibodies. This would provide information about the kinase(s) that could be affected by GAS2L3 depletion. Possible kinases could be PLK1 or CDK1. Recent research identified S676 as a PLK1-specific phosphorylation site on BUBR1. A prerequisite for PLK1 phosphorylation is the kinetochore localization of BUBR1 and the CDK1 dependent phosphorylation at T620. PLK1 phosphorylation was also shown to be responsible for causing the characteristic mitotic electrophoretic BUBR1 upshift (Elowe et al., 2007; Matsumura et al., 2007). Additionally, Elowe et al demonstrated that PLK1 dependent BUBR1 phosphorylation at kinetochores is only essential for stabilizing kinetochore-microtubule interaction and chromosome congression, but is not required for the SAC functions of BUBR1 (Elowe et al., 2007). On the one hand, these data argue against a direct effect of GAS2L3 in compromising SAC activity by regulating the BUBR1 phosphorylation status. On the other hand, BUBR1 phosphorylation upon GAS2L3 depletion was only reduced and not completely abolished (Fig. 3.27 & data not shown). This argues against PLK1 as the affected kinase.

However, literature concerning the consequence of BUBR1 phosphorylation and SAC function is still controversial. For example Huang et al identified in 2008 four new mitosis specific BUBR1 phosphorylation sites that are not targets of PLK1. The most conserved residue S670 was, unlike the PLK1 dependent S676 phosphorylation site, sensitive to microtubule attachments but not to kinetochore tension. Additionally, *in vitro* data suggested that S670 phosphorylation is important for SAC inhibition of the APC/C and thus, is also a critical determinant of SAC activity (Huang et al., 2008).

The discrepancy of those studies might be dependent on whether compromised BUBR1 phosphorylation has impact on BUBR1 kinase activity, encoded by the C-terminus. Even though the role of this kinase domain in SAC function, and in mitosis generally, is also still controversial, evidence is coming from data in *Xenopus* extracts, in MEFs and in human cells that BUBR1 kinase activity is essential for sustaining SAC signaling (Kops et al., 2004; Malureanu et al., 2009; Mao et al., 2003).

At kinetochores, BUBR1 kinase activity is turned on through phosphorylation by the microtubule motor protein CENP-E and vice versa, BUBR1 kinetochore localization is also essential for CENP-E kinetochore association (Mao et al., 2003; Mao et al., 2005). Whereas kinase-dead BUBR1 has been shown to still localize to kinetochores in the absence of endogenous BUBR1, SAC activity could only be partially restored (Malureanu et al., 2009). This suggests that prolonged SAC signaling requires BUBR1 kinase activity at kinetochores. The identification of the substrates through which kinetochore bound BUBR1 acts to sustain SAC signaling will be important future experiments.

It could be possible that the affected kinase upon GAS2L3 depletion might be CENP-E. Therefore, the next important experiment would be an *in vitro* BUBR1 kinase assay to investigate, if the compromised phosphorylation upon GAS2L3 depletion weakens BUBR1 kinase activity. Interestingly, the BUBR1 kinase activity is not required for CDC20 binding and for BUBR1 kinetochore localization (Malureanu et al., 2009; Tang et al., 2001). So it is still possible that albeit BUBR1/CDC20 interaction and BUBR1 kinetochore localization were not compromised upon GAS2L3 depletion (Fig. 3.26 & 3.27), BUBR1 kinase activity might be affected.

4.6 Hypothesis

Aneuploidy is the most common characteristic of human solid tumors and has therefore been proposed to contribute to, or even to drive, tumor development. The SAC guards against chromosome mis-segregation by delaying cell cycle progression through mitosis until all chromosomes have successfully made spindle microtubule attachments. Defects in the SAC generate aneuploidy and hence might facilitate tumorigenesis. In this study, I could demonstrate that GAS2L3 is essential for proper SAC function and furthermore for proper cytokinesis, but the underlying mechanism is so far unknown.

The molecular mechanism of cytokinesis is still not completely understood. One important open question is the mechanism linking the contractile ring to the plasma membrane or the mechanism stabilizing the interaction of the contractile ring and the spindle midzone. A possibility is that proteins, containing actin as well as microtubule binding domains, function as specific linker proteins. One of the proteins known to have a pivotal role as linker protein is the actin binding protein Anillin. Recent studies indicated that Anillin is not only necessary for the

organization of the contractile ring, but also for linking structural components of the ring to signaling proteins that control cytokinesis and mitotic exit (D'Avino et al., 2008; Piekny and Glotzer, 2008). Moreover, Anillin establishes a direct connection between the contractile ring and spindle microtubules at the cell division site (D'Avino et al., 2008; Gregory et al., 2008). Except for Anillin, to date, remarkably few actin binding proteins have been identified among the genes implicated in cytokinesis (Glotzer, 2005). Since I could demonstrate that midbody localization of GAS2L3 during cytokinesis is not only dependent on the microtubule binding domains but also on the CH domain, it is tempting to speculate that GAS2L3 might be such a linker protein.

Concerning GAS2L3 function at the SAC, it is difficult to propose a hypothesis due to the complexity of this checkpoint. What I can conclude from my experiments is that in the absence of microtubules (nocodazole treatment) GAS2L3 is more or less dispensable for proper SAC function, whereas in the presence of microtubules that do not create tension (taxol treatment), GAS2L3 is necessary to generate and sustain SAC signaling. This argues for GAS2L3 playing a role similar to Aurora B and not for being a direct participant in SAC signaling. It is thinkable that by localizing to mitotic spindle microtubules, GAS2L3 acts as a transducer protein in the Aurora B pathway, known to be responsible for sensing the tension between attached kinetochores. In this scenario, GAS2L3 would transduce the mechanical property sensed by Aurora B into a biochemical signal, therefore rendering the cell capable to communicate a lack of tension back to the SAC.

An obvious phenotype upon GAS2L3 depletion and SAC activation was also the reduced phosphorylation of BUBR1. However, the impact of the BUBR1 phosphorylation status in relation to SAC function is highly dependent on the affected phosphorylation sites. PLK1 phosphorylation at S676 has been shown to be not essential for SAC function and only for stable kinetochore microtubule attachments. In contrast, phosphorylation by CENP-E affects BUBR1 kinase activity and BUBR1 kinase activity has been shown to be essential for sustained SAC signaling. Therefore, it is possible that GAS2L3 might be a direct effector of the SAC and essential for sustained SAC signaling. This would be an explanation for the premature SAC silencing in nocodazole treated cells upon GAS2L3 depletion. However, before proposing any hypothesis, it is crucial to find out whether reduced BUBR1 phosphorylation is cause or consequence of the weakened SAC.

Since a complete understanding of mitotic regulation is central to dissecting the basic mechanisms of tumorigenesis, further research on GAS2L3 is indispensable.

5 APPENDIX

5.1 List of Figures & Tables

Figures

Fig. 1.1. Simplified illustration of the human cell cycle.....	3
Fig. 1.2. Overview of different M phase stages.....	5
Fig. 1.3. Schematic illustration of a dividing cell in telophase	7
Fig. 1.4. Schematic illustration of the human GAS2 family members	13
Fig. 3.1. <i>GAS2L3</i> is a LINC target gene in human cells	40
Fig. 3.2. <i>GAS2L3</i> is a G2/M regulated gene	42
Fig. 3.3. <i>GAS2L3</i> G2/M specific gene expression is LINC dependent	43
Fig. 3.4. <i>GAS2L3</i> shows distinct subcellular localization during the cell cycle	45
Fig. 3.5. <i>GAS2L3</i> localizes to the midbody during cytokinesis	46
Fig. 3.6. MB localization of <i>GAS2L3</i> is not HeLa cell specific.....	46
Fig. 3.7. <i>GAS2L3</i> shows a distinct mitotic localization pattern.....	48
Fig. 3.8. <i>GAS2L3</i> mainly colocalizes with the microtubule network during mitosis.....	50
Fig. 3.9. Endogenous <i>GAS2L3</i> localizes to the midbody during cytokinesis	51
Fig. 3.10. (A) Diagram of <i>GAS2L3</i> deletion mutants (B) Summary of the results obtained by microscopic examination in Fig. 3.11 – 13	51
Fig. 3.11. Only full length <i>GAS2L3</i> can localize to the MB	53
Fig. 3.12. <i>GAS2L3</i> mutants show different localization pattern during interphase	54
Fig. 3.13. <i>GAS2L3</i> mut 3 and mut 4 induce the formation of actin stress fibers.....	55
Fig. 3.14. Protein characteristics of <i>GAS2L3</i> mutants are remarkably different	56
Fig. 3.15. Endogenous <i>GAS2L3</i> protein cannot be detected by immunoblot analysis	57
Fig. 3.16. Newly designed <i>Gas2l3</i> siRNAs are highly efficient	58
Fig. 3.17. <i>GAS2L3</i> depletion has no effect on cell cycle distribution in HeLa cells.....	59
Fig. 3.18. <i>GAS2L3</i> depletion induces enrichment of cytokinesis and multinucleated cells.....	60
Fig. 3.19. <i>GAS2L3</i> depletion has no effect on cell cycle distribution in BJ-ET cells	61
Fig. 3.20. Stable <i>GAS2L3</i> depletion leads to reduced proliferation of BJ-ET cells	62
Fig. 3.21. <i>GAS2L3</i> depletion leads to a weakened SAC after nocodazole treatment.....	64
Fig. 3.22. <i>GAS2L3</i> depleted cells show faster SAC recovery	65
Fig. 3.23. <i>GAS2L3</i> depletion leads to a highly weakened SAC after taxol treatment.....	67
Fig. 3.24. MAD2 can still localize to kinetochores in <i>GAS2L3</i> depleted cells	68
Fig. 3.25. MAD2/CDC20 interaction is compromised in <i>GAS2L3</i> depleted cells	69
Fig. 3.26. BUBR1 can still localize to kinetochores in <i>GAS2L3</i> depleted cells	70
Fig. 3.27. BUBR1 phosphorylation is compromised after <i>GAS2L3</i> depletion	71

Table

Table 1.1. Genes downregulated upon <i>Lin9</i> depletion	12
--	----

5.2 Abbreviations

ABD	Actin binding domain
APC/C	Anaphase promoting complex/Cyclosome
APS	Ammonium persulfate
AS	Anti sense
bp	base pairs
BSA	Bovine serum albumine
CDK	Cyclin dependent kinase
CH	Calponin homology
ChIP	Chromatin immunoprecipitation
DMEM	Dulbecco`s modified eagle medium
DMSO	Dimethylsulfoxyde
DNA	Deoxyribonucleic acid
DTT	Dithiothreitol
dNTP	Deoxyribonucleotide triphosphate
EDTA	Ethylenediaminetetraacetic acid
ESB	Electrophoresis sample buffer
FACS	Fluorescence-associated cell sorting
FCS	Fetal calf serum
Fig.	Figure
G0, G1, G2	Gap phases
GAS	Growth arrest specific
GAPDH	Glyceraldehyde-3-phosphate dehydrogenase
GST	Glutathione S-transferase
h	Hours
HRP	Horseradish peroxydase
IF	Immunofluorescence
IP	Immunoprecipitation
kDa	kiloDalton
LB	Luria Bertani
LINC	LIN complex
MB	Midbody
MBD	Microtubule binding domain
MBR	Midbody ring
M phase	Mitosis and cytokinesis
MT	Microtubules
PBS	Phosphate buffered saline
PH3	Phosphorylated histone H3 (Ser10)
PI	Protease Inhibitor
PMSF	Phenylmethylsulphonyl fluoride
pRB	Retinoblastoma protein
qRT-PCR	Quantitative real-time polymerase chain reaction
RNA	Ribonucleic acid
RNAi	RNA interference
shRNA	short hairpin RNA
siRNA	small interfering RNA
rpm	Revolutions per minute
RT	Reverse transcriptase / Room temperature
SDS	Sodium dodecyl sulfata
S phase	Synthesis phase
TAE	Tris-acetate-EDTA
TBS	Tris-buffered saline
WB	Western blot

5.3 References

- Akiyoshi, B., Nelson, C. R., Ranish, J. A., and Biggins, S. (2009). Quantitative proteomic analysis of purified yeast kinetochores identifies a PP1 regulatory subunit. *Genes Dev* 23, 2887-2899.
- Baker, D. J., Jeganathan, K. B., Cameron, J. D., Thompson, M., Juneja, S., Kopecka, A., Kumar, R., Jenkins, R. B., de Groen, P. C., Roche, P., and van Deursen, J. M. (2004). BubR1 insufficiency causes early onset of aging-associated phenotypes and infertility in mice. *Nat Genet* 36, 744-749.
- Baker, D. J., Perez-Terzic, C., Jin, F., Pitel, K., Niederlander, N. J., Jeganathan, K., Yamada, S., Reyes, S., Rowe, L., Hiddinga, H. J., *et al.* (2008). Opposing roles for p16Ink4a and p19Arf in senescence and ageing caused by BubR1 insufficiency. *Nat Cell Biol* 10, 825-836.
- Benetti, R., Copetti, T., Dell'Orso, S., Melloni, E., Brancolini, C., Monte, M., and Schneider, C. (2005). The calpain system is involved in the constitutive regulation of beta-catenin signaling functions. *J Biol Chem* 280, 22070-22080.
- Benetti, R., Del Sal, G., Monte, M., Paroni, G., Brancolini, C., and Schneider, C. (2001). The death substrate Gas2 binds m-calpain and increases susceptibility to p53-dependent apoptosis. *EMBO J* 20, 2702-2714.
- Bharadwaj, R., and Yu, H. (2004). The spindle checkpoint, aneuploidy, and cancer. *Oncogene* 23, 2016-2027.
- Biggins, S., and Murray, A. W. (2001). The budding yeast protein kinase Ipl1/Aurora allows the absence of tension to activate the spindle checkpoint. *Genes Dev* 15, 3118-3129.
- Bradford, M. M. (1976). A rapid and sensitive method for the quantitation of microgram quantities of protein utilizing the principle of protein-dye binding. *Anal Biochem* 72, 248-254.
- Brancolini, C., Benedetti, M., and Schneider, C. (1995). Microfilament reorganization during apoptosis: the role of Gas2, a possible substrate for ICE-like proteases. *EMBO J* 14, 5179-5190.
- Brancolini, C., Bottega, S., and Schneider, C. (1992). Gas2, a growth arrest-specific protein, is a component of the microfilament network system. *J Cell Biol* 117, 1251-1261.
- Brancolini, C., and Schneider, C. (1994). Phosphorylation of the growth arrest-specific protein Gas2 is coupled to actin rearrangements during Go-->G1 transition in NIH 3T3 cells. *J Cell Biol* 124, 743-756.
- Brito, D. A., and Rieder, C. L. (2006). Mitotic checkpoint slippage in humans occurs via cyclin B destruction in the presence of an active checkpoint. *Curr Biol* 16, 1194-1200.
- Ciliberto, A., and Shah, J. V. (2009). A quantitative systems view of the spindle assembly checkpoint. *EMBO J* 28, 2162-2173.
- Cleveland, D. W., Mao, Y., and Sullivan, K. F. (2003). Centromeres and kinetochores: from epigenetics to mitotic checkpoint signaling. *Cell* 112, 407-421.
- Cobb, J., Miyaike, M., Kikuchi, A., and Handel, M. A. (1999). Meiotic events at the centromeric heterochromatin: histone H3 phosphorylation, topoisomerase II alpha localization and chromosome condensation. *Chromosoma* 108, 412-425.
- Coller, H. A. (2007). What's taking so long? S-phase entry from quiescence versus proliferation. *Nat Rev Mol Cell Biol* 8, 667-670.

- Coughlin, S. R., Lee, W. M., Williams, P. W., Giels, G. M., and Williams, L. T. (1985). c-myc gene expression is stimulated by agents that activate protein kinase C and does not account for the mitogenic effect of PDGF. *Cell* **43**, 243-251.
- D'Avino, P. P. (2009). How to scaffold the contractile ring for a safe cytokinesis - lessons from Anillin-related proteins. *J Cell Sci* **122**, 1071-1079.
- D'Avino, P. P., Takeda, T., Capalbo, L., Zhang, W., Lilley, K. S., Laue, E. D., and Glover, D. M. (2008). Interaction between Anillin and RacGAP50C connects the actomyosin contractile ring with spindle microtubules at the cell division site. *J Cell Sci* **121**, 1151-1158.
- Ditchfield, C., Johnson, V. L., Tighe, A., Ellston, R., Haworth, C., Johnson, T., Mortlock, A., Keen, N., and Taylor, S. S. (2003). Aurora B couples chromosome alignment with anaphase by targeting BubR1, Mad2, and Cenp-E to kinetochores. *J Cell Biol* **161**, 267-280.
- do Carmo Avides, M., and Glover, D. M. (1999). Abnormal spindle protein, Asp, and the integrity of mitotic centrosomal microtubule organizing centers. *Science* **283**, 1733-1735.
- Dobles, M., Liberal, V., Scott, M. L., Benezra, R., and Sorger, P. K. (2000). Chromosome missegregation and apoptosis in mice lacking the mitotic checkpoint protein Mad2. *Cell* **101**, 635-645.
- Doree, M., and Galas, S. (1994). The cyclin-dependent protein kinases and the control of cell division. *FASEB J* **8**, 1114-1121.
- Dyson, N. (1998). The regulation of E2F by pRB-family proteins. *Genes Dev* **12**, 2245-2262.
- Eggert, U. S., Mitchison, T. J., and Field, C. M. (2006). Animal cytokinesis: from parts list to mechanisms. *Annu Rev Biochem* **75**, 543-566.
- Elowe, S., Hummer, S., Uldschmid, A., Li, X., and Nigg, E. A. (2007). Tension-sensitive Plk1 phosphorylation on BubR1 regulates the stability of kinetochore microtubule interactions. *Genes Dev* **21**, 2205-2219.
- Fang, G. (2002). Checkpoint protein BubR1 acts synergistically with Mad2 to inhibit anaphase-promoting complex. *Mol Biol Cell* **13**, 755-766.
- Feng, J., Huang, H., and Yen, T. J. (2006). CENP-F is a novel microtubule-binding protein that is essential for kinetochore attachments and affects the duration of the mitotic checkpoint delay. *Chromosoma* **115**, 320-329.
- Fish, J. L., Kosodo, Y., Enard, W., Paabo, S., and Huttner, W. B. (2006). Aspm specifically maintains symmetric proliferative divisions of neuroepithelial cells. *Proc Natl Acad Sci U S A* **103**, 10438-10443.
- Fontijn, R. D., Goud, B., Echard, A., Jollivet, F., van Marle, J., Pannekoek, H., and Horrevoets, A. J. (2001). The human kinesin-like protein RB6K is under tight cell cycle control and is essential for cytokinesis. *Mol Cell Biol* **21**, 2944-2955.
- Fu, J., Bian, M., Jiang, Q., and Zhang, C. (2007). Roles of Aurora kinases in mitosis and tumorigenesis. *Mol Cancer Res* **5**, 1-10.
- Gavet, O., and Pines, J. (2010). Progressive activation of CyclinB1-Cdk1 coordinates entry to mitosis. *Dev Cell* **18**, 533-543.
- Gimona, M., and Mital, R. (1998). The single CH domain of calponin is neither sufficient nor necessary for F-actin binding. *J Cell Sci* **111** (Pt 13), 1813-1821.
- Gimona, M., and Winder, S. J. (1998). Single calponin homology domains are not actin-binding domains. *Curr Biol* **8**, R674-675.
- Glotzer, M. (2005). The molecular requirements for cytokinesis. *Science* **307**, 1735-1739.

- Glotzer, M. (2009a). The 3Ms of central spindle assembly: microtubules, motors and MAPs. *Nat Rev Mol Cell Biol* *10*, 9-20.
- Glotzer, M. (2009b). Cytokinesis: GAP gap. *Curr Biol* *19*, R162-165.
- Gonzalez, C., Saunders, R. D., Casal, J., Molina, I., Carmena, M., Ripoll, P., and Glover, D. M. (1990). Mutations at the *asp* locus of *Drosophila* lead to multiple free centrosomes in syncytial embryos, but restrict centrosome duplication in larval neuroblasts. *J Cell Sci* *96* (Pt 4), 605-616.
- Goriounov, D., Leung, C. L., and Liem, R. K. (2003). Protein products of human Gas2-related genes on chromosomes 17 and 22 (hGAR17 and hGAR22) associate with both microfilaments and microtubules. *J Cell Sci* *116*, 1045-1058.
- Greenberg, M. E., and Ziff, E. B. (1984). Stimulation of 3T3 cells induces transcription of the *c-fos* proto-oncogene. *Nature* *311*, 433-438.
- Gregory, S. L., Ebrahimi, S., Milverton, J., Jones, W. M., Bejsovec, A., and Saint, R. (2008). Cell division requires a direct link between microtubule-bound RacGAP and Anillin in the contractile ring. *Curr Biol* *18*, 25-29.
- Hardwick, K. G., Johnston, R. C., Smith, D. L., and Murray, A. W. (2000). MAD3 encodes a novel component of the spindle checkpoint which interacts with Bub3p, Cdc20p, and Mad2p. *J Cell Biol* *148*, 871-882.
- Hart, G. W., Housley, M. P., and Slawson, C. (2007). Cycling of O-linked beta-N-acetylglucosamine on nucleocytoplasmic proteins. *Nature* *446*, 1017-1022.
- Hauf, S., Cole, R. W., LaTerra, S., Zimmer, C., Schnapp, G., Walter, R., Heckel, A., van Meel, J., Rieder, C. L., and Peters, J. M. (2003). The small molecule Hesperadin reveals a role for Aurora B in correcting kinetochore-microtubule attachment and in maintaining the spindle assembly checkpoint. *J Cell Biol* *161*, 281-294.
- Hauf, S., and Watanabe, Y. (2004). Kinetochore orientation in mitosis and meiosis. *Cell* *119*, 317-327.
- Horvath, S., Zhang, B., Carlson, M., Lu, K. V., Zhu, S., Felciano, R. M., Laurance, M. F., Zhao, W., Qi, S., Chen, Z., *et al.* (2006). Analysis of oncogenic signaling networks in glioblastoma identifies ASPM as a molecular target. *Proc Natl Acad Sci U S A* *103*, 17402-17407.
- Hoyt, M. A., Totis, L., and Roberts, B. T. (1991). *S. cerevisiae* genes required for cell cycle arrest in response to loss of microtubule function. *Cell* *66*, 507-517.
- Huang, H., Hittle, J., Zappacosta, F., Annan, R. S., Hershko, A., and Yen, T. J. (2008). Phosphorylation sites in BubR1 that regulate kinetochore attachment, tension, and mitotic exit. *J Cell Biol* *183*, 667-680.
- Humbert, P. O., Verona, R., Trimarchi, J. M., Rogers, C., Dandapani, S., and Lees, J. A. (2000). E2f3 is critical for normal cellular proliferation. *Genes Dev* *14*, 690-703.
- Jeganathan, K., Malureanu, L., Baker, D. J., Abraham, S. C., and van Deursen, J. M. (2007). Bub1 mediates cell death in response to chromosome missegregation and acts to suppress spontaneous tumorigenesis. *J Cell Biol* *179*, 255-267.
- Joglekar, A. P., Bloom, K. S., and Salmon, E. D. (2010). Mechanisms of force generation by end-on kinetochore-microtubule attachments. *Curr Opin Cell Biol* *22*, 57-67.
- Johnson, R. P., and Craig, S. W. (1994). An intramolecular association between the head and tail domains of vinculin modulates talin binding. *J Biol Chem* *269*, 12611-12619.
- Johnson, R. P., and Craig, S. W. (1995). F-actin binding site masked by the intramolecular association of vinculin head and tail domains. *Nature* *373*, 261-264.

- Kalitsis, P., Fowler, K. J., Earle, E., Griffiths, B., Howman, E., Newson, A. J., and Choo, K. H. (2003). Partially functional Cenpa-GFP fusion protein causes increased chromosome missegregation and apoptosis during mouse embryogenesis. *Chromosome Res* 11, 345-357.
- Kamijo, K., Ohara, N., Abe, M., Uchimura, T., Hosoya, H., Lee, J. S., and Miki, T. (2006). Dissecting the role of Rho-mediated signaling in contractile ring formation. *Mol Biol Cell* 17, 43-55.
- Kastan, M. B., and Bartek, J. (2004). Cell-cycle checkpoints and cancer. *Nature* 432, 316-323.
- Kops, G. J., Foltz, D. R., and Cleveland, D. W. (2004). Lethality to human cancer cells through massive chromosome loss by inhibition of the mitotic checkpoint. *Proc Natl Acad Sci U.S.A* 101, 8699-8704.
- Kouprina, N., Pavlicek, A., Collins, N. K., Nakano, M., Noskov, V. N., Ohzeki, J., Mochida, G. H., Risinger, J. I., Goldsmith, P., Gunsior, M., *et al.* (2005). The microcephaly ASPM gene is expressed in proliferating tissues and encodes for a mitotic spindle protein. *Hum Mol Genet* 14, 2155-2165.
- Kraft, C., Gmachl, M., and Peters, J. M. (2006). Methods to measure ubiquitin-dependent proteolysis mediated by the anaphase-promoting complex. *Methods* 38, 39-51.
- Kramer, E. R., Scheuringer, N., Podtelejnikov, A. V., Mann, M., and Peters, J. M. (2000). Mitotic regulation of the APC activator proteins CDC20 and CDH1. *Mol Biol Cell* 11, 1555-1569.
- Lampson, M. A., and Kapoor, T. M. (2005). The human mitotic checkpoint protein BubR1 regulates chromosome-spindle attachments. *Nat Cell Biol* 7, 93-98.
- Lee, D. H., and Goldberg, A. L. (1998). Proteasome inhibitors: valuable new tools for cell biologists. *Trends Cell Biol* 8, 397-403.
- Lee, K. K., Tang, M. K., Yew, D. T., Chow, P. H., Yee, S. P., Schneider, C., and Brancolini, C. (1999). *gas2* is a multifunctional gene involved in the regulation of apoptosis and chondrogenesis in the developing mouse limb. *Dev Biol* 207, 14-25.
- Lee, W. H., Bookstein, R., Hong, F., Young, L. J., Shew, J. Y., and Lee, E. Y. (1987a). Human retinoblastoma susceptibility gene: cloning, identification, and sequence. *Science* 235, 1394-1399.
- Lee, W. H., Shew, J. Y., Hong, F. D., Sery, T. W., Donoso, L. A., Young, L. J., Bookstein, R., and Lee, E. Y. (1987b). The retinoblastoma susceptibility gene encodes a nuclear phosphoprotein associated with DNA binding activity. *Nature* 329, 642-645.
- Lens, S. M., and Medema, R. H. (2003). The survivin/Aurora B complex: its role in coordinating tension and attachment. *Cell Cycle* 2, 507-510.
- Li, M., Fang, X., Wei, Z., York, J. P., and Zhang, P. (2009). Loss of spindle assembly checkpoint-mediated inhibition of Cdc20 promotes tumorigenesis in mice. *J Cell Biol* 185, 983-994.
- Li, R., and Murray, A. W. (1991). Feedback control of mitosis in budding yeast. *Cell* 66, 519-531.
- Li, W., Lan, Z., Wu, H., Wu, S., Meadows, J., Chen, J., Zhu, V., and Dai, W. (1999). BUBR1 phosphorylation is regulated during mitotic checkpoint activation. *Cell Growth Differ* 10, 769-775.
- Li, X., and Nicklas, R. B. (1995). Mitotic forces control a cell-cycle checkpoint. *Nature* 373, 630-632.
- Maiato, H., DeLuca, J., Salmon, E. D., and Earnshaw, W. C. (2004a). The dynamic kinetochore-microtubule interface. *J Cell Sci* 117, 5461-5477.

- Maiato, H., Sampaio, P., and Sunkel, C. E. (2004b). Microtubule-associated proteins and their essential roles during mitosis. *Int Rev Cytol* **241**, 53-153.
- Malureanu, L. A., Jeganathan, K. B., Hamada, M., Wasilewski, L., Davenport, J., and van Deursen, J. M. (2009). BubR1 N terminus acts as a soluble inhibitor of cyclin B degradation by APC/C(Cdc20) in interphase. *Dev Cell* **16**, 118-131.
- Mao, Y., Abrieu, A., and Cleveland, D. W. (2003). Activating and silencing the mitotic checkpoint through CENP-E-dependent activation/inactivation of BubR1. *Cell* **114**, 87-98.
- Mao, Y., Desai, A., and Cleveland, D. W. (2005). Microtubule capture by CENP-E silences BubR1-dependent mitotic checkpoint signaling. *J Cell Biol* **170**, 873-880.
- Matsumura, S., Toyoshima, F., and Nishida, E. (2007). Polo-like kinase 1 facilitates chromosome alignment during prometaphase through BubR1. *J Biol Chem* **282**, 15217-15227.
- Michel, L. S., Liberal, V., Chatterjee, A., Kirchwegger, R., Pasche, B., Gerald, W., Dobles, M., Sorger, P. K., Murty, V. V., and Benezra, R. (2001). MAD2 haplo-insufficiency causes premature anaphase and chromosome instability in mammalian cells. *Nature* **409**, 355-359.
- Morgan, D. O. (1997). Cyclin-dependent kinases: engines, clocks, and microprocessors. *Annu Rev Cell Dev Biol* **13**, 261-291.
- Morrow, C. J., Tighe, A., Johnson, V. L., Scott, M. I., Ditchfield, C., and Taylor, S. S. (2005). Bub1 and aurora B cooperate to maintain BubR1-mediated inhibition of APC/CCdc20. *J Cell Sci* **118**, 3639-3652.
- Murray, A. W. (2004). Recycling the cell cycle: cyclins revisited. *Cell* **116**, 221-234.
- Nasmyth, K. (2002). Segregating sister genomes: the molecular biology of chromosome separation. *Science* **297**, 559-565.
- Neef, R., Klein, U. R., Kopajtich, R., and Barr, F. A. (2006). Cooperation between mitotic kinesins controls the late stages of cytokinesis. *Curr Biol* **16**, 301-307.
- Nevins, J. R. (1992). E2F: a link between the Rb tumor suppressor protein and viral oncoproteins. *Science* **258**, 424-429.
- Nishimura, Y., and Yonemura, S. (2006). Centralspindlin regulates ECT2 and RhoA accumulation at the equatorial cortex during cytokinesis. *J Cell Sci* **119**, 104-114.
- Oegema, K., Savoian, M. S., Mitchison, T. J., and Field, C. M. (2000). Functional analysis of a human homologue of the *Drosophila* actin binding protein anillin suggests a role in cytokinesis. *J Cell Biol* **150**, 539-552.
- Osterloh, L., von Eyss, B., Schmit, F., Rein, L., Hubner, D., Samans, B., Hauser, S., and Gaubatz, S. (2007). The human synMuv-like protein LIN-9 is required for transcription of G2/M genes and for entry into mitosis. *EMBO J* **26**, 144-157.
- Paramasivam, M., Chang, Y. J., and LoTurco, J. J. (2007). ASPM and citron kinase co-localize to the midbody ring during cytokinesis. *Cell Cycle* **6**, 1605-1612.
- Pardee, A. B. (1974). A restriction point for control of normal animal cell proliferation. *Proc Natl Acad Sci U S A* **71**, 1286-1290.
- Paweletz, N. (2001). Walther Flemming: pioneer of mitosis research. *Nat Rev Mol Cell Biol* **2**, 72-75.
- Pearson, M. A., Reczek, D., Bretscher, A., and Karplus, P. A. (2000). Structure of the ERM protein moesin reveals the FERM domain fold masked by an extended actin binding tail domain. *Cell* **101**, 259-270.

- Perera, D., Tilston, V., Hopwood, J. A., Barchi, M., Boot-Handford, R. P., and Taylor, S. S. (2007). Bub1 maintains centromeric cohesion by activation of the spindle checkpoint. *Dev Cell* *13*, 566-579.
- Peters, J. M. (2002). The anaphase-promoting complex: proteolysis in mitosis and beyond. *Mol Cell* *9*, 931-943.
- Peters, J. M. (2006). The anaphase promoting complex/cyclosome: a machine designed to destroy. *Nat Rev Mol Cell Biol* *7*, 644-656.
- Peterson, J. R., and Mitchison, T. J. (2002). Small molecules, big impact: a history of chemical inhibitors and the cytoskeleton. *Chem Biol* *9*, 1275-1285.
- Petronczki, M., Lenart, P., and Peters, J. M. (2008). Polo on the Rise-from Mitotic Entry to Cytokinesis with Plk1. *Dev Cell* *14*, 646-659.
- Piekny, A., Werner, M., and Glotzer, M. (2005). Cytokinesis: welcome to the Rho zone. *Trends Cell Biol* *15*, 651-658.
- Piekny, A. J., and Glotzer, M. (2008). Anillin is a scaffold protein that links RhoA, actin, and myosin during cytokinesis. *Curr Biol* *18*, 30-36.
- Planas-Silva, M. D., and Weinberg, R. A. (1997). The restriction point and control of cell proliferation. *Curr Opin Cell Biol* *9*, 768-772.
- Pohl, C., and Jentsch, S. (2008). Final stages of cytokinesis and midbody ring formation are controlled by BRUCE. *Cell* *132*, 832-845.
- Porter, L. A., and Donoghue, D. J. (2003). Cyclin B1 and CDK1: nuclear localization and upstream regulators. *Prog Cell Cycle Res* *5*, 335-347.
- Raemaekers, T., Ribbeck, K., Beaudouin, J., Annaert, W., Van Camp, M., Stockmans, I., Smets, N., Bouillon, R., Ellenberg, J., and Carmeliet, G. (2003). NuSAP, a novel microtubule-associated protein involved in mitotic spindle organization. *J Cell Biol* *162*, 1017-1029.
- Rao, C. V., Yamada, H. Y., Yao, Y., and Dai, W. (2009). Enhanced genomic instabilities caused by deregulated microtubule dynamics and chromosome segregation: a perspective from genetic studies in mice. *Carcinogenesis* *30*, 1469-1474.
- Reichert, N., Wurster, S., Ulrich, T., Schmitt, K., Hauser, S., Probst, L., Gotz, R., Ceteci, F., Moll, R., Rapp, U., and Gaubatz, S. (2010). Lin9, a subunit of the mammalian DREAM complex, is essential for embryonic development, for survival of adult mice, and for tumor suppression. *Mol Cell Biol* *30*, 2896-2908.
- Ribbeck, K., Raemaekers, T., Carmeliet, G., and Mattaj, I. W. (2007). A role for NuSAP in linking microtubules to mitotic chromosomes. *Curr Biol* *17*, 230-236.
- Rieder, C. L., Cole, R. W., Khodjakov, A., and Sluder, G. (1995). The checkpoint delaying anaphase in response to chromosome monoorientation is mediated by an inhibitory signal produced by unattached kinetochores. *J Cell Biol* *130*, 941-948.
- Rieder, C. L., and Maiato, H. (2004). Stuck in division or passing through: what happens when cells cannot satisfy the spindle assembly checkpoint. *Dev Cell* *7*, 637-651.
- Sagona, A. P., and Stenmark, H. (2010). Cytokinesis and cancer. *FEBS Lett* *584*, 2652-2661.
- Schiel, J. A., and Prekeris, R. (2010). Making the final cut - mechanisms mediating the abscission step of cytokinesis. *ScientificWorldJournal* *10*, 1424-1434.
- Schmit, F., Korenjak, M., Mannefeld, M., Schmitt, K., Franke, C., von Eyss, B., Gagrlica, S., Hanel, F., Brehm, A., and Gaubatz, S. (2007). LINC, a human complex that is related to pRB-containing complexes in invertebrates regulates the expression of G2/M genes. *Cell Cycle* *6*, 1903-1913.

- Schneider, C., King, R. M., and Philipson, L. (1988). Genes specifically expressed at growth arrest of mammalian cells. *Cell* **54**, 787-793.
- Shackelford, R. E., Kaufmann, W. K., and Paules, R. S. (1999). Cell cycle control, checkpoint mechanisms, and genotoxic stress. *Environ Health Perspect* **107 Suppl 1**, 5-24.
- Shannon, K. B., Canman, J. C., and Salmon, E. D. (2002). Mad2 and BubR1 function in a single checkpoint pathway that responds to a loss of tension. *Mol Biol Cell* **13**, 3706-3719.
- Sherr, C. J. (1994a). G1 phase progression: cycling on cue. *Cell* **79**, 551-555.
- Sherr, C. J. (1994b). The ins and outs of RB: coupling gene expression to the cell cycle clock. *Trends Cell Biol* **4**, 15-18.
- Sherr, C. J. (1996). Cancer cell cycles. *Science* **274**, 1672-1677.
- Sherr, C. J., Kato, J., Quelle, D. E., Matsuoka, M., and Roussel, M. F. (1994). D-type cyclins and their cyclin-dependent kinases: G1 phase integrators of the mitogenic response. *Cold Spring Harb Symp Quant Biol* **59**, 11-19.
- Skop, A. R., Liu, H., Yates, J., 3rd, Meyer, B. J., and Heald, R. (2004). Dissection of the mammalian midbody proteome reveals conserved cytokinesis mechanisms. *Science* **305**, 61-66.
- Skoufias, D. A., Andreassen, P. R., Lacroix, F. B., Wilson, L., and Margolis, R. L. (2001). Mammalian mad2 and bub1/bubR1 recognize distinct spindle-attachment and kinetochore-tension checkpoints. *Proc Natl Acad Sci U S A* **98**, 4492-4497.
- Slawson, C., Zachara, N. E., Vosseller, K., Cheung, W. D., Lane, M. D., and Hart, G. W. (2005). Perturbations in O-linked beta-N-acetylglucosamine protein modification cause severe defects in mitotic progression and cytokinesis. *J Biol Chem* **280**, 32944-32956.
- Stein, G. H. (1979). T98G: an anchorage-independent human tumor cell line that exhibits stationary phase G1 arrest in vitro. *J Cell Physiol* **99**, 43-54.
- Stern, B. M., and Murray, A. W. (2001). Lack of tension at kinetochores activates the spindle checkpoint in budding yeast. *Curr Biol* **11**, 1462-1467.
- Stevaux, O., and Dyson, N. J. (2002). A revised picture of the E2F transcriptional network and RB function. *Curr Opin Cell Biol* **14**, 684-691.
- Stradal, T., Kranewitter, W., Winder, S. J., and Gimona, M. (1998). CH domains revisited. *FEBS Lett* **431**, 134-137.
- Sudakin, V., Chan, G. K., and Yen, T. J. (2001). Checkpoint inhibition of the APC/C in HeLa cells is mediated by a complex of BUBR1, BUB3, CDC20, and MAD2. *J Cell Biol* **154**, 925-936.
- Sun, D., Leung, C. L., and Liem, R. K. (2001). Characterization of the microtubule binding domain of microtubule actin crosslinking factor (MACF): identification of a novel group of microtubule associated proteins. *J Cell Sci* **114**, 161-172.
- Tanaka, T. U., Rachidi, N., Janke, C., Pereira, G., Galova, M., Schiebel, E., Stark, M. J., and Nasmyth, K. (2002). Evidence that the lpl1-Sli15 (Aurora kinase-INCENP) complex promotes chromosome bi-orientation by altering kinetochore-spindle pole connections. *Cell* **108**, 317-329.
- Tang, Z., Bharadwaj, R., Li, B., and Yu, H. (2001). Mad2-Independent inhibition of APCCdc20 by the mitotic checkpoint protein BubR1. *Dev Cell* **1**, 227-237.

- Taylor, S. S., Hussein, D., Wang, Y., Elderkin, S., and Morrow, C. J. (2001). Kinetochore localisation and phosphorylation of the mitotic checkpoint components Bub1 and BubR1 are differentially regulated by spindle events in human cells. *J Cell Sci* *114*, 4385-4395.
- Taylor, S. S., Scott, M. I., and Holland, A. J. (2004). The spindle checkpoint: a quality control mechanism which ensures accurate chromosome segregation. *Chromosome Res* *12*, 599-616.
- Torras-Llort, M., Moreno-Moreno, O., and Azorin, F. (2009). Focus on the centre: the role of chromatin on the regulation of centromere identity and function. *EMBO J* *28*, 2337-2348.
- Trimarchi, J. M., and Lees, J. A. (2002). Sibling rivalry in the E2F family. *Nat Rev Mol Cell Biol* *3*, 11-20.
- Trinkle-Mulcahy, L., and Lamond, A. I. (2006). Mitotic phosphatases: no longer silent partners. *Curr Opin Cell Biol* *18*, 623-631.
- Vanoosthuyse, V., and Hardwick, K. G. (2009a). A novel protein phosphatase 1-dependent spindle checkpoint silencing mechanism. *Curr Biol* *19*, 1176-1181.
- Vanoosthuyse, V., and Hardwick, K. G. (2009b). Overcoming inhibition in the spindle checkpoint. *Genes Dev* *23*, 2799-2805.
- Vanoosthuyse, V., Meadows, J. C., van der Sar, S. J., Millar, J. B., and Hardwick, K. G. (2009). Bub3p facilitates spindle checkpoint silencing in fission yeast. *Mol Biol Cell* *20*, 5096-5105.
- Varis, A., Salmela, A. L., and Kallio, M. J. (2006). Cenp-F (mitosin) is more than a mitotic marker. *Chromosoma* *115*, 288-295.
- Vassilev, L. T. (2006). Cell cycle synchronization at the G2/M phase border by reversible inhibition of CDK1. *Cell Cycle* *5*, 2555-2556.
- Vassilev, L. T., Tovar, C., Chen, S., Knezevic, D., Zhao, X., Sun, H., Heimbrook, D. C., and Chen, L. (2006). Selective small-molecule inhibitor reveals critical mitotic functions of human CDK1. *Proc Natl Acad Sci U S A* *103*, 10660-10665.
- Wang, Q., Liu, T., Fang, Y., Xie, S., Huang, X., Mahmood, R., Ramaswamy, G., Sakamoto, K. M., Darzynkiewicz, Z., Xu, M., and Dai, W. (2004). BUBR1 deficiency results in abnormal megakaryopoiesis. *Blood* *103*, 1278-1285.
- Wang, Z., Udeshi, N. D., Slawson, C., Compton, P. D., Sakabe, K., Cheung, W. D., Shabanowitz, J., Hunt, D. F., and Hart, G. W. (2010). Extensive crosstalk between O-GlcNAcylation and phosphorylation regulates cytokinesis. *Sci Signal* *3*, ra2.
- Waters, J. C., Chen, R. H., Murray, A. W., and Salmon, E. D. (1998). Localization of Mad2 to kinetochores depends on microtubule attachment, not tension. *J Cell Biol* *141*, 1181-1191.
- Weaver, B. A., and Cleveland, D. W. (2006). Does aneuploidy cause cancer? *Curr Opin Cell Biol* *18*, 658-667.
- Weaver, B. A., Silk, A. D., Montagna, C., Verdier-Pinard, P., and Cleveland, D. W. (2007). Aneuploidy acts both oncogenically and as a tumor suppressor. *Cancer Cell* *11*, 25-36.
- Wei, Y., Yu, L., Bowen, J., Gorovsky, M. A., and Allis, C. D. (1999). Phosphorylation of histone H3 is required for proper chromosome condensation and segregation. *Cell* *97*, 99-109.
- Whitfield, M. L., Sherlock, G., Saldanha, A. J., Murray, J. I., Ball, C. A., Alexander, K. E., Matese, J. C., Perou, C. M., Hurt, M. M., Brown, P. O., and Botstein, D. (2002). Identification of genes periodically expressed in the human cell cycle and their expression in tumors. *Mol Biol Cell* *13*, 1977-2000.

- Woods, C. G., Bond, J., and Enard, W. (2005). Autosomal recessive primary microcephaly (MCPH): a review of clinical, molecular, and evolutionary findings. *Am J Hum Genet* 76, 717-728.
- Wu, H., Lan, Z., Li, W., Wu, S., Weinstein, J., Sakamoto, K. M., and Dai, W. (2000). p55CDC/hCDC20 is associated with BUBR1 and may be a downstream target of the spindle checkpoint kinase. *Oncogene* 19, 4557-4562.
- Wulf, E., Deboen, A., Bautz, F. A., Faulstich, H., and Wieland, T. (1979). Fluorescent phalloxin, a tool for the visualization of cellular actin. *Proc Natl Acad Sci U S A* 76, 4498-4502.
- Yu, H. (2002). Regulation of APC-Cdc20 by the spindle checkpoint. *Curr Opin Cell Biol* 14, 706-714.
- Zhao, W. M., and Fang, G. (2005). Anillin is a substrate of anaphase-promoting complex/cyclosome (APC/C) that controls spatial contractility of myosin during late cytokinesis. *J Biol Chem* 280, 33516-33524.
- Zhong, X., Liu, L., Zhao, A., Pfeifer, G. P., and Xu, X. (2005). The abnormal spindle-like, microcephaly-associated (ASPM) gene encodes a centrosomal protein. *Cell Cycle* 4, 1227-1229.
- Zhu, C., Bossy-Wetzel, E., and Jiang, W. (2005a). Recruitment of MKLP1 to the spindle midzone/midbody by INCENP is essential for midbody formation and completion of cytokinesis in human cells. *Biochem J* 389, 373-381.
- Zhu, C., Zhao, J., Bibikova, M., Levenson, J. D., Bossy-Wetzel, E., Fan, J. B., Abraham, R. T., and Jiang, W. (2005b). Functional analysis of human microtubule-based motor proteins, the kinesins and dyneins, in mitosis/cytokinesis using RNA interference. *Mol Biol Cell* 16, 3187-3199.
- Zucman-Rossi, J., Legoix, P., and Thomas, G. (1996). Identification of new members of the Gas2 and Ras families in the 22q12 chromosome region. *Genomics* 38, 247-254.

5.4 Own publications

- in preparation Schmitt K, Kremling H, Wolpert P, Probst L and Gaubatz S. The LINC target gene GAS2L3 is a novel regulator of mitosis and cytokinesis.
- 2010 Reichert N, Wurster S, Ulrich T, Schmitt K, Hauser S, Probst L, Götz R, Ceteci F, Moll R, Rapp U and Gaubatz S. LIN9, a subunit of the mammalian DREAM complex is essential for embryonic development, for survival of adult mice and for tumor suppression. *Molecular and Cellular Biology* 2010 June;30(12):2896-908.
- 2007 Schmit F, Korenjak M, Mannefeld M, Schmitt K, Franke C, von Eyss B, Gargica S, Hänel F, Brehm A and Gaubatz S. LINC, a human complex that is related to pRb-containing complexes in invertebrates regulates the expression of G2/M genes. *Cell Cycle* 2007 August 1;6(15):1903-13.

Conference contributions (Talks & Posters)

- 06.-08.10.2010 Meeting "The Puzzling World of Cancer", Integrated Graduate College of the SFB Transregio 17, Universität Würzburg

Talk: Schmitt K, Kremling H, Wolter P, Probst L and Gaubatz S. The LINC Target Gene GAS2L3 is a Novel Regulator of Mitosis and Cytokinesis.
- 21.-23.08.2008 Meeting "Cancer and the Cell Cycle", ISREC, Lausanne (Schweiz)

Poster: Mannefeld M, Schmitt K, Gaubatz S. Regulation of G2/M gene expression by the human DREAM/ LIN complex in response to DNA damage.
- 06.-07.02.2008 Sonderforschungsbereich Transregio 17 Meeting, Universität Würzburg

Poster: Reichert N, Schmitt K, Spahr S, Götz R, Rapp UR, Gaubatz S. The role of LIN9 in Ras-dependent tumorigenesis.

5.6 Eidesstattliche Erklärung

Hiermit erkläre ich, Kathrin Schmitt, geboren am 9. November 1977 in Freiburg im Breisgau, an Eides statt, dass ich die vorliegende Dissertation selbständig verfasst habe und dabei keine anderen als die von mir angegebenen Hilfsmittel und Quellen benutzt habe. Zitate sind als solche gekennzeichnet.

Ich erkläre außerdem, dass die vorliegende Dissertation weder in gleicher noch in ähnlicher Form bereits in einem anderen Prüfungsverfahren vorgelegen hat.

Ich habe früher, außer den mit dem Zulassungsantrag urkundlich vorgelegten Graden, keine weiteren akademischen Grade erworben oder zu erwerben versucht.

Würzburg, 30. September 2010

Kathrin Schmitt

ACKNOWLEDGEMENTS

I am grateful to Prof. Dr. Stefan Gaubatz for the opportunity to work in his lab and for supervising my PhD thesis. Thank you for your continued scientific support and helpful suggestions.

Thank you to Prof. Dr. Georg Krohne for the supervision of my PhD thesis as a representative of the Faculty of Biology.

Many thanks to all my colleagues in the PCI, PCII & EBC for your help and advice. In particular, I would like to thank my present lab mates for the pleasant working atmosphere, help, advice and support: Tanja Ulrich, Jasmina Esterlechner, Piero Ocone, Stefanie Hauser, Susi Spahr and Adelgunde Wolpert. Special thanks go to Leona Probst, Heidi Kremling and Patrick Wolter for your assistance to my project.

Above all, I want to express my gratitude to my former lab mates: Mirjam Mannefeld, Nina Reichert, Fabienne Schmit, Lisa Osterloh and Markus Kleinschmidt. Without your enthusiasm for science, your unfailing optimism and your friendship I would have never started my PhD.

Special thanks go to my parents, sisters and Benjamin for your love, continued encouragement and because I could always rely on you.